Investigation of dissolution behavior of Mo-CerMet fuel in reprocessing by means of nano-electrospray ionization mass spectrometry

Von der Fakultät für Mathematik und Physik
der Gottfried Wilhelm Leibniz Universität Hannover
zur Erlangung des akademischen Grades
Doktorin der Naturwissenschaften
Dr. rer. nat.

genehmigte Dissertation von

M.Sc. Meijie Cheng

2019

Referent: Prof. Dr. Clemens Walther

Korreferent: Prof. Dr. Georg Steinhauser

Korreferent: Prof. Dr. Christian Ekberg

Tag der Promotion: 14.11.2019

Abstract

Dissolution behavior of Mo-CerMet fuel in reprocessing was investigated by use of *nano* ESI-MS. Pure Mo solution as well as 4 mixed systems (Mo-Fe, Mo-Zr, Mo-Th and Mo-Eu) solutions are qualitative and quantitative analyzed in 0.5 - 3 mol/L nitric acid.

In the pure Mo solutions, Mo dimer is the dominant species in the sample of 1 mol/L and 3 mol/L nitric acid, at lower acid concentration 0.5 mol/L nitric acid, the tendency towards formation of polymeric species increases. The solution species are measured during the dissolutions of the Mo pellet. With increasing concentration of Mo and increasing dissolution time, larger polymeric species form. The species distribution becomes more complicated during dissolution of the pellet, due to the increasing Mo concentration. Therefore, we can conclude that higher acidic strengths and low Mo concentration are favorable to the reprocessing step.

The addition of Fe(III) nitrate not only lead to significantly increase of the solubility of molybdenum and dissolution rate in nitric acid but also the formation of Mo-Fe species prevents formation of precipitates. Throughout the three mixed system Mo-Zr, Mo-Th and Mo-Eu, higher acidic strengths and the presence of Zr, Th or Eu suppresses the formation of pure Mo species and the formation of large Mo polymeric species. High concentration of nitric acid can suppress the formation of mixed Mo-Th species and mixed Mo-Eu species. In contrast, in higher concentration of nitric acid more mixed Mo-Zr species are formed. This could be due to the particularity of the ZMH precipitate precursors.

Since each species could behave differently in liquid-liquid extraction steps, solutions containing less different species are easier to be handled in reprocessing. Working at higher acid strengths could be advantageous for future reprocessing processes, as there are significantly fewer dissolution species in the system.

Keywords

Molybdenum, Nanoelectrospray, Polymerization, Solution species

List of Abbreviations

ADS	Accelerator Driven Systems
ASGARD	Advanced Fuels for Generation IV Reactors: Reprocessing and Dissolution
CerMet	Ceramic Metal
CID	collisionally induced dissociation
CMPO	Octyl(phenyl)-*N*,*N*-diisobutylcarbamoylmethylphosphine oxide
CRM	Charged residue model
d_{M-L}	distance between the centers of metal and ligand ions
E_k	kinetic energy
E_e	electric energy
ESI-MS	Electrospray ionization mass spectrometry
EXAFS	extended X-ray absorption fine structure
FPs	fission products
GWd/tHM	gigawatt-days per tonne of heavy metal
HEXS	high energy X-ray scattering
HLW	High-level wastes
I	Ionic strength
IAEA	International Atomic Energy Agency
ICP-MS	Inductively coupled plasma mass spectrometry
ICP-OES	Inductively Coupled Plasma Optical Emission Spectrometry
IEM	Ion evaporation model
IMF	Inert Matrix Fuels
L	distance
LWR	light-water reactor
$\log ß_{1n}^{0}$	complexation constant
m	mass
MA	Minor actinide
mM	mmol/L

MOX	Mixed oxide fuel
m/q	mass to charge ratio
NA	nicotianamine
NEA	Nuclear Energy Agency
NMR	nuclear magnetic resonance
P&T	partitioning and transmutation
PUREX	Plutonium Uranium Redox Extraction
PWR	pressurized water reactor
R&D	research and development
SNF	spent nuclear fuel
t	time
TBP	tributyl phosphate
TOF	time of flight
TOPO	trioctylphosphine oxide
TRUS	transuranium elements
TWh	tera watt hours
XAFS	X-ray absorption fine structure spectroscopy
XAS	X-ray absorption spectroscopy
V	velocity
V_s	potential
ZMH	$[ZrMo_2O_7(OH)_2]\cdot 2H_2O$
z_M	charge of the metal ion

Contents

1 Motivation and Introduction

Due to the strong increase of global population reaching 10 billion peoples in the next decades and their need for better living conditions, there is no doubt today that the demand for energy will continuously increase over the next few decades. A safe, clean, yet economic energy supply will be increasingly sought. Nuclear energy can make an important contribution to this. Today, around 11% of the world's electricity is provided by about 450 nuclear power reactors [1]. Nuclear and hydro power accounting for the largest share of any single nongreenhouse-gas-emitting source [1, 2]. In 2017 nuclear plants supplied 2503 TWh of electricity, up from 2477 TWh in 2016 [1, 3]. This is the fifth consecutive year that global nuclear generation has risen. The increase of nuclear energy in recent years has undoubtedly provided the most important contribution to reducing the CO_2-problem. To continue this benefit, new systems will be needed to replace plants as they retire. Many countries are therefore convinced that increased use of nuclear energy will be needed to secure energy supplies. To improve the nuclear energy systems, Generation IV roadmap defines and plans the necessary R&D to support a generation of innovative nuclear energy systems. Generation IV nuclear energy systems cover the entire system of nuclear energy, from uranium extraction to disposal, nuclear reactors and the nuclear fuel cycle [4]. The goals for Generation IV are defined in the four broad areas of sustainability, economic competitiveness, safety and reliability, proliferation resistance, and physical protection.

How to treat nuclear waste

However, nuclear power constantly produces radioactive waste (spent nuclear fuel, SNF). Long lived fission and activation products are hazardous when released into the environment. Most of the hazards from spent fuel stems from only a few chemical elements: plutonium, neptunium, americium, curium and some long-lived fission products (FPs) such as iodine and technetium. Several classifications of radioactive wastes exist, the most widely used by the specific activity and by the half-life of the istotopes [5]. High-level wastes (HLW) containing large proportions of long-lived isotopes (> 30y) represent a significant long-term risk. HLW of SNF contains actinides, particularly the transuranium elements (TRUs), and also long-lived fission products. Some of the latter are particularly mobile and pose an environmental and health risk if released into the geosphere biosphere [6]. Sustainable nuclear energy is defined with focus on waste management and resource utilization in the roadmap. The solution of the nuclear waste problem plays an important role for the new types of fuel design. The two strategies are followed now, namely direct spent fuel disposal

(once-through fuel cycle) and reprocessing-recycling (closed fuel cycle).

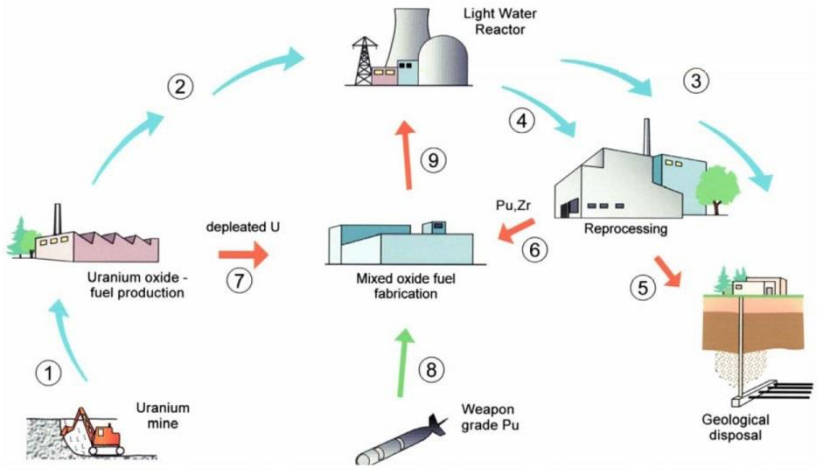

Figure 1-1: Nuclear fuel cycle. The arrows (1, 2, 3) denote the classical step of basic nuclear fuel cycle from the uranium mine to the disposal of the non-reprocessed fuel element (Once-through fuel cycle). The arrow (4) introduce the reprocessing step, Pu is produced and stocked (a small amount of waste that needs to be disposed of is also produced (5). The arrows (6, 7, 9, 4) present potential extension for the MOX option. The arrows (6, 8, 9, 3) depict the suggested fuel cycle extension. It includes spent U-fuel reprocessing plutonium fuel fabrication (U-free), Pu burning in the reactor, intermediate storage and direct geological disposal of the rock-like spent fuel [7].

First, in the once-through fuel cycle, spent fuel is stored several decades in interim storage sites to take credit of decay of short-lived isotopes and heat reduction. Subsequently, the SNF will be disposed in deep underground repositories. In Germany, the HLW was solidified prior to disposal *i.e.* the radionuclides were dispersed and confined in a matrix of borosilicate glass. The glass was filled into stainless steel containers (coquilles), which will be buried in an underground repository [8]. Since 2005, this reprocessing was stopped leaving direct disposal of fuel rods the only remaining option. While many technical questions of building and operating a repository are solved, the long-term safety of a repository cannot be guaranteed by technical systems alone.

The closed fuel cycle

Closing of the nuclear fuel cycle is an important alternative for achieving the sustainability goal. This objective can be attained by recovering the long-lived isotopes from the spent fuel and converting them into short-lived or stable nuclides by irradiation in a dedicated reactor. Several states with the largest nuclear programs (France, China, Japan, the Russian Federation and the UK) have adopted the policy of reprocessing nuclear fuel and recycling the separated material. This strategy is referred to as partitioning and transmutation (P&T). Partitioning is the separation of the

radiotoxic elements out of spent fuel. Transmutation is the change of long-lived nuclides into shorter-lived or stable nuclides by nuclear reactions in connection with waste management. P&T strategies are very powerful and unique tools that can drastically reduce the radiotoxicity level of the wastes as well as the time needed to reach the reference level, which is typically taken as the radiotoxicity of the amount of natural uranium the fuel was fabricated from [9-11]. Figure 1-2 shows as an example the radiotoxicity of spent fuel of a light water reactor after a burn up of 50 GWd/tHM. Spent fuel directly sent to long term storage without P&T in the open cycle will take 130 000 years until the radiotoxicity (ingestion dose) reaches the reference level. This time span can strongly be reduced to less than 1000 years if the long-lived actinides are separated from the waste prior to storage (Figure 1-2, red line). This route is called partitioning. One possible way to deal with the separated long-lived radionuclides is subsequent transmutation by an undercritical reactor (accelerator driven system). If, in addition to the actinides, also all long lives fission products are separated, the radiotoxicity curve reaches the level of natural uranium even after about 270 years. The separated plutonium and uranium are used to produce mixed uranium plutonium fuels (MOX) suitable for LWRs or fast reactors. Therefore, the P&T strategy not only reduces the necessary capacity of a final repository, but also increases efficiency of the resource exploitation.

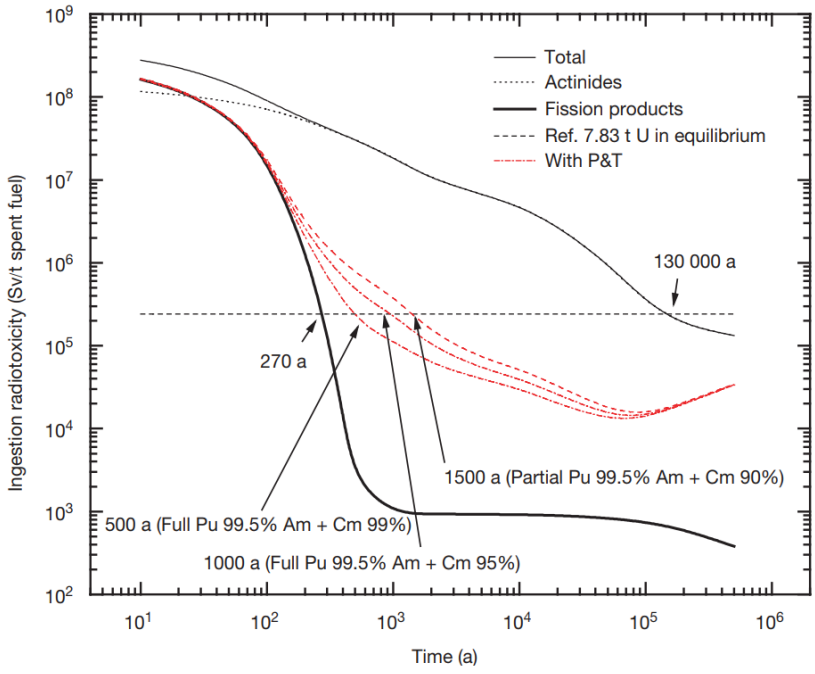

Figure 1-2: radiotoxicity of one ton of spent fuel from a pressurized light water reactor [6].

The PUREX Process

Pu and U separation from the SNF is performed by the PUREX process (Plutonium

Uranium Redox Extraction). It is used for almost all commercial fuel reprocessing today [12]. Pure uranium and plutonium oxides are produced by separation using a hydrometallurgical process based on liquid-liquid extraction between aqueous and organic phases. In the PUREX process, the fuel is dissolved in hot concentrated nitric acid, actinide ions are extracted from nitric acid into tributyl phosphate (TBP) diluted in a paraffinic diluent such as odorless Kerosene [12]. The overall reactions are

$$UO_{2(aq)}{}^{2+} + 2NO_3{}^{-}(aq) + 2TBP_{(org)} \rightarrow UO_2(NO_3)_2 \cdot 2TBP_{(org)}$$

Whereas the plutonium reacts

$$Pu_{(aq)}{}^{4+} + 4NO_3{}^{-}(aq) + 2TBP_{(org)} \rightarrow Pu(NO_3)_4 \cdot 2TBP_{(org)}$$

In the first step, fission products and minor actinides are separated from uranium and plutonium. Subsequently, the U and Pu loaded TBP solution is treated with a dilute nitric acid solution containing a reducing agent, such as ferrous sulfamate or U(IV), which reduces the plutonium to a trivalent state but leaves the uranium in a hexavalent state. Plutonium will then transfer to the aqueous phase, leaving uranium in the organic phase. The purified aqueous uranium and plutonium solutions are converted to storage as solid products through direct thermal denitration in the case of uranium and, for plutonium, oxalate precipitation and calcination. The waste solution containing fission products and minor actinides is evaporated to reduce its storage volume before being converted to its final waste form by calcination and vitrification. Insoluble fission products arising from the fuel dissolution process are incorporated with the calcined fission products prior to vitrification [13].

Transmutation

Besides generating energy, transmutation entails the advantage that plutonium and minor actinides will no longer exist in the HLW. In the transmutation of nuclear wastes, plutonium and MA can be fissioned directly by neutrons in the core of a nuclear reactor or transformed into other fissile nuclides (neutron-capture reactions). However, for efficient transmutation the fission reaction is needed. By comparison the fission/absorption ratios for dominant actinides in a PWR and a sodium cooled fast reactor, actinides are preferentially fissioned in a fast spectrum, not transmuted into higher actinides [11]. The accelerator-driven system (ADS) is a potential transmutation system option as part of partitioning and transmutation strategies for radioactive waste in advanced nuclear fuel cycles. The concept of ADS combines a particle accelerator, a spallation target, and a nuclear reactor with a subcritical core. The term subcritical means that, on average, for each generation of neutrons, less than one

secondary neutron is capable of initiating a subsequent nuclear fission. In a particle accelerator, high energy protons impinge on a spallation target made of a heavy metal like lead produce supplementary neutrons for the subcritical core. An ADS allows a greater flexibility with respect to the fuel composition and it has a potentially enhances safety.

Future nuclear fuels

The inert matrix fuels (IMF) are designed for transmutation in Accelerator Driven Systems (ADS) involving multi-recycling of actinides. In the IMF ^{238}U is replaced with a neutron-transparent matrix. This eliminates plutonium breeding as a result of neutron capture, thereby reducing the proliferation risk and promoting environmental safety. The desired properties of the inert matrix material are a high melting point, good thermal conductivity, good compatibility with the cladding, low solubility in the coolant, good mechanical properties, and high density [7]. At present, one of the favored candidates is Mo-CerMet fuels. In particular, the fuel type considered is a composite, in which the actinide phase is a U-free oxide $(Pu,Am)O_{2-x}$, and the inert matrix phase is Mo. The IMF with molybdenum attracts much attention especially from the viewpoint of its superior performance. The fuels shows good transmutation properties and low fission gas release can be reached [14]. Due to its inertness versus oxygen, the Mo-CerMet fuel can be fabricated relatively simple [15]. In addition, Mo based CerMet fuel has the advantage to behave favorably under transient and accident conditions [16-19].

Natural Mo contains ca. 24% of the isotope ^{98}Mo which has a non-negligible cross section for neutron absorption and forms ^{99}Mo, which in turn decays to ^{99}Tc. To minimize the build-up of ^{99}Tc, which due to its long half live of 210 000 years is regarded as one of the problematic isotopes for disposal (and also is a high yield fission product). Highly enriched ^{92}Mo is used for the Mo matrix [19, 20]. To avoid enrichment costs, the highly enriched molybdenum should be recycled for further use. On the other side, since complete actinide transmutation cannot be achieved in a single step, multi-recycling of the fuel including recovery of the not transmuted minor actinides is required. For these proposes, methods of separating the matrix from the not yet burned actinides and fission products need to be developed. This was one of the objectives within the ASGARD project.

The FP7 project ASGARD

The project ASGARD focusses on the separation processes of the fissile material from the matrix, in order to recycle it for new reactor fuel. The purpose of this work is trying to acquire knowledge of the behavior of the Mo matrix in reprocessing. In the first step of reprocessing, Mo based spent oxide fuel is dissolved in nitric acid. However, with

high Mo concentrations, formation of Mo containing precipitates that also might include actinides will occur over time [21]. Therefore, strategies are needed to investigation the dissolution process of the molybdenum matrix fuel.

As mentioned before, spent nuclear fuel is reprocessed by PUREX process as basis for all current commercial scale reprocessing plants, which base on liquid-liquid extraction. It is important to note that the aqua chemistry of actinides, particularly hydrolysis, is of major importance for understanding their aqueous chemistry [22]. For instance, speciation strongly influences solubility and sorption processes and consequently impacts mobility and migration behavior [23]. Chemistry in highly acidic media such as required in separation processes is complicated due to a rich redox chemistry of some of the light actinides including Pu. Mo has a complicated solution chemistry. The oxidation state in aqueous solutions can range from +2 to +6. Furthermore, Mo complexes in aqueous solutions readily undergo protonation and polymerization reactions, giving rise to plenty of coexisting species [24].

Experimental approach

Within ASGARD, the present work focuses on the species, which form upon dissolution of the Mo-Matrix. It is very important to understand whether the Mo with embedded actinide forms mixed Mo-actinide complexes or polymers. The Mo species formed in the dissolution process in strong acid have to be characterized and quantified comprehensively. For this purpose, *nano* electrospray ionization mass spectrometry (*nano* ESI-MS), which can probe the stoichiometry and relative abundances of solution species, is applied in this work. The method delivers unique insights into the solution speciation of molybdenum in strongly acidic media.

First developed for biological applications, ESI-MS allows for investigating very high masses by making multicharged species [25, 26]. it is also very suitable for direct speciation studies in solution due to its soft mode of ionization. This technique has been used successfully and increasingly in a variety of fields of inorganic, organometallic, analytical and environmental chemistry. ESI-MS is a technique that can be used for detection, identification and possible quantification of a number of species in equilibrium, whose distribution depends on the pH and the stoichiometric concentrations, among other factors. In recent years, this technique has been used successfully and increasingly in a variety of fields of metal-ligand systems. The results obtained by ESI-MS and other techniques have shown that ESI-MS obtains information on the stoichiometry of the metal-ligand complexes [27-30]. Investigations on hydrolysis products of metal cations in various acidic media and various acid concentrations have been performed including Zr(IV) [29], Th(IV) [30, 31], Pu(IV) [32], U(VI) [33] or Pu(VI) [34]. Moreover, the ESI-MS technique has been applied to different

aqueous molybdenum systems, for instance for investigations on isopolyoxymolybdate species [35], on heteropolymolybdates [36], polyoxymolybdates [37] and on molybdosilicate species [38]. Recently, Vilà-Nadal *et al.* showed that a combination of theoretical and mass spectrometric methods proves useful in order to elucidate the formation and fragmentation processes of small polyoxomolybdates [39].

The present work focuses on the investigations on pure Mo solutions species as well as on formation of the mixed species, Mo forms with Zr and Th (analogues for tetravalent actinides, particularly Pu), Eu (analogue for the trivalent actinides, particularly Am). Possible implications of the formation of the solution species on reprocessing steps will be discussed.

2 Chemistry Background

The understanding of chemical behavior of pure inert matrix Mo, and the inert matrix loaded with tetravalent and trivalent actinides, respectively, in the PUREX process is of major importance in the design of nuclear fuel and in relation to nuclear fuel reprocessing cycles. The aqua chemistries of molybdenum and actinides, particularly hydrolysis has been studied for over half a century [40-48]. However, due to the existence of anionic, cationic and polymeric species, the behavior of molybdenum in aqueous solutions is complicated to understand. In the PUREX process, the fuel is dissolved in concentrated nitric acid. Therefore, our work is focused on the investigation of Mo solutions as well as mixed solutions of Mo-Zr, Mo-Th and Mo-Eu in strongly acidic media.

2.1 Molybdenum

Molybdenum is a transition metal with atomic number 42. Mo has seven naturally occurring isotopes with atomic masses of 92, 94, 95, 96, 97, 98, and 100. As a transition metal Mo has the electron configuration $4d^5 5s^1$. In its compounds, Mo occurs in the oxidation states -2, -1, 0, +1, +2, +3, +4, +5, +6, and in aqueous solutions, from +2 to +6 [24]. Standard reduction potentials of Mo at pH = 0 are shown in Figure 2-1.

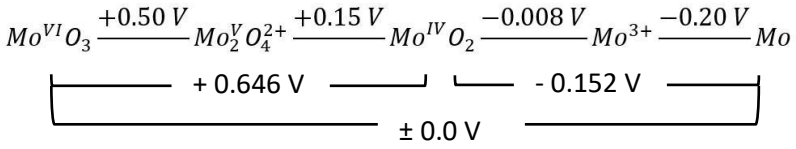

Figure 2-1: Standard reduction potentials for Mo at pH = 0.

Some of the safety advantages of the Mo-CerMet fuel are the high thermal conductivity, high melting temperature and low thermal expansion. Molybdenum isotopically enriched with ^{92}Mo is favored for use as inert matrix compared to natural Mo, because of its advantageous behaviour during (thermal-)neutron irradiation as described above. Additionally, ^{92}Mo has a much lower neutron capture cross-section in the fast spectrum region than natural molybdenum (especially the ^{95}Mo and ^{97}Mo isotopes). Neutron irradiation of ^{92}Mo will lead to ^{93}Mo which is only little radioactive (positron emission) and not radiotoxic and then to the stable ^{94}Mo [19]. To minimize enrichment costs, the isotopically enriched matrix needs to be recycled.

2.1.1 Aqua chemistry of Mo (VI)

The species distribution of Mo (VI) in aqueous solutions strongly depends on the acidity and Mo concentration [44, 45, 49-51]. Above pH 6.5 the $[MoO_4]^{2-}$ ion is the most stable species, in the range of pH 4.5 to 6.5, the paramolybdate $[Mo_7O_{24}]^{6-}$ exists in equilibrium with $[MoO_4]^{2-}$. Further acidification leads to the formation of the octamolybdate anion $[Mo_8O_{26}]^{4-}$ between pH 2.9 and 1.5. Tytko and Schonfeld showed that the anion $[Mo_{36}O_{112}]^{8-}$ is present in solution below a pH of 2.0. At the isoelectric point at pH 0.9 molybdic acid $MoO_3 \cdot H_2O$ tends to precipitate [52, 53]. With further decreasing pH, ongoing protonation and condensation reactions lead to predominant formation of cation species e.g. $[MoO_2(OH)]^+$ and $[MoO_2]^+$ [24, 54]. The monomeric cationic species $[HMoO_3]^+$ and $[H_2MoO_3]^{2+}$ are the predominant species in solution as long as the total molybdenum concentration is lower than 10^{-4} mol/L [44]. In nitric acid, the existence of the hydroxomolybdenyl cation $[MoO_2(OH)]^+$ is assumed at molybdenum concentrations on the order of 10^{-3} mol/L [51]. Banik *et al.* showed that at higher molybdenum concentrations of 10^{-2} mol/L, mononuclear species are practically absent [55]. As the concentration of Mo increases, the existence of dimeric cationic species in strongly acidic media was postulated in the early studies [56-60]. In the following years, dimeric cations $[Mo_2O_5]^{2+}$ have been found in several studies with increasing acid concentration and molybdenum concentrations in the mmol/L range [43, 44, 53, 61-64]. Ojo *et al.* showed by spectrophotometric methods that in 0.2-3 mol/L perchloric acid solutions, beside two monomeric species, $[HMoO_3]^+$ and $[H_2MoO_3]^{2+}$, two dimeric species $[H_2Mo_2O_6]^{2+}$ and $[H_3Mo_2O_6]^{3+}$ are present in solution. The group around Cruywagen performed many spectrophotometric investigations on the Mo(VI) system in strongly acidic media and deduced formation constants for monomeric and dimeric species with different degrees of protonation [43, 44, 64]. The notation of the different molybdenum species varies in the different publications. Table 2-1 gives an overview on the different notations of the proposed species together with the notations used throughout the present work.

Table 2-1: different notations used in the literature for the proposed solution species of Mo(VI) in acid solutions. The bold notations are the ones used in the present work.

species	Alternative notations
MoO_4^{2}	
$HMoO_4^-$	$MoO_3(OH)^-$, $MoO(OH)_5^-$
H_2MoO_4	$Mo(OH)_6$, $MoO_3 \cdot 3H_2O$, $MoO_3 \cdot H_2O$
$HMoO_3^+$	$Mo(OH)_5$,$\cdot H_2O$, $H_3MoO_4^+$, **$MoO_2(OH)^+$**
$H_2MoO_3^{2+}$	$MoO_2(H_2O)_4^{2+}$, $Mo(OH)_4(H_2O)_2^{2+}$, $H_4MoO_4^{2+}$, $MoO(OH)_2^{2+}$, **MoO_2^{2+}**
$HMo_2O_6^{2+}$	$Mo_2O(OH)_9(H_2O)^+$, $Mo_2O_6H(H_2O)_m^+$, **$Mo_2O_5(OH)^+$**
$H_2Mo_2O_6^{2+}$	$Mo_2O_5(H_2O)_m^{2+}$, $Mo_2O_2(OH)_6^{2+}$, **$Mo_2O_5^{2+}$**
$H_3Mo_2O_6^{3+}$	$Mo_2O(OH)_7(H_2O)_3^{3+}$, $Mo_2O_5H(H_2O)_m^{3+}$

Figure 2-2 shows the species plot calculated from the formation constants that were summarized in [45, 62, 65]. Due to the complicated aqua chemistry of Mo (VI) in strongly acidic media, few direct speciation studies have been performed. Esbelin *et al.* investigated comparable systems and reevaluated spectrophotometric data of the Mo monomer-dimer equilibria in perchloric acid media and determined conditional dimerization constants [66]. In their studies, the authors found the acidity to have a slight effect on the dimerization equilibrium. A much greater effects have variations in water activity, including the effects of ion strength and perchlorate anion concentration. Structural information on the dimeric complexes were gained by investigation of solids [67, 68]. The structure of the dimeric solution species was determined by Raman spectroscopy [53, 63], ^{95}Mo NMR [53] and X-ray absorption spectroscopy [69, 70]. The studies suggested that Mo(VI) forms a cationic dinuclear complex with an oxo bridge $[Mo_2O_5]^{2+}$.

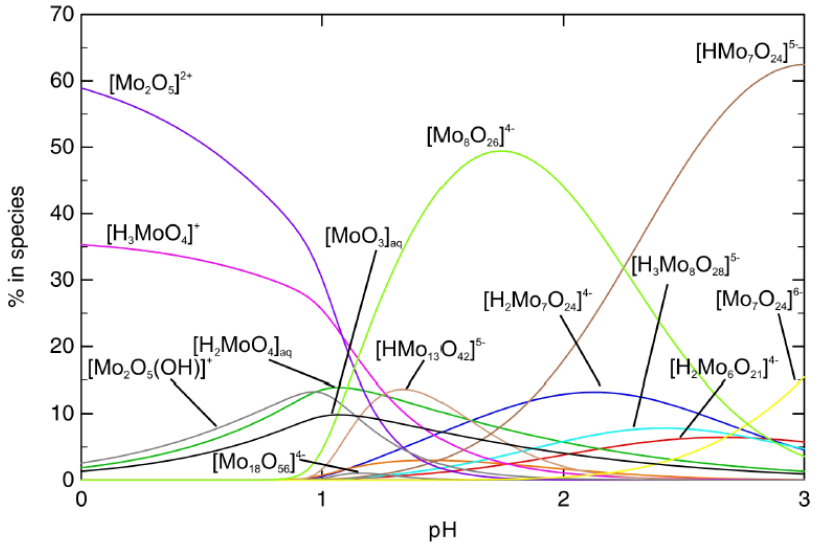

Figure 2-2: Distribution diagram of molybdenum in aqueous medium with varying pH values at [Mo] = 10 mmol/L and I = 1 mol/L. The stability constants for the calculation of the diagram were taken from [45, 62, 65]. The dimeric molybdenum species $Mo_2O_5^{2+}$ is the predominant species at pH values lower than 1. Formation constants of larger cationic species have not been reported, even if the presence of larger polymeric species was proposed in the literature below the isoelectric point at pH 0.9.

Beside the afore mentioned methods, liquid-liquid extraction methods were also used in order to identify the cationic solution species [49, 51, 71]. Only monomeric species were extracted by the extraction ligands TBP, TOPO and CMPO. The concentration of molybdenum are in the low mmol/L range in publications [49] and [71], this concentration range may have caused only monomeric molybdenum species to be extracted. Sato *et al.* showed, that depending on the acid concentrations of [HCl] > 0.5 mol/L and $[HNO_3]$ > 1 mol/L molybdenyl nitrato- or chloro-complexes $[MoO_2(X)_2]$ (with X = Cl^-, NO_3^-) are extracted respectively [71]. In the study of Tkac and Paulenova, the authors argue, that it is likely, that dimeric or even trimeric cationic

molybdenum species are present in solution, but that these do not have an influence on the extraction yields [51].

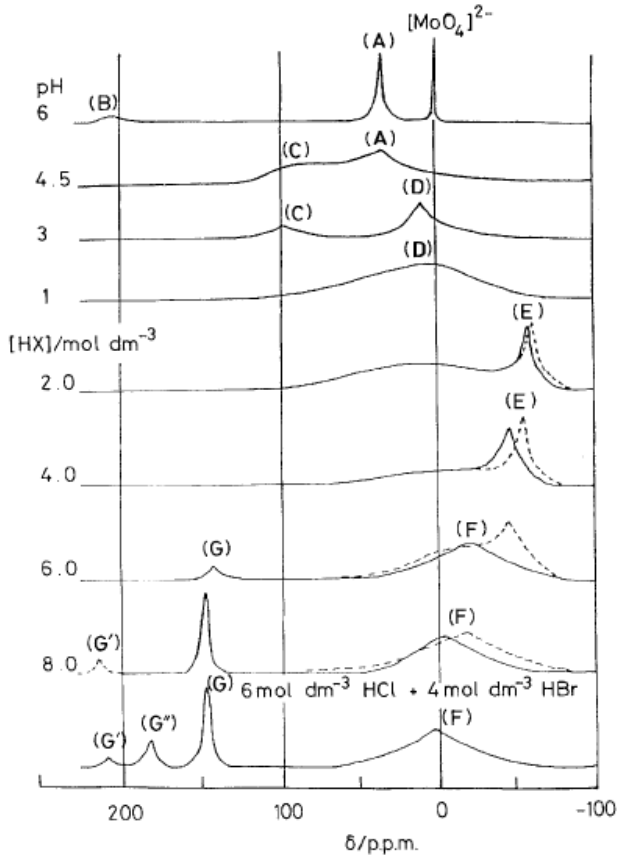

Figure 2-3: Molybdenum-95 NMR spectra of molybdenum (VI) species in aqueous HCl (full line) or HBr (dotted line) solutions of $Na_2[MoO_4]$ (0.5 mol/L). Species (E) causes a strongly signal at δ -60 ppm in solutions of $[HNO_3]$ = 2.0 mol/L and $[HClO_4]$ = 3.0 or 4.5 mol/L. This signal is attributed to the $[Mo_2O_5]^{2+}$ complex. At higher acidic solutions, species (F) and (G), (G'), (G'') are showed in the spectra. Species (F) are cationic *cis*-dioxomolybdenum(VI) polymers involving octahedrally co-ordinated molybdenum. Species (G), (G'), (G'') are discrete complexes $[MoO_2X_2(H_2O)_2]$ (X = Cl, Br) [53].

Two studies hinted on the formation of more species than the proposed monomeric and dimeric cationic species below the isoelectric point of molybdic acid (pH 0.9) [52, 53]. Ng *et al.* observed by use of light scattering techniques a rapid increase of the molecular weight of the species in solution at a pH of 0.8. The authors deduced, that below the isoelectric point of molybdic acid, there is at least one additional polymeric species present in solution, that is possibly positively charged [52]. In the study of Coddington *et al.* the authors also see strong evidence for the presence of larger oligomeric cationic species in the ^{95}Mo-NMR (Figure 2-3) and Raman-spectroscopy data [53]. The data did not provide enough information for the detailed determination of the structure of these species, but the Raman spectra indicated an octahedral coordination of Mo and a presence of cis dioxomolybdenum moieties in the oligomers. With increasing acid concentration, the size of the Mo species decreased, leading to a

predominant formation of dimeric $[Mo_2O_5]^{2+}$ at acid concentrations of 2 to 4 mol/L. With even higher acid concentrations monomeric species with coordinated anions $[MoO_2X]^+$ (with X = Cl, Br) are formed [53, 70]. Formation of cationic nitrato molybdenum complexes has been reported in the literature for concentrations higher than 0.05 mol/L [72-74]. Vorobev *et al.* proposed the formation of two different nitrato complexes $[MoO_2(NO_3)_i]^{(2-i)+}$ with i = 1-2 [72].

2.1.2 Aqua chemistry of Mo (V)

Mo (V) species in aqueous HCl were investigated by use of Mo K- and $L_{2,3}$-edge X-ray absorption and Raman spectroscopic methods by Jalilehvand [75]. In 0.2 mol/L solutions of $MoCl_5$, different dominant species are verified in three acid ranges: mononuclear $[MoOCl_4(OH_2)]^-$ in 7.4-9.4 mol/L HCl, dinuclear $[Mo_2O_4Cl_{6-n}(OH_2)_n]^{n-4}$ (n=2,3) in 1.7 mol/L HCl, and three coexisting classes of Mo(V) complexes in 3.7-6.3 mol/L HCl, i.e. mononuclear complexes, dinuclear mono-oxo (e.g., $[Mo_2O_3Cl_6(H_2O)_2]^{2-}$) and dioxo bridged species [75]. A reversible redox couple consisting of monomeric Mo(VI) and Mo(V) ions can be observed in highly dilute acidic solutions of Mo(VI). The aquemolybenum(V) ion undergoes spontaneous dimerization to form the stable Mo_2(V) ion [60]. Ardon *et al.* proposed a dioxo-bridged structure without chloro ligands for Mo(V) in 1-2 M HCl solutions (Figure 2-4,a) from a comparison with UV-Vis spectra of the diamagnetic Mo(V) oxalate complex [76]. Himeno *et al.* proposed structures (Figure 2-4, b and c) for Mo(V) in 1 M HCl by investigation of Raman spectra, which differ from the previously suggested structure a. The authors state that the mono-oxo and dioxo bridged species c and b would coexist in 2 M HCl solution [77, 78].

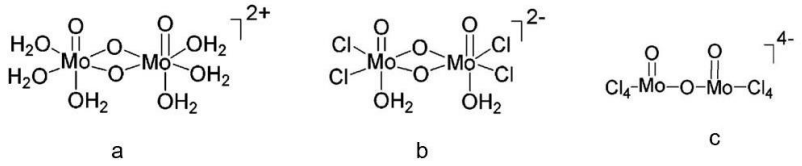

Figure 2-4: The previously proposed structures for dominating Mo(V) species in 1-2 M HCl [76-78].

2.1.3 The addition of iron(III)nitrate

As molybdenum shows poor solubility as well as slow dissolution kinetics in nitric acid, strategies are needed to enhance the dissolution process of the matrix. The addition of iron(III)nitrate leads to an increased solubility of the molybdenum matrix and enhances the dissolution kinetics, because a soluble Fe-Mo complex is formed [79-82]. Heteropolymolybdate ions are formed by reactions similar to the following [83]:

$$2Fe^{3+} + 12MoO_3 + 6H_2O \rightleftharpoons (Fe_2Mo_{12}O_{42})^{6-} + 12H^+$$

Uranium-molybdenum alloys dissolved in nitric acid-ferric nitrate solutions more rapidly than in nitric acid alone for each of the investigated acid concentrations. In order to understand the effect of Fe(III) on the process, the solution species formed by Mo in the presence of iron are investigated by means of *nano* ESI-MS in this work.

ESI-MS was also applied to the speciation of different Fe(III)-chelate complexes [84-87]. Rellán-Álvarez *et al.* have used electrospray ionization mass spectrometry to study the complexation of metal-nicotianamine complexes. A redox form of Fe(III) was apparent in the Fe(III) spectra, although this reduction is not expected when considering the redox potentials [86]. About 5% Fe(III) complex was detected in a Fe(II)-nicotianamine (NA) solution by both positive and negative nano-ESI ion mode, although oxidation is unlikely to occur in negative ESI ion mode [87]. However, no Fe(II) complex was observed in the Fe(III) solutions in both of two ESI ion modes. The authors suggest that the oxidation of Fe(II) to Fe(III) appeared already in solution resulting in NA-Fe(III) complex formation.

The free aquatic Fe^{3+} ion has a 6-fold coordination [88] and a strong tendency to hydrolyze to form $Fe(OH)_y^{3-y}$ (y≤4) [89]. It can be seen in Figure 2-5, that the predominant species at pH = 0 is free Fe^{3+}.

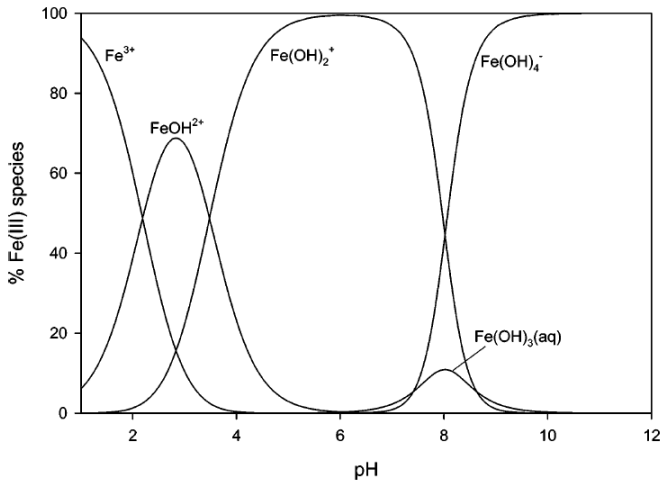

Figure 2-5: Distribution diagram of iron in aqueous medium with varying pH values at [Fe] = 10 μmol/L. The stability constants for the calculation of the diagram were taken from [90].

2.2 Aqua chemistry of Zr

In order to save expensive, rare material, and in order to avoid issues such as radiation induced redox transformations, homologue are often used for preliminary or

preparatory experiment instead of the radionuclide of interest. Experiments for the investigation of Pu(IV) are not easy to perform not only because of the complex redox behavior of plutonium but also due to its high radiotoxicity. The two most frequently used homologues for tetravalent plutonium are Zr(IV) and the very long lived actinide isotope ^{232}Th(IV). Under environmental conditions, zirconium always occurs in the oxidation state +IV in aqueous solution.

The remarkable similarities of Zr(IV) and Pu(IV) ions in solution are their strong tendency towards hydrolysis and colloid formation and low solubility. The first hydrolysis constants for $M(OH)^{3+}$ are $\beta_{1,1}^0 = 14.3$ [8] and $\beta_{1,1}^0 = 14.6$ [48] for Zr(IV) and Pu(IV), respectively. Figure 2-6 compares the species distribution in very dilute solutions at (I = 1 mol/L HCl/NaCl) when polynuclear complexes do not play a role. It became evident that the Zr^{4+} ion is stable only under very acidic conditions (pH<0), and that mononuclear hydroxide complexes dominate only in very dilute solutions ([Zr] < 10^{-5} M). For both metal ions, the first hydroxide complex starts to form in 1 M acid (calculated for HCl), and the second complex $M(OH)_2^{2+}$ dominates up to pH 3.

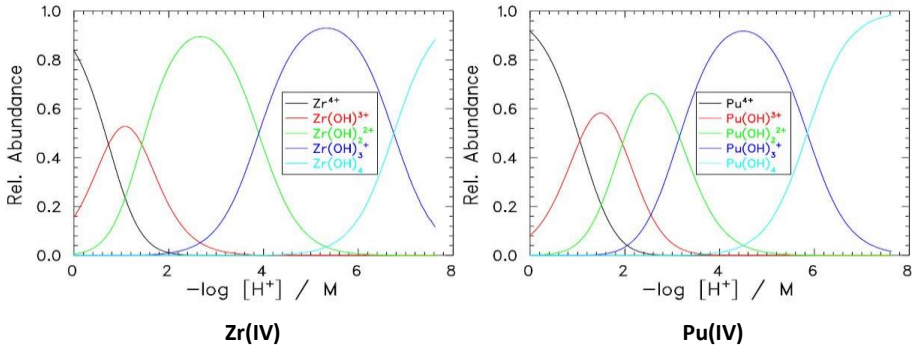

Figure 2-6: Calculated distribution of mononuclear hydroxide complexes (HCl/NaCl solutions of I = 0.5 M) in the absence of polynuclear species [8], e.g., at very low metal ion concentration. (a) Zr(IV), hydrolysis constants from [91]. (b) Pu(IV), hydrolysis constants from [92].

Zirconium itself is a high priority element for the assessment of radioactive nuclear waste repositories, therefore, at the beginning of this century the properties of Zr polyspecies in aqueous solutions gained renewed interest [93, 94]. Zirconium exists in aqueous solution only in the oxidation state IV. The study of Ekberg *et al.* covers the solubility of $Zr(OH)_4$ over a wide pH range [93]. The results indicate the presence of the monomeric species $Zr(OH)^{3+}$, $Zr(OH)_2^{2+}$, $Zr(OH)_3^{+}$, and $Zr(OH)_4^0$(aq) as well as the polymeric species $Zr_4(OH)_8^{8+}$ and $Zr_2(OH)_6^{2+}$. Walther *et al.* investigated the distribution of zirconium species directly by ESI-MS. In contrast to many other methods all species are observed independently – the signal does not average over many or all species. They detected the formation of zirconium monomers, tetramers and pentamers, octamers and larger polymers in acidic aqueous solution between pH_C 0 and pH_C 3 for [Zr] = 1.5–10 mM. Monomers and tetramers account for > 80% of the species at 1-

molar acidity, larger polymers form with increasing pH [29]. At pH<0.7, the tetramer dominates the species distribution which is well in line with the NEA model. The number of OH^- ligands per Zr(IV) ion increases with increasing pH, explained by the authors being a charge compensation mechanism [29]. There is a common agreement that the dominant hydrolysis species is the tetranuclear complex $[Zr_4(OH)_8^{8+} \cdot 16H_2O]$, which was investigated in detail in the past [95-100]. Recently, in Brown and Ekberg's [89] review a predominance diagram for the speciation of the Zr(IV) ion at 25°C and in 1 mol/L (H, Na)ClO_4 was given. In the region below pH 2 it resembles the diagram given in the review by Brown *et al.* [101], except for an additional predominance region for $Zr_4(OH)_8^{8+}$. However, this tetramer has been identified in X-ray studies in both the solid and aqueous state, therefore a predominance region of this species must be existing.

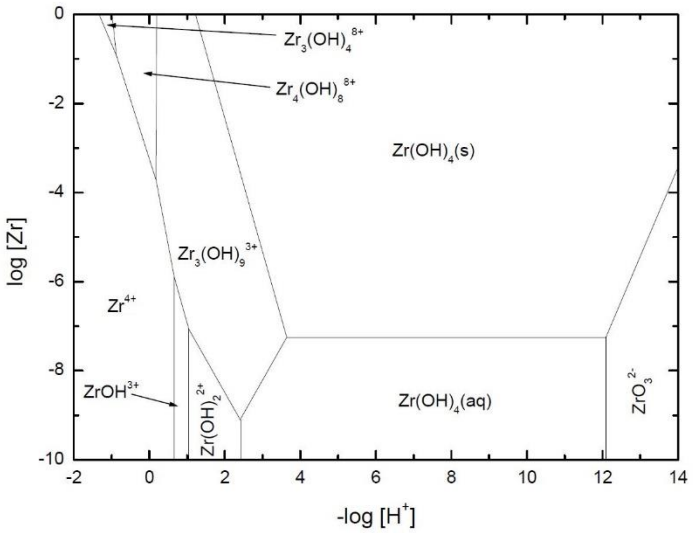

Figure 2-7: Predominance diagram for the speciation of the Zr(IV) ion at 25°C and in 1 mol/L (H,Na)ClO_4 [89].

The structure with the $[Zr_4(OH)_8^{8+} \cdot 16H_2O]$ unit was first analyzed by Clearfield et. al. [95] and has been refined since then by several authors. The tetrameric hydrolysis species has a square Zr_4 core stabilized by 8 μ_2-OH bridges. The presence of the tetranuclear hydrolysis complex in aqueous solution was first independently described by Muha *et al.* [97] and Åberg [98] based on X-ray scattering measurements and has been recently confirmed by Hagfeldt *et al.* [100] with Zr K-edge EXAFS. For increasing pH, the degree of polymerization increases leading to the formation of large polymers close to the solubility limit which is yet another parallel to Pu(IV).

Experimental data on zirconium nitrate complexation are limited. One of the few publications, the PSI/Nagra report, states that zirconium nitrate complexes are rather weak [102].

2.3 Aqua chemistry of Th

^{232}Th has the longest half-life of actinides ($1.405 \cdot 10^{10}$ years). Small amounts of millimolar solutions remain far below the permitted limit that can be handled in inactive laboratories. The effective charge of the Th(IV) ion in solution is 3.88 [103]. The aqua chemistry of Th(IV) parallels the one of Pu(IV) in many respects. However, due to the significant larger radius of the tetravalent thorium ion [104] hydrolysis is weaker than in the case of Pu(IV) and plays a significant role only at significantly higher pH. Accordingly, ^{232}Th is used as homologue for tetravalent plutonium at higher pH besides zirconium. Due to the actinide contraction, the Th(IV) Ion is the largest tetravalent cation and Th(IV) has the largest M-O bond length among the tetravalent actinides d(Th^{4+}-O) = 2.46 ± 0.02 Å [105], significantly larger than the value of d(Pu^{4+}-O) = 2.39 ± 0.01 Å [105], hence complexation with anionic ligands is much stronger for Pu(IV) than for Th(IV).

In the review of Johnson and Toth, the authors concluded that although Pu(IV) beings to hydrolyze at considerably lower pH, the 'hydrolytic behavior of Th(IV) and Pu(IV) (i.e. the mechanism) is quite similar' [106]. Close to the solubility limit, the presence of extensive polymerization reactions leads to extremely complex hydrolytic behavior of the ion. Various sets of species are detected or postulated in various media, at various ionic strength and temperature and different total thorium concentrations. In the review of Neck *et al.* [48] the solubility and hydrolysis of Th(IV) was critically revisited. At thorium concentrations of 10^{-4} – 10^{-2} mol/L, mononuclear species are usually found to be much less abundant than polynuclear species. Ekberg *et al.* show that $Th(OH)^{+3}$ is the dominant hydrolysis species at lower pH values [107]. Moulin *et al.* studied the hydrolysis of thorium by use of ESI-MS for the first time at high acidity. Due to rather harsh declustering conditions used in this study only the first thorium hydroxo complex $[Th(OH)]^{3+}$ was detected. $[Th(OH)]^{3+}$ appears above pH 1 and reaches maximum abundance at pH 2. No reduction of thorium was observed in the ESI-MS measurement, since the IV state is the only stable oxidation state [31]. By using much milder conditions of ESI-MS Walther et al. identified dimers and pentamers, which are the dominant polymeric complexes close to the solubility limit [30, 46]. The structure of the dimeric solution species $[Th_2(\mu_2\text{-}OH)_2(NO_3)_6(H_2O)_4]H_2O$ and $[Th_2(\mu_2\text{-}OH)_2(NO_3)_4(H_2O)_8](NO_3)_2$ were identified previously. The Th(IV) ions bridges with double μ^2O-hydroxo, the nitrate groups are bidentate, giving each thorium atom a coordination number of 11 and 10, respectively [108, 109]. Subsequently, Walther *et al*. [47] investigated the Th(IV)-hydroxo pentamer structure by combining X-ray absorption fine structure (XAFS) spectroscopy, high energy X-ray scattering (HEXS) measurements, and quantum chemical calculations. The most favourable structure is represented by two Th(IV) dimers linked by a central Th(IV) cation through hydroxide bridges. An important finding of their study was that even low concentrated samples may contain a high fraction of polymers as the solubility limit is approached. On the

basis of these facts, at the condition of our work (millimolar thorium concentrations) predominantly monomers and a small fraction of dimers at low pH are expected.

2.4 Aqua chemistry of Eu

Although europium is of limited relevance to spent nuclear fuel, it is widely used in laboratory experiments as analogue of trivalent actinides like americium(III). Americium is contained in all the nuclear waste produced by a nuclear power plant and one of the elements that contributes most to the radio toxicity of spent nuclear fuel. Americium has a high and lasting radiotoxicity with a high yield in nuclear fuel depending on burnup. Therefore, transmutation of americium is considered a favourable option. The effect on lowering radiotoxicity exceeds the one of all other MAs [110]. The ionic radius of Eu(III) is similar to the one of most trivalent actinide ions, which results in similar physical and chemical characteristics [111]. The evaluation of Nagra/PSI shows that the majority of the Eu(III) hydrolysis constants are fairly close to the corresponding values for Am(III). Europium is the only rare earth element which can be easily reduced to the divalent state in aqueous solutions. The standard potential for the reduction of europic to europeous ion lies slightly above that for reduction of divalent to metallic iron (-0.44 V).

$$Eu^{3+} + e^{-} \Leftrightarrow Eu^{2+},\ Eu^{0}_{(red)} = -0.35\ V \ \text{[112]}$$

Neck *et al.* reviewed the aqua chemistry of trivalent actinides, including a few data available for Eu(III) [111]. By inspecting the conditional formation/equilibrium constants for complexation of trivalent actinides, the authors conclude that, if a consistent method is applied to derive zero ionic strength constants, no significant differences are found among corresponding constants for Am(III), Cm(III), Eu(III) and Nd(III). Based on a Pitzer development, Neck *et al.* proposed the following unique set of equilibrium constants for hydrolysis of the mentioned trivalent ions at I = 0:

$$\log_{10}\ {}^{*}ß^{0}_{1,1} = -7.3 \pm 0.3$$

$$\log_{10}\ {}^{*}ß^{0}_{1,2} = -15.2 \pm 0.8$$

$$\log_{10}\ {}^{*}ß^{0}_{1,3} = -27.5 \pm 0.6$$

referring to the general reaction:

$$M^{3+} + nH_2O \Leftrightarrow M(OH)^{3-n}_{n} + nH^{+}.$$

The stable crystal structure $[Eu(NO_3)_3(H_2O)_4]$ was reported in 1986 [113], in which three bidentate nitrates and four coordinated water molecules produce a 10-coordinated Eu atom. However, to our knowledge the definite structures of Am(III) or Eu(III) cations in nitrate acid solution are still not available. Suzuki [114] investigated the stoichiometry of Eu(III)-citrate complexes at pH 7 by ESI-MS. The Eu dimer $Eu_2(C_6H_4O_7)_2^{2-}$ is the predominant complex species in 0.5 mmol/L Eu(III) and 0.5 mmol/L citrate solution, in the presence of excess citric acid, the abundance of Eu monomeric species $Eu(HC_6H_4O_7)_2^{3-}$ exceeds the one of the dimeric species. Bentouhami *et al.* [115] postulated the formation of the polynuclear hydrolysis product for trivalent europium $Eu_2(OH)_3^{3+}$ with the logarithm of the stability constant being -15.4 ± 0.2. However, the data are no confirmatory evidence for the formation of this species. Plancque *et al.* investigated Eu(III) complexation with acetic, glycolic and 4-hydroxyphenylacetic acids. The results show, that only one inorganic species is formed at acidic pH: free europium Eu^{3+}, since no hydrolysis or carbonatation occurs at pH values below 7. Figure 2-8 shows a species-distribution diagram obtained from the stabiliy constants of hydrolysis products of europium with $[Eu^{3+}]_{tot} = 2 \cdot 10^{-4}$ mol/L by Jimenez-Reyes et. al. [116]. Only free europium Eu^{3+} is present in solution below pH 5.5.

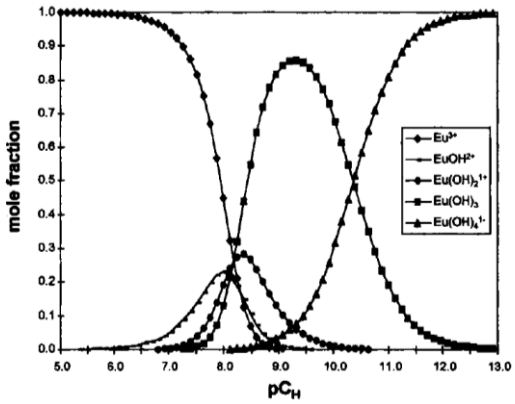

Figure 2-8: species-distribution diagram obtained from the stabiliy constant of hydrolysis products of europium with $[Eu^{3+}]_{tot} = 2 \cdot 10^{-4}$ mol/L [116].

2.5 The correlation of hydrolysis of Zr(IV), Pu(IV), Th(IV) and Eu(III)

Because of the high electric charge, tetravalent actinide ions form hydroxide complexes in aqueous solution even at high acidity (pH<1) and undergo polynucleation and colloid formation. Different from tetravalent actinides, hydrolysis reactions of Am(III) and Eu(III) are not significant at near neutral pH or below [111, 117].

Neck *et al.* [48] gave the evaluation of a comprehensive set of thermodynamic data at I=0 and 25°C for the aqueous hydrolysis species of tetravalent actinides. The effect of hydrolysis increases for the heavier actinides due to the increasing charge density of

the ions analogously as known for the lanthanides (lanthanide contraction). An empirical linear correlation is usually applied to the first complexation constant:

$$\log \beta^0_{(1n)} \propto {}^{el}E_{M-L} \propto (z_M/d_{M-L})$$

z_M is the charge of the metal ion and $d_{M\text{-}L}$ is the distance between the centers of metal and ligand ions. Figure 2-9 shows the application of this correlation to the known hydrolysis constants for Am(III) and Cm(III), Np(IV), Pu(IV), NpO_2^+ and UO_2^{2+}. The correlation may be used to estimate the unknown constants and the correlation of hydrolysis of the metal ions that we measured in this work. The distances $d_{M\text{-}OH}$ of Zr(IV), Th(IV) and Eu(III) are given in Table 2-2. Since the quotient Z_M / $d_{M\text{-}OH}$ decreases in the series: $Zr^{4+} > Th^{4+} > Eu^{3+}$, a corresponding decrease is expected for the constants $\log \beta^0_{1n}$ for these ions. This assumption holds quite well for the interesting pH range of this work, Zr(IV) and Th(IV) begin hydrolysis or undergo polynucleation. In contrast europium Eu(III) dominantly remains Eu^{3+}_{aq} in the acidic solution.

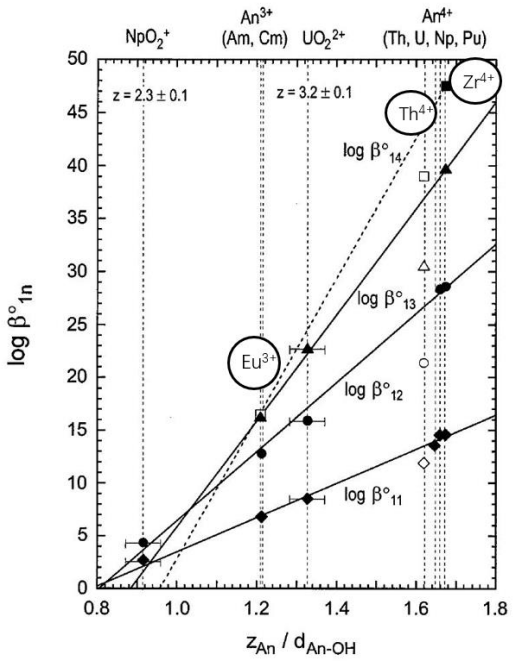

Figure 2-9: Correlation of the formation constants $\log \beta^0_{1n}$ of actinide hydroxide complexes with the electrostatic interaction energy ${}^{el}E_{An\text{-}OH}$ between the actinide and OH^- ions [48].

Table 2-2: Distances $d_{M\text{-}OH}$ of Zr(IV), Th(IV) and Eu(III). a: Crystal radii at given coordination number (CN) from Ref. [104], b: calculated according to $d_{M\text{-}OH} = r_M + r_{H2O}$

	Crystal radius/Å [a]	$d_{M\text{-}OH}$/Å [b]	Z_M / $d_{M\text{-}OH}$
Zr^{4+}	0.89 (CN=9)	2.27	1.76
Th^{4+}	1.09 (CN=9)	2.47	1.62
Eu^{3+}	1.066 (CN=8)	2.45	1.23

2.6 ZMH

ZMH phases were found in reprocessing equipment and these phases accumulated on walls of pipes and containers. This substance with stoichiometric formula $[ZrMo_2O_7(OH)_2]\cdot 2H_2O$ causes twofold major issues during reprocessing of spent nuclear fuel [118-120]: On the one hand, the accumulation can carry significant quantities of plutonium and other actinides due to coprecipitation or structural incorporation to cause major problems in the PUREX process [118, 121-123]. Lloyd described that ZMH can carry 0.02 mg Pu per mg Zr and Mo from reprocessing solutions [118]. On the other hand, the accumulation of ZMH on the equipment wall may hinder the heat transfer to the nitric acid solution [124, 125]. It is essential to understand ZMH formation in acidic solution and specifically which solution species are involved in the formation of the precipitate, in order to effectively minimize formation of ZMH and hence improve reprocessing conditions. For this purpose, a number of studies have been carried out to characterize ZMH and its precipitation kinetics, such as structural investigations [120, 122, 126], nucleation kinetics [127-130], or crystal growth in simulated spent nuclear fuel reprocessing solutions [125, 131-133] and irradiation effects in ZMH [134]. The formation of ZMH is affected by both, temperature and nitric acid concentration. The higher the temperature and the lower the concentration of nitric acid the higher becomes the precipitation rate of ZMH phases [127].

3 Experimental Section

3.1 nano electrospray time of flight mass spectrometer

The samples were measured by an ALBATROS electrospray time of flight mass spectrometer (hereinafter referred to as: ALBATROS ESI-MS). The ALBATROS ESI-MS was built by T. Bergmann and the construction is described in detail in [135-137]. It consists of a home-built *nano* electrospray ion source (ESI) and a high resolution reflectron time-of-flight mass spectrometer (TOF-MS). The main components of the ESI-MS are shown schematically in Figure 3-1.

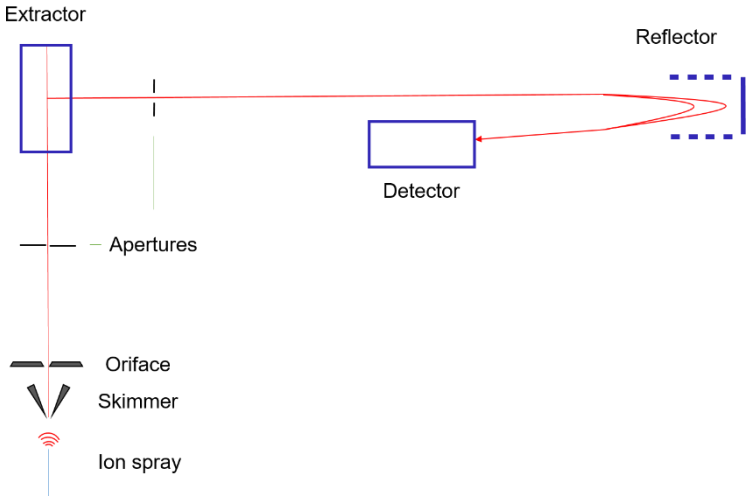

Figure 3-1: ALBATROS ESI-MS consists of a homemade nano-ESI source and a high resolution reflectron time-of-flight mass spectrometer.

The ion source is equipped with metal coated borosilicate spray capillaries with an inner tip diameter of 2 µm from New Objective Inc. (Woburn, MA, USA) known as nano electrospray emitters. The source can be operated in positive and negative ion mode. All results presented in this work were obtained in the positive ion mode. About 10 µL of the sample solutions are injected into the capillaries and a positive voltage of 2100 V is applied to the capillaries to generate the electrospray.

Under the influence of the high electric field (in this work 2 kV), positive ions move towards the surface of the liquid at the tip, whereas negative ions migrate away from the surface (Figure 3-2). Due to the mutual repulsion of positive charges at the liquid surface, the liquid surface is distorted and a so called 'TAYLOR cone' is formed [138, 139].

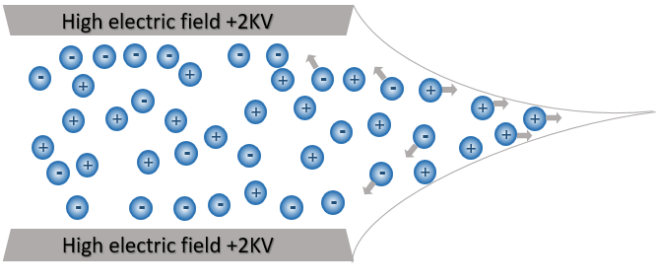

Figure 3-2: Schematic representation of the processes that are assumed to occur in electrospray of positive ion mode. The positive ions are enriched towards the surface of the liquid at the tip, whereas negative ions migrate away from the surface.

From this TAYLOR cone, small droplets are released and accelerated due to the high charge of the needle tip. As the droplet size decreases by solvent evaporation, the surface tension cannot compensate for the charge of the droplet any more at the "RAYLEIGH limit". Thus, the droplets undergo COULOMB explosions, leading to smaller charged droplets. These generated droplets undergo solvent evaporation, reach the Rayleigh limit and break into smaller droplets. After the charged droplet creation, the process keeps going, solvent evaporation and Coulomb explosions lead to a decrease of droplets size until droplets contain only one charge. This mechanisms of the formation of gas phase ions is the charged residue model (CRM) suggested by Dole [140, 141] and is shown in Figure 3-3. Alternatively to CRM, the ion evaporation model (IEM) of Iribarne and Thomson [142, 143] was suggested IEM assumes that when a droplet reaches the critical size and charge density, solvated ions desorb directly from the droplet surface. The major difference between these two models is how the final ions are produced, by solvent evaporation or by desorption. There is very strong evidence that small ions with radii of R ≤ 10 nm are produced by IEM. Macroions such as bio-macroions are more likely produced by CRM [144, 145].

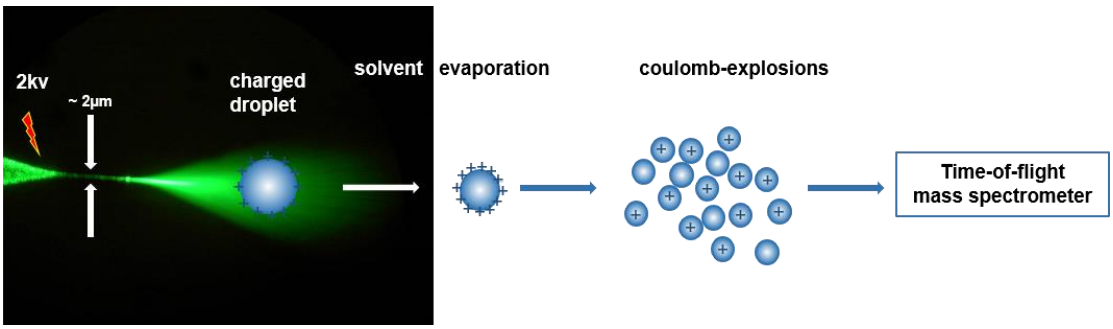

Figure 3-3: Charged residue model (CRM). Mechanism for the generation of gas phase ions. Charged droplets are generated through a controlled electrostatic spraying process. After the charged droplet creation, solvent evaporation and Coulomb explosions lead to a decrease of droplets size and droplets contain only one charge. In the spray, there may be present single ions, an ion with accompanying solvation, or bulk paired electrolyte species.

Sample flow of the ion source is approximately 20 nL/min (thus the name "*nano* ESI"). A static nitrogen pressure of < 0.5 bar is applied at the end of the capillary and adjusted according to the mass spectrometric signal in order to achieve a stable flow. In order to avoid fragmentation of the ionic species, the source is operated at low declustering conditions, that means, low curtain flow rate and a lower voltage setting between the orifice and skimmer [146]. The voltage between the sampling plate and the skimmer is very important as it provides a collision region. As the solvated metal ion is entering into this region, the electric field will lead to loss of some solvent ligands. This is commonly referred to as collisionally induced dissociation (CID) [147]. In this work, a nitrogen gas curtain flow rate of < 0.1 L min^{-1} at room temperature is used. The sampling plate voltage is kept at 42 V. This choice of parameters ensure that the detected molecules remain in droplets of some 10-30 water molecules. The addition of organic solvents such as methanol, often used in ESI-MS investigations to reduce the surface tension, is strictly avoided in the present work, in order to not alter the solution compositions.

After passing differential pumping stages, the ions are injected orthogonally into the time-of-flight mass-spectrometer. The time-of-flight mass-analyzer has a maximum resolution of m/Δm = 30000. In order to increase the sensitivity, the instrument is typically operated at m/Δm = 15000 in the present work, still providing isobaric resolution. During the whole measurement process, the ions remain in a small solvent shell of water molecules.

The ions with small solvent shell are separated by their mass to charge ratio (m/q) in the time-of-flight mass spectrometer (TOF). With this technique ions with mass m and total charge $q = ze$ are accelerated by a potential V_s, and afterwards drift in a free-field region (Drift region in Figure 3-4) to the detector. After acceleration all ions have acquired the same kinetic energy E_k (equak to the electric energy E_e)

$$E_k = \frac{mv^2}{2} = qV_S = zeV_S = E_e.$$

Ions of different masses m need the time *t* to drift over the distance L to the detector according to their velocities *v.* The velocity v is proportional to the m/q value of the ion, so that by measuring the time of flight, one can calculate this value.

$$v = \sqrt{\frac{2zeV_S}{m}}$$

$$t = \frac{L}{v}$$

As a continuous ion beam is generated in the ESI source, the ions cannot be directly transferred into the time of flight region, as for the measurement of the time of flight a defined starting point is needed. Thus, ion packages are pulsed from this ion beam by the orthogonal injection method into the drift region. The acceleration of the ions into the drift region is performed by the WILEY-MCLAREN-Focus method. This reduces the kinetic energy spread among ions with the same m/q ratio leaving the source, by a two-step acceleration (see Figure 3-4 region 2s). In this so called delayed pulsed extraction mode, the extraction pulse applied after a certain delay transmits more energy to the ions which remained for a longer time in the source. Consequently, the initially less energetic ions receive more kinetic energy and join the initially more energetic ions at the detector [148]. This method improves the resolution of the TOF-MS.

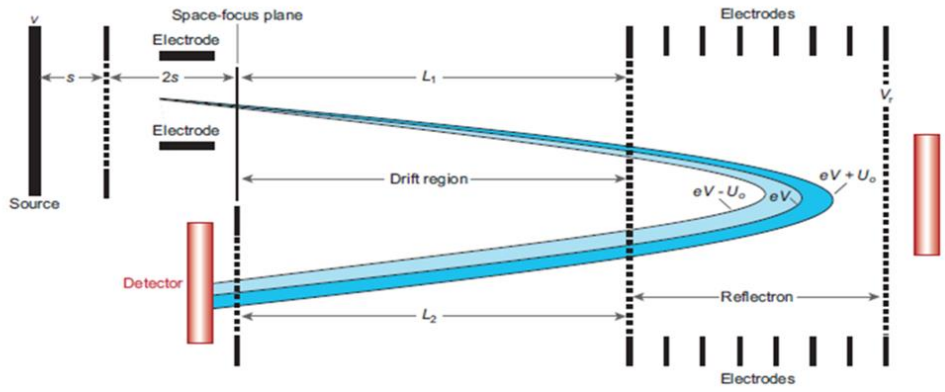

Figure 3-4: Schematic drawing of a reflectron time-of-flight mass spectrometer (TOF)[149]. Ions with higher kinetic energy and hence with more velocity will penetrate the reflectron more deeply than ions with lower kinetic energy. The faster ions will spend more time in the reflectron and will reach the detector at the same time than slower ions with the same m/q.

Another possibility to improve mass resolution is to use an electrostatic reflector (reflectron). This device corrects the kinetic energy dispersion of the ions leaving the source with the same m/q ratio. As shown in Figure 3-4, the reflectron is situated behind the drift region and increases the flight path without increasing the dimensions of the mass spectrometer. Ions with the same m/q, but higher kinetic energy (and hence with higher velocity) penetrate the reflectron more deeply than ions with lower kinetic energy. Consequently, the faster ions will travel a longer trajectory, spend more time in the reflectron and will be delayed with respect to slower ions. As a net result, slow and fast ions of equal m/q reach the detector simultaneously, correcting the kinetic energy dispersion of the ions leaving the source. Eventually, the mass resolution is increased [148].

3.2 Fitting routine and calculation of relative abundance

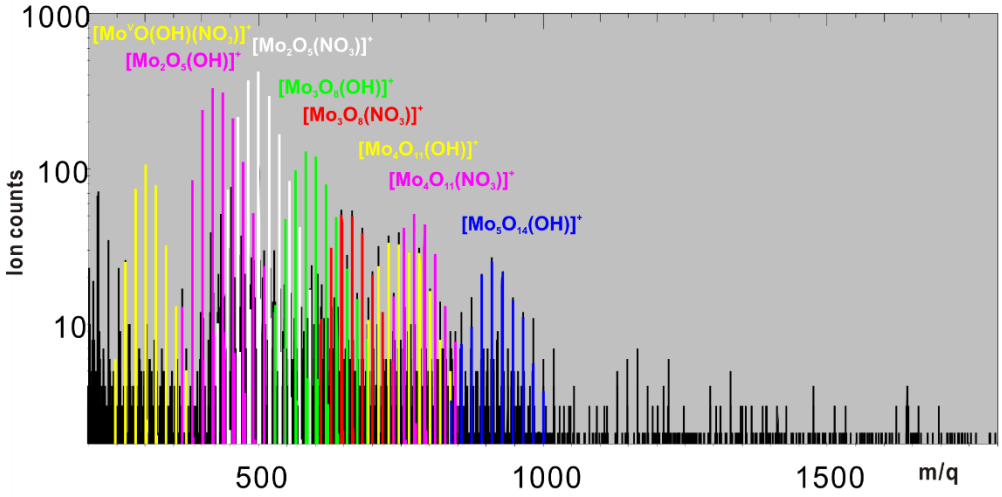

Figure 3-5: Part of an ESI-MS spectrum (m/q region 200-1800) of sample **M1** with [^{98}Mo] = 10.0 mmol/L, [HNO_3] = 3 mol/L.

Sample **M1** (Figure 3-5) is used here exemplarily to illustrate the composition and interpretation of ESI-MS spectra: the ionic counts are plotted versus the mass-divided by charge ratio. A logarithmic representation of the y-axis was chosen due to the large difference in abundance of the various species. Minor species will therefore be visualized easily. The data are plotted in black, the fits to the data indicating individual species are plotted as colored lines. The fits are calculated by a homebuilt C++ fitting routine taking into account isotope distributions and mass resolution of the time-of-flight analyzer. The spectra evaluation is performed as described in [29]. Since the peaks observed at m/q < 200 are not attributed to Mo species, they are not shown in Figure 3-5. At m/q > 1800 almost no species are detected. During the ESI-MS measurement the solution species remain in small water droplets, the number n of the H_2O molecules varies between 0 to 40. Thus, each species gives rise to formation of a peak cluster rather than one single line in the spectrum. As mentioned the fitting routine fits all possible combinations, in this system $[(Mo)_x(O)_y(OH)_z(NO_3)_{6x-2y-z-q'}]^{q'}\cdot nH_2O$ with x = 1 to 13, q' = 1 or 2, y = 0 to (6x-z-q'), z = 0 to (6x-y-q') and n = 0 to 40, to the data.

The peak clusters of equal color reflect the shell of water molecules around one sort of ionic species. For each species, the peak areas of all isotope combinations and all different numbers of water molecules n are summed up, giving a total number of ions:

$$N\left[Mo_xO_y(OH)_z(NO_3)_{6x-2y-z-q'}\right]^{q'} = \sum_n N\left[Mo_xO_y(OH)_z(NO_3)_{6x-2y-z-q'}\right]^{q'} \cdot nH_2O.$$

The percentage of one species with respect to all detected species is the relative abundance of this species in the sample. In this work, for the sake of simplicity, the water molecules are omitted in the following sum formulas of species.

3.3 ESI-TOF artefacts

ESI-MS is a technique which can be used for detection, identification and possible quantification of a number of species in equilibrium, whose distribution depends on the pH and the stoichiometric concentrations, among other factors. This technique has been used successfully and increasingly in a variety of fields of inorganic, organometallic, analytical and environmental chemistry. Some issues that need to be considered arise (will be discussed in detail in this section) in the practical application of ESI-MS, however, when the results are compared with data obtained by other methods. Particularly when used in conjunction with other speciation techniques the major advantages of ESI MS led to a growing number of works dedicated to its use for the study of solution equilibria in different branches of chemistry and biology. [27, 150]

An intriguing question of ESI, however, is to what extent the ions observed in ESI mass spectra represent the species present in solution. Some issues that need to be considered arise in the practical application of ESI-MS, artefacts can be generated during analysis process. The main factors that can generate artefacts are possible disturbances of the equilibrium conditions during ionization and the possibility of gas phase reactions that may occur before reaching the analyzer.

The correlation between the ions detected in the gas phase by ESI-MS and the species present in solution is controversially discussed in the literature. Schröder gives an overview about this in reference [151]. Many publications address artefacts-ion formation in ESI process, which can hamper quantitative and qualitative determinations [152]. However, many publications described, that ESI does not generally create ions, more it tends to facilitate the transfer of pre-existing solutions ions to the gas phase. Stewart examined a lanthanum nitrate solution in methanol under different conditions for the voltage between the sampling plate and the skimmer [147]. Under relatively gentle conditions (skimmer potential), lanthanum is observed in oxidation state 3+, as was originally present in solution. There are three main distributions of ion species observable $La(OH)(H_2O)_x^{2+}$, $La(OCH_3)(H_2O)_y^{2+}$ and

$La(NO_3)(H_2O)_z^{2+}$. The species observed are surrounded by water molecules. As the skimmer potential increases, the conditions between orifice and skimmer get harsher. As a consequence, the mean number of water molecules attached to the species (H_2O = 2) decreases. At higher m/q range $La(OH)_2^+$ is observed as the small number of solvating molecules are no longer able to stabilize the 2+ charge completely. As the voltage continues to increase the trend is either to doubly-charge-reduce species by coordination of two OH^- ions forming $La(OH)_2^+$ or lose further ligands to give the bare molecular $La(OH)^{2+}$ or $La(OCH_3)^{2+}$ species. Hence the $La(OH)_2^+$ species undergo a loss of protons due to the collisions with the gas molecules in the orifice skimmer region. This leads to the formation of LaO^+ species and at even higher potentials a loss of hydroxide molecules leading to the formation of La^{2+} species. The formation of these artefacts depending on the settings of the transfer region of the ions from ambient conditions to the vacuum is commonly referred to as collision induced dissociation (CID).

$$La(OH)(H_2O)^{2+} \rightarrow La(OH)^{2+} + H_2O$$

$$La(OH)^{2+} \rightarrow LaO^+ + H^+$$

$$\rightarrow La^{2+} + OH$$

$$La(OH)_2{}^+ \rightarrow LaO^+ + H_2O$$

$$LaO^+ \rightarrow La^+ + O$$

These effects however only occur when rather harsh declustering conditions are chosen, that the metal cations have low ligand (about 2 water) number. The example emphasizes the point that the type of ions observed is dependent on the sampling conditions and parameters [147]. Another method that has been used by several groups is to complex the metal ion with stabilizing ligands in order to avoid reaction during ionization and ensure a stable spray to maximize the information obtained.

4 Pure Mo-powder and Mo-pellet system

In order to work as closely to the acid concentration conditions of fuel reprocessing as possible and at the same time use a feasible acid range for nano ESI-MS measurements, ^{98}Mo metal powder in three different acid strength 0.5 to 3 mol/L nitric acid were measured.

Additionally, the kinetics of Mo-Pellet dissolution in 1 mol/L nitric acid and the variation of Mo species during dissolution processes were investigated.

4.1 ^{98}Mo-powder

4.1.1 ^{98}Mo-sample preparation

Since there are seven naturally occurring Mo isotopes, ion count intensities in mass spectrometric measurements will be dispersed over all isotopes. In order to achieve larger signal intensities during the very time consuming measurements by ESI-MS at the high acid concentrations used for this investigation, isotopically enriched ^{98}Mo is used in the present work.

Three ^{98}Mo metal powder samples (**M1**, **M2**, **M3**) and three $^{98}MoO_3$ oxide powder samples (**O1**, **O2**, **O3**) were measured. The concentration of ^{98}Mo and $^{98}MoO_3$ remains around 10 mmol/L, isotopically pure ^{98}Mo metal powder (> 98% ^{98}Mo) and isotopically pure $^{98}MoO_3$ powder were purchased from STB Isotope GmbH, Hamburg, Germany. 3 mol/L, 1 mol/L and 0.5 mol/L nitric acid stock solutions were prepared by dilution of appropriate amounts of HNO_3 (Merck, Darmstadt, Germany; 37%, analytical grade) with Milli-Q water. ^{98}Mo metal powder samples were prepared by dissolving appropriate amounts of ^{98}Mo in [HNO_3] = 3 mol/L, 1 mol/L and 0.5 mol/L, respectively. To reduce the time needed for the dissolution, the samples were stirred and heated in a water bath to 60ºC during the dissolution. The concentrations of Mo in fresh samples **M1**, **M2** and **M3** were not determined by ICP-MS, but rather calculated with weighted amount of ^{98}Mo metal powder and volume of nitric acid because of the completely dissolution of the powder. Sample **M3** was measured again after a time span of 258 days by use of *nano* ESI-MS, to see the changes of the Mo speciation over time. The concentration of dissolved Mo in aged sample **M3** was determined by ICP-MS. Using the same approach, $^{98}MoO_3$ samples **O1**, **O2** and **O3** were prepared in 3 mol/L, 1 mol/L and 0.5 mol/L nitric acid, respectively. Because $^{98}MoO_3$ powder did not completely dissolve in 0.5 mol/L nitric acid after 20 days, final concentrations of Mo in solutions were measured by ICP-MS respectively. The concentrations of the fresh samples are summarized in Table 4-1. All samples were prepared without the addition of any electrolyte in order to avoid clogging of the ESI needle tip.

Table 4-1: Mo concentrations in fresh samples **M1**, **M2** and **M3** are calculated: weighed amounts of the ^{98}Mo metal powder were dissolved in the nitric acid resulting in [^{98}Mo] = 10 mmol/L. Mo concentrations in samples **O1**, **O2** and **O3** were determined by ICP-MS.

Sample	Sample ID	[HNO_3] mol/L	[$_{98}$Mo] mmol/L
^{98}Mo metal	**M1**	3	10.0
	M2	1	10.0
	M3	0.5	10.0
	aged M3	0.5	10.7
$^{98}MoO_3$	**O1**	3	12.8
	O2	1	12.8
	O3	0.5	11.0

4.1.2 Results of ^{98}Mo metal, $^{98}MoO_3$ oxide powder samples and discussion

At first, we will begin with the samples prepared from ^{98}Mo metal powder (**M1**, **M2**, **M3** and aged **M3**). In order to check the influence of the acid concentration on the species distribution, 3 different concentrations nitric acid 3 mol/L, 1 mol/L and 0.5 mol/L are investigated. ^{98}Mo metal powder was complete dissolved in nitric acid, respectively. The ^{98}Mo concentration in the samples was 10 mmol/L (concentrations are calculated weight per volume).

General features of the ESI-MS spectra have been discussed exemplarily using the spectrum of sample **M1** containing [^{98}Mo] = 10.0 mmol/L in 3 mol/L nitric acid plotted in chapter 3.2 Figure 3-5. In the spectrum, eight peak-clusters marked with different colors were identified in the mass region of m/q 200-1800. That means eight species are distinctly observed in sample **M1**. For an overview, the detected species and their relative abundances are summarized in Table 4-2. Different Mo species $[(Mo)_x(O)_y(OH)_z(NO_3)_{6x-2y-z-q'}]^{q'}\cdot nH_2O$ with x = 1-7 are present in sample **M1** solution. The species range from the mononuclear complex (containing one Mo(VI) ion and called monomers), dinuclear complexes (containing two Mo(VI) ion and called dimers) to pentamers (containing five Mo(VI) ions). Two types of dimeric, two types of trimeric and two types of tetrameric species distinctly observed respectively. For dimeric species, one with a hydroxide ion $[Mo_2O_5(OH)]^+$ (magenta, + 4 ~ 14 H_2O, m/q = 365 ~ 545, relative abundance 22.9%), and another with a nitrate anion: $[Mo_2O_5(NO_3)]^+$ (white, + 4 ~ 14 H_2O, m/q = 410 ~ 590, relative abundance 29.6%) are detected. Trimerics $[Mo_3O_8(OH)]^+$ (green, + 5 ~ 14 H_2O, m/q = 528 ~ 690, relative abundance 16%), $[Mo_3O_8(NO_3)]^+$ (red, + 7 ~ 14 H_2O, m/q = 609 ~ 735, relative abundance 6.3%), tetramerics $[Mo_4O_{11}(OH)]^+$ (yellow, + 6 ~ 14 H_2O, m/q = 692 ~ 836, relative abundance 7.6%), $[Mo_4O_{11}(NO_3)]^+$ (magenta, + 6 ~ 12 H_2O, m/q = 737 ~ 845, relative abundance 8.3%) and pentameric $[Mo_5O_{14}(OH)]^+$ (blue, + 6 ~ 15 H_2O, m/q = 838 ~ 1000, relative abundance 6.7%) are detected. A small fraction of a heptameric species $[Mo_7O_{20}(OH)]^+$ is present (m/q = 1022, with a relative abundance of about 3.8% with respect to the total amount of Mo present in the solution).

The low intensity of the peak does not allow fitting to the data, therefore, it is not included in the relative abundance calculation and not being plotted as colored lines in the spectrum.

It is noteworthy that there is no cationic hexameric Mo-species detected in sample **M1**. This is also true for other two sample **M2** and **M3** and all other ESI-MS measurements of samples containing Mo, which we performed in this work. The ESI-MS spectra of these samples (**M2** and **M3**) are depicted in Figure 4-1 top and Figure 4-1 middle, respectively. In Figure 4-2 illustrates the relative abundance of different monomeric or polymeric species in sample **M1**, **M2** and **M3**. There are two possibilities for the absence of hexameric Mo species in the spectra. One possibility would be that no cationic hexameric species are present in solution at the conditions of present investigation. Or there might be a favorable configuration for *neutral* hexamers, which cannot be detected by ESI-MS, a technique which only transfers ions from the solution into the gas phase.

Besides stable Mo (VI) species, a fraction of molybdenum in the oxidation state +V is observed in the spectrum. In sample **M1**, one Mo (V) species $[MoO(OH)(NO_3)]^+$ is detected, plotted in yellow (+ 4 ~ 9 H_2O, m/q = 265 ~ 355, relative abundance 2.5%).

Our results show, that no monomeric Mo species is detected in the system with a nitric acid concentration of 3 mol/L. As can be seen in Figure 2-2, a dominance of the dimeric Mo species is to be expected. The distribution diagram shows the calculated species abundances for a molybdenum concentration of 10 mmol/L. The relative abundance of dimeric Mo species decreases with increasing pH in the pH range 0 – 1.5. The most abundant Mo species detected by ESI-MS is the Mo dimer with a total relative abundance of 52.5% ($[Mo_2O_5(OH)]^+$ 22.9% and $[Mo_2O_5(NO_3)]^+$ 29.6%). According to Cruywagen [43, 62] the doubly charged dimeric species $[Mo_2O_5]^{2+}$ should be the domination species. The structure of the Mo dimer was described as two cis-dioxo-molybdenum moieties that are bridged by an oxygen atom [24]. As previously mentioned, two types of dimeric Molybdenum species appear in the ESI-MS spectra, one with hydroxide ion $[Mo_2O_5(OH)]^+$, one with nitrate anion $[Mo_2O_5(NO_3)]^+$, instead of the doubly charged dimeric species $[Mo_2O_5]^{2+}$. The thermodynamic date would suggest the formation of hydroxide dimeric species $[Mo_2O_5(OH)]^+$ only at lower acid concentrations and to a much lesser extent. The appearance of the hydroxide ion could be due to a charge compensation effect as described in the literature [153-155]. In the ESI process due to the droplet shrinkage and the loss of water molecules a hydrolysis reaction sets in the shrinking droplets, leading to a formation of metal cation hydroxides and protons (see equation below). The protons, or hydronium ions are then repulsed from the cationic species and eventually end up in another droplet in the secondary droplet formation processes. Similar species have been observed by our group before, such as by the measurement of Th [46], Zr [29].

$$M^{2+}(H_2O)_x = MOH^+(H_2O)_{x-2} + H_3O^+$$

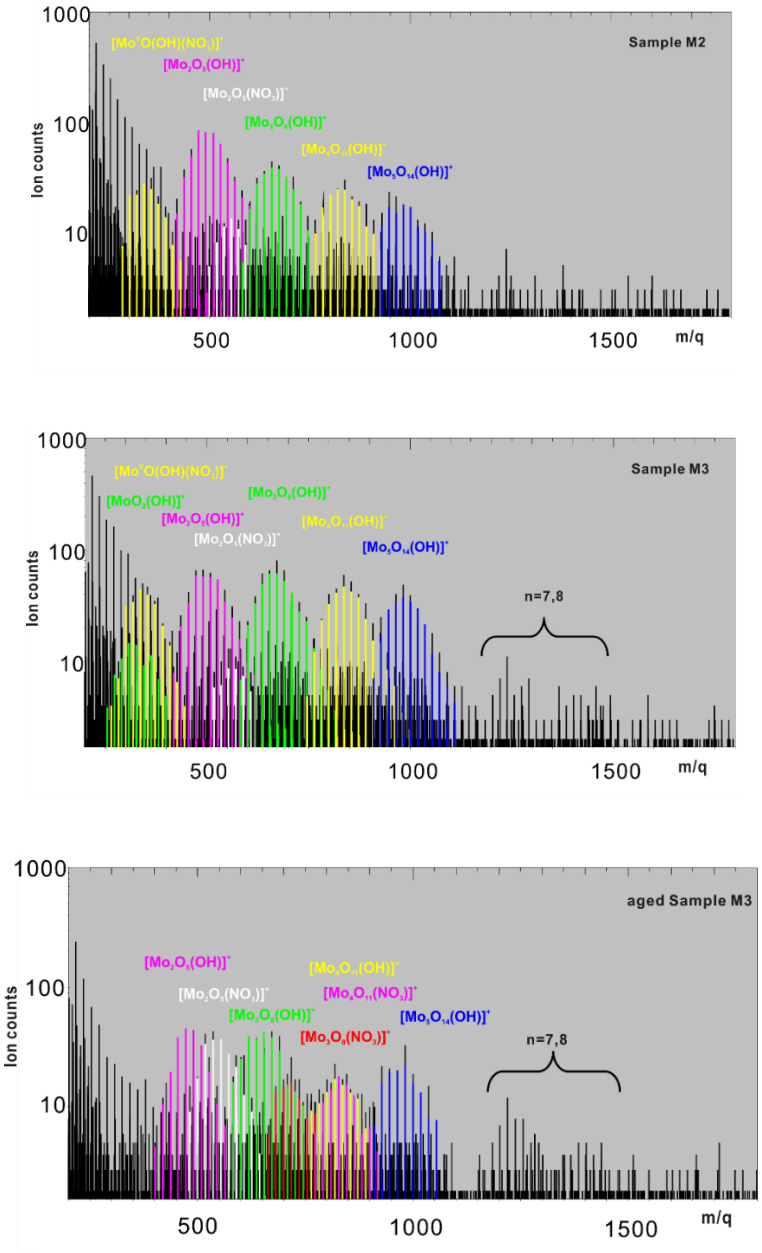

Figure 4-1: ESI-MS spectrum of samples **M2**, **M3** and aged **M3**. In the spectra, each peak cluster represents a species, which is detected in the sample solution. $[Mo^{V}O(OH)(NO_3)]^+$ (yellow), $[MoO_2(OH)]^+$ (green), $[Mo_2O_5(OH)]^+$ (magenta), $[Mo_2O_5(NO_3)]^+$ (white), $[Mo_3O_8(OH)]^+$ (green), $[Mo_3O_8(NO_3)]^+$ (red), $[Mo_4O_{11}(OH)]^+$ (yellow), $[Mo_4O_{11}(NO_3)]^+$ (magenta), $[Mo_5O_{14}(OH)]^+$ (blue). TOP: Spectrum of sample **M2** with $[^{98}Mo]$ = 10.0 mmol/L, $[HNO_3]$ = 1 mol/L. Five Mo(VI) species and one Mo(V) species are detected. MIDDLE: Spectrum of sample **M3** with $[^{98}Mo]$ = 10.0 mmol/L, $[HNO_3]$ = 0.5 mol/L. Six Mo(VI) species and one Mo(V) species are detected. BOTTOM: Spectrum of **M3** measured after 258 days. Compared to the fresh sample **M3**, no Mo(V) signal and no Mo(VI) monomers are detected. The Mo(V) species seem to have been oxidized with time. The relative abundances of the other Mo(VI) species do not change considerably.

Table 4-2: Relative abundance of species in sample **M1**, **M2**, **M3** and aged **M3**. **M1** with [^{98}Mo] = 10.0 mmol/L, [HNO_3] = 3 mol/L **M2** with [^{98}Mo] = 10.0 mmol/L, [HNO_3] = 1 mol/L, **M3** with [^{98}Mo] = 10.0 mmol/L, [HNO_3] = 0.5 mol/L

species	**Sum formula**	**m/q**	**relative abundance in%**			
			Sample M1 [HNO_3] = 3 mol/L	**Sample M2** [HNO_3] = 1 mol/L	**Sample M3** [HNO_3] = 0.5 mol/L	**Sample aged M3** [HNO_3] = 0.5 mol/L
Mo(V) monomers	$[Mo^{V}O(OH)(NO_3)]^+$	192.91	2.5	3.9	3.8	
Monomers	$[MoO_2(OH)]^+$	146.91			1.3	
Dimers	$[Mo_2O_5(OH)]^+$	292.81	22.9	29.9	13.7	12.8
	$[Mo_2O_5(NO_3)]^+$	337.81	29.6	3.3	1.5	11.6
Trimers	$[Mo_3O_8(OH)]^+$	438.71	16.0	22.6	24.3	23.1
	$[Mo_3O_8(NO_3)]^+$	483.71	6.3			7.0
Tetramers	$[Mo_4O_{11}(OH)]^+$	584.62	7.6	21.5	27.5	12.2
	$[Mo_4O_{11}(NO_3)]^+$	629.61	8.3			11.7
Pentamers	$[Mo_5O_{14}(OH)]^+$	730.52	6.7	18.8	27.9	21.6

The formation of nitrato complexes of Mo dimeric $[Mo_2O_5]^{2+}$ have not been reported before, while nitrato complexes of monomeric molybdyl-ions have been reported in the literature [72-74]. The formation of $[MoO_2(NO_3)_i]^{(2-i)+}$ (with i = 1-2) species was proposed to start from nitric acid concentrations exceeding 0.05 mol/L [72, 74].

In order to check the influence of the acid concentration on the species distribution, nitric acid concentration is decreased to 1 mol/L (samples **M2**) and 0.5 mol/L (samples **M3**. Different species distributions are observed in the other two acid concentrations. The relative abundance of dimers (including hydroxide species and nitrate species) decreases with decreasing nitric acid concentration, until it is no longer the domination species. In Sample **M3** only a total of 2% dimer is detected, whereas the pentamers $[Mo_5O_{14}(OH)]^+$ become dominant with a relative abundance of 27.9%. At lower acid concentration, the tendency towards formation of (larger) polymeric species increases. In sample **M2** more large polymeric species form than in sample **M1**. Thus, the trend towards a formation of dimeric Mo species at high acidic strength is in good agreement also with earlier findings. Cruywagen suggested that Mo has a strong tendency to form dimers at high acid concentration and high Mo concentration $[Mo]_{aq} > 10^{-3}$ mmol/L [45, 62]. Trimeric $[Mo_3O_8(OH)]^+$ (green, m/q = 438.71), $[Mo_3O_8(NO_3)]^+$ (red, m/q = 483.70), tetrameric $[Mo_4O_{11}(OH)]^+$ (yellow, m/q = 584.62) $[Mo_4O_{11}(NO_3)]^+$ (magenta, m/q = 629.61) and pentameric $[Mo_5O_{14}(OH)]^+$ (blue, m/q = 730.52) species are detected in all of the three samples. In sample **M3**, there are small fractions of heptameric and octameric species $[[Mo_7O_{20}(OH)]^+$ and $[[Mo_8O_{23}(OH)]^+$, but both of these peaks are too low to fit the data well enough. They are therefore not counted in the relative abundance calculation. These species might be the "large" cationic molybdenum species in solution, which were described by Dement'ev et al [24], Coddington *et al.* [53] and Ng *et al.* [52] before. As described by Dement'ev et al, a formation of trimeric species was hypothesized or could at least not be excluded. From both studies [52, 53] either information on the sum formulas nor structures of the species could be determined. The applied methods also average over all species simultaneously, but the authors have seen strong evidence that polymeric species larger than the dimers are involved. Coddington *et al.* investigated a Molybdenum(VI) solution in $[HNO_3]$ = 6.0 mol/L by applying nuclear magnetic resonance (NMR) and Raman spectroscopy. The Raman spectroscopy bands at 952 cm^{-1} and 925 cm^{-1} attributable to ν_{sym}(Mo-O) and ν_{asym}(Mo-O) respectively, and the band at 830 cm^{-1} suggests an oxo-bridged structure ν(Mo-O-Mo), so the authors suggest these are cationic *cis*-dioxomolybdenum polymers with octahedrally coordinated molybdenum [53].There are very broad resonances in the ^{95}Mo-NMR spectra, which were explained due to existence of equilibria between the various polymeric molybdenyl ions. By use of Raman spectroscopy and light scatting Ng *et al.* suggested, that below the isoelectric point of molybdic acid (pH 0.9), there is a polymeric species (possibly positively charged) with an average molecular weight 2500 existing in very acidic solution [52].

The complex $[Mo_2O_5(H_2O)_6]^+$ has a formula weight of 380, hence if this species is present in the acid, as the Raman spectra of Coddington [53] suggest, it must be accompanied by high-molecular-weight material. Our ESI results show, that more large polymeric species are formed in the HNO_3 solutions at high pH range. The molecular weight 2500 is measured at pH 0.8 [52], the pH value is higher than the one of sample **M3** (about pH 0.3, maximum molecular-weight about 1022). At pH 0.8 more large polymeric Mo species are estimated to be formed.

Comparing three samples (**M1**, **M2** and **M3**), the proportion of nitrate species $[Mo_2O_5(NO_3)]^+$ is increased with increasing concentration of nitric acid (from 0.5 mol/L to 3 mol/L), and the proportion of hydroxide species $[Mo_2O_5(OH)]^+$ thereby decreases. A third dimeric species $[Mo_2O_4(OH)(H_2O)_6]^{3+}$ [61, 62], due to the protonation of $[Mo_2O_5]^{2+}$, is not observed in this work.

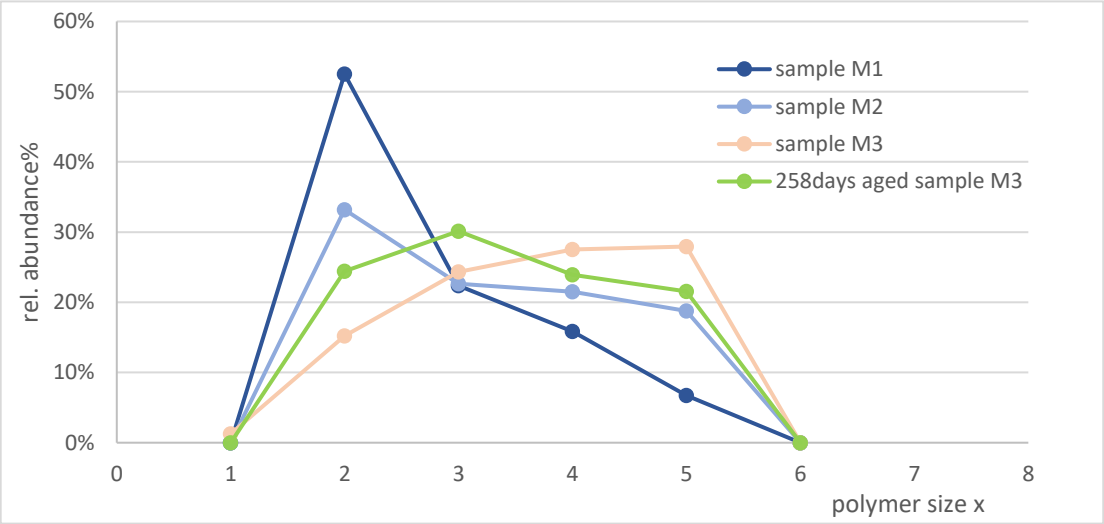

Figure 4-2: Relative species abundance of the samples **M1** with [^{98}Mo] = 10.0 mmol/L, [HNO_3] = 3 mol/L, samples **M2** with [^{98}Mo] = 10.0 mmol/L, [HNO_3] = 1 mol/L, samples **M3** with [^{98}Mo] = 10.0 mmol/L, [HNO_3] = 0.5 mol/L and sample **M3** after 258 days.

ESI results show, only one hexavalent monomer $[MoO_2(OH)]^+$ is detected in these three samples. Mononuclear Mo(VI) complexes referred to by Dement'ev [24], contain two short Mo=O bonds in the *cis* position in strongly acidic media. The previously published results suggested that the monomer $[MoO_2(OH)]^+$ has a relative abundance about 80% ~ 90% at a very low molybdenum concentration ($2.5 \cdot 10^{-5}$ mol/L) in a perchloric acid concentration range from 0.5 mol/L to 3mol/L [44, 45]. The monomer plotted in green in Figure 4-1 middle spectrum has only 1.3% relative abundance in the fresh sample **M3**. It seems to play a subordinate role in the system with the Mo concentration of 10 mmol/L. In order to see, whether the species change with time, the sample **M3** was measured after a timespan of eight months. The monomer $[MoO_2(OH)]^+$ seems to be unstable in the solution, that would not be detected after eight months.

A fraction of molybdenum in the oxidation state +V $[MoO(OH)(NO_3)]^+$ (plotted in yellow) is also detected in sample **M2** and **M3** just as in sample **M1**. The relative abundances are also very small (2.5% in sample **M1**, 3.9% in sample **M2** and 3.8% in sample **M3**). There is no significant change in the relative abundance trends. Mo(V) species were stabilized by Jalilehvand *et al.* in HCl medium [75]. Paffet *et al.* also described the presence of monomeric Mo(V) species in 1 to 2 mol/L trifluoromethanesulfonic acid [60]. The species seems to exhibit the Mo=O moiety typical for Mo(V) species [24, 75]. Dimeric Mo(V) species, which were reported before [24, 156], were not detected in our ESI-MS spectra. However, the reason for the appearance of Mo(V) species is unclear. It might be an intermediate product of the oxidation process of Mo from metal (oxidation state 0) towards the oxidation state VI. This explanation seemed to be corroborated the measurements after eight months **aged M3** (spectrum see Figure 4-1 bottom). No Mo(V) signal can be observed in the spectrum of **aged M3**. To further confirm this explanation, solutions prepared from $^{98}MoO_3$ instead of ^{98}Mo metal are measured, which has the initial oxidation state VI. Three $^{98}MoO_3$ samples **O1**, **O2** and **O3** are measured. $^{98}MoO_3$ concentrations remain around 10 mmol/L in 3 mol/L, 1 mol/L and 0.5 mol/L nitric acid, respectively (concentration see Table 4-1). The spectra are shown in Figure 4-3 top **O1**, middle **O2** and bottom **O3**, respectively. As can be seen in the spectra, Mo(V) species are present in samples with 3 mol/L (**O1**) and 1 mol/L (**O2**) nitric acid (rel. abundance between 0.4 - 6.3%), so that the explanation of intermediate product of the oxidation process does not hold.

Another possibility is that Mo(V) is not present in the solution, but rather forms in the ESI process. An apparent reduction of metal cations due to the ESI process has been reported before by Stewart and Horlick [147], which is describe in chapter 3.3. Moulin *et al.* [157] and Galindo *et al.* [158] have observed in their ESI-MS study a reduced form of UO_2^+ (pentavalent) in uranyl solutions (hexavalent). The proposed mechanism is reduction of uranyl when all water molecules around the uranium have been removed. In the study Moulin [157] confirmed, that the increase of voltage between orifice and skimmer causes fragmentation of the uranyl, and reduction of UO_2^{2+}. In contrast, Steppert *et al.* did not measure any reduced species [159], when hexavalent uranium solutions at pH values from 3 to 5.3, were measured by ESI MS. However, in the latter study, the parameters were chosen in a way that the detected molecules remained in droplets of some 10–30 water molecules. These parameters should also avoid CID processes.

In our measurement, we chose the settings in a way, that a water shell of 4-21 water molecules remains around the species, this makes a CID process for the reduction of the metal cation rather unlikely. However, although the Mo(V) species is embedded in droplets of 4-10 water molecules, the reduced form of Mo is observed nevertheless.

Our study reveals, that the system of Mo species in acidic solutions might be much more complicated, than one would expect from the data in the literature. In order to investigate the Mo polymeric and Mo(V) species formed during the dissolution and gain a closer insight into the dissolution steps the dissolution of a ^{98}Mo-pellet in 1 mol/L nitric acid was studied.

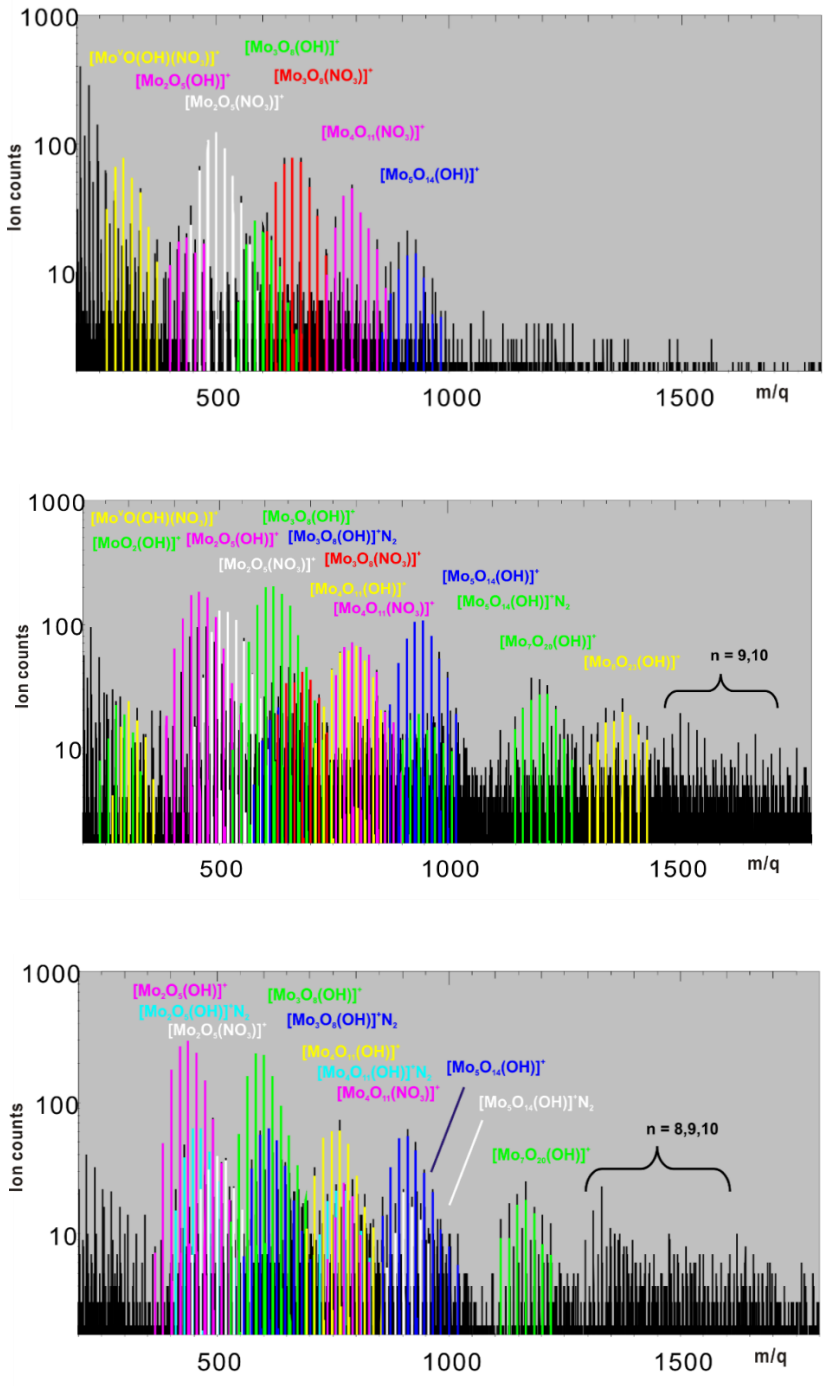

Figure 4-3: ESI-MS spectrum of sample **O1**, **O2**, and **O3**. TOP: Spectrum of sample **O1** with $[^{98}MoO_3]$ = 10.0 mmol/L, $[HNO_3]$ = 3 mol/L. MIDDLE: Spectrum of sample **O2** with $[^{98}MoO_3]$ = 10.0 mmol/L, $[HNO_3]$ = 1 mol/L. BOTTOM: Spectrum of sample **O3** with $[^{98}MoO_3]$ = 10.0 mmol/L, $[HNO_3]$ = 0.5 mol/L. Mo(V) $[MoO(OH)(NO_3)]^+$ species are detected in sample **O1** (6.3%) and **O2** (0.4%).

4.2 ^{98}Mo-pellet

The ^{98}Mo-pellet dissolution is performed in 1 mol/L nitric acid and the solutions species are measured during the dissolutions of the pellet by use of *nano* ESI-MS.

4.2.1 Sample preparation

The ^{98}Mo-pellet sample was made by our project partner Forschungszentrum Jülich. Isotopically pure ^{98}Mo metal powder (STB Isotope GmbH, Hamburg, Germany) was compacted at a pressure of 640 MPa using a cold uniaxial press. The pellet was then sintered under argon atmosphere. During a first heating period, the pellet was heated to 500 °C within 2.5 h and this temperature was kept stable for 2 h. The pellet was then further heated to 1600 °C within 5.5 h and sintered at this temperature for 5 h. The dissolution of the pellet and Mo-speciation were studied in our lab. The ^{98}Mo-pellet was placed in 1 mol/L nitric acid. The complete dissolution of the pellet took place within 10 days, the concentrations of the supernatant were measured by ESI-MS after 3, 5, 6, 10 and 461 days after the pellet was placed into the nitric acid. These samples are labelled **P1** through **P5.** The molybdenum concentration of the supernatant was determined by ICP-MS as a function of time during the dissolution process and is summarized in Table 4-3.

Table 4-3: Mo concentrations in samples **P1** to **P5**. The molybdenum concentration of the supernatant was determined by ICP-MS after the pellet placed into the nitric acid.

Sample	Sample ID	time intervals	[^{98}Mo] mmol/L
^{98}Mo pellet	**P1**	3 days	2.4
	P2	5 days	7.6
	P3	6 days	11.4
	P4	10 days	19.7
	P5	461 days	19.3

4.2.2 Results and discussion

The concentration of ^{98}Mo in the nitric acid increases with time. After 3 days, sample **P1**, the ^{98}Mo-concentration reaches 2.4 mmol/L. After 10 days, sample **P4** the pellet seems fully dissolved and the concentration of ^{98}Mo is 19.7 mmol/L. The project partner Forschungszentrum Jülich measured the supernatant of ^{98}Mo-pellet sample after 6 months, the concentration of ^{98}Mo increases up to 22.7 mol/L [160]. After 461 days, the concentration decreases to 19.3 mmol/L. It seems like, the ^{98}Mo-pellet dissolved further after 10 days, the concentration of ^{98}Mo in supernatant increases after 6 months. Subsequently, the concentration decreases slightly, due to the solvent

evaporation over time. The samples were collected from the supernatant and measured by use of ESI-MS. Several trends can be seen in this measurement system.

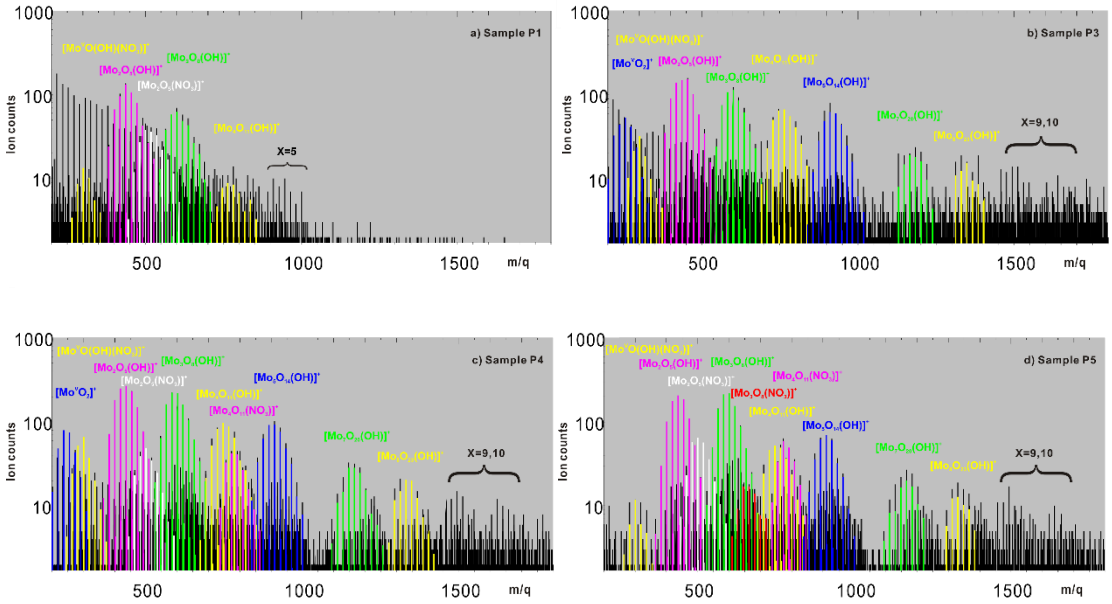

Figure 4-4: ESI-MS spectra taken from a solution containing 1 mol/L nitric acid during the dissolution of a ^{98}Mo pellet after various contact times. The concentrations of ^{98}Mo vary for the samples depicted. a): Sample **P1** taken after 3 days of contact time with a ^{98}Mo concentration of 2.4 mmol/L. Only a small number of different species are present in solution. The dimeric species $[Mo_2O_5(OH)]^+$ (m/q 292.81), relative abundance 41.5%), plotted in magenta is the dominating Mo-species. b): With increasing time and concentration ([^{98}Mo] = 11.4 mmol/L) more and more species are detected in sample **P3**. The dimeric species are not dominating the species distribution any more. c): **P4** After 10 days the pellet is fully dissolved, leading to a Mo concentration of 19.7 mmol/L. The abundances do not change considerably, but there is a slight tendency towards the formation of larger polymeric species. d): **P5** After 461 days, the relative abundances of the Mo polymers did not change significantly any more. The fraction of Mo(V) species has completely vanished and was obviously oxidized.

Figure 4-4 shows the ESI-MS spectra of supernatant solutions **P1**, **P3**, **P4** and **P5**. The spectrum of sample **P2** was omitted, as only little changes are detected in this spectrum. During the dissolution process of the Mo-pellet show that the Mo-dimer is the dominant species in the samples **P1** (Figure 4-4 a) at the beginning of the pellet dissolution (plotted in magenta, m/q 292.81, rel. abundance 41.5%), followed by the trimer $[Mo_3O_8(OH)]^+$ (green, m/q 438.72, rel. abundance 34.3%). Other species are only present to a much lesser extent. Pentameric species with the sum formula $[Mo_5O_{14}(OH)]^+$ give rise to a small signal in the m/q region 850-1000. Due to the low intensity of these peaks, we refrained from calculating the relative abundance of this species due to the poor statistics. The relative abundances of each detected Mo species in samples **P1** to **P5** are summarizes in Table 4-4. After 6 days, in sample **P3** when the Mo concentration reaches 11.4 mmol/L, trimers become the dominant species. This behaviour can be seen by comparison with ESI-MS spectra from sample **P1** to **P3**: With increasing concentration of Mo and increasing dissolution time, larger

polymeric species form. After a time interval of 6 days, in the spectrum of **P3**, when the Mo concentration reaches 11.4 mmol/L, more larger species $[Mo_xO_{3x-1}(OH)]^+$ with x = 3-10 and $[Mo_2O_5(NO_3)]^+$ are detected. The signal intensity of nonamers and decamers are rather low, so that due to the low statistics they were not considered for the relative abundance calculation. That means the species distribution becomes more complicated during dissolution of the pellet, due to the increasing Mo concentration. After 10 days, after the pellet was fully dissolved, the concentration of Mo reached 19.7 mol/L, decamers $[Mo_{10}O_{29}(OH)]^+$ are the largest detected species. No signal at the m/q region between 1020-1170 are detected in all the spectra, where a hexameric Mo species would be expected. The absence of hexameric Mo species has been discussed in chapter 4.1.2.. However, we can only speculate the reason about the absence of mass spectrometric signals for these species.

Figure 4-5 gives the comparison of the concentration of the different solution species correlated to the total concentration of the dissolved Mo after different time intervals. As can be seen in the distribution diagram of Figure 2-2, with the stability constant taken from [45, 62, 65], one would expect an abundance of the monomers $[MoO_2(OH)]^+$ of about 56% and for the dimers $[Mo_2O_5]^{2+}$ of about 36% at a Mo concentration of 2.4 mmol/L. The relative abundance of the trimeric species $[Mo_3O_8(OH)]^+$ increases with increasing Mo concentration in the solution, and larger species form with the dissolution of Mo pellet, where the thermodynamic model would predict a predominance of the dimeric Mo species $[Mo_2O_5]^{2+}$. Moreover, the relative abundances of the larger polymers like the heptameric and octameric species rises with increasing Mo concentration.

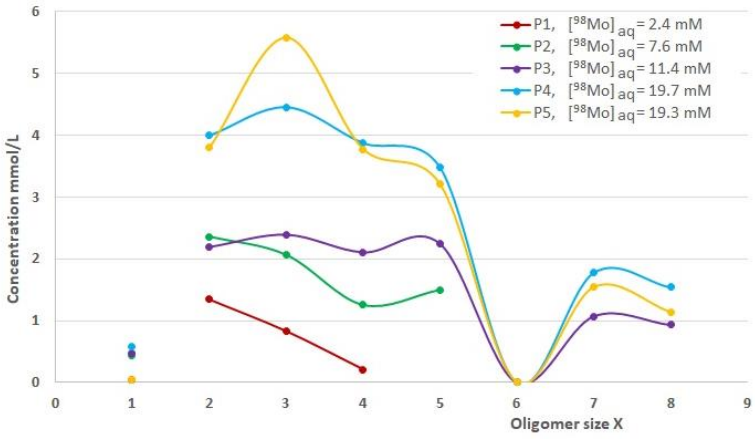

Figure 4-5: Concentration distribution of Mo species of the supernatant solutions during a Mo pellet dissolution. ^{98}Mo-pellet placed in 1 mol/L nitric acid. Different spectra were taken reflecting different contact times of the pellet. The plot shows that with increasing concentration of Mo and increasing dissolution time, larger polymeric species form. At concentrations >7.6 mmol/L the trimeric species $[Mo_3O_8(OH)]^+$ start to dominate the species distribution.

As in the case of metal powder samples, in addition to the Mo (VI) species, a small fraction of Mo (V) is observed in all pellet samples. Beside $[MoO(OH)(NO_3)]^+$, a second Mo(V) species with a sum formula of $[MoO_2]^+$ (blue, m/q 129.90) is observed in the spectra of samples **P2**, **P3** and **P4**. The relative abundances of the Mo(V) species vary in the different samples. In sample **P1** the Mo(V) species $[MoO(OH)(NO_3)]^+$ account for 1.5% of the total amount of Mo in solution. It increases to 5.7% in sample **P2** and then decreases again in samples **P3** and **P4**. In the aged sample for 461 days **P5** the Mo(V) species are nearly absent. This tendency seems to be a dependency of the contact time of the Mo pellet with the nitric acid on the amount of Mo(V) detected in the spectra. This could indicate a small fraction of Mo(V) present in solutions, which is oxidized to Mo(VI) over time. However, the presence of a small fraction of Mo(V) in solution prepared from MoO_3 contradicts this assumption. A formation of this species as an artefact due to the ESI process induces by collision induced dissociation processes is rather unlikely, as all the measurement are performed with the same settings of the orifice-skimmer region of the ESI-MS, leading to the same low declustering conditions. Thus, the variations of the Mo(V) signal in this measurement series cannot be explained by this mechanism and seems to be related with species actually present in fresh solution.

4.3 Conclusions

By use of ESI-MS the sum formulas and relative abundances of many molybdenum solution species can be investigated at the same time, even if the system of aqua molybdenum is rather complicated. For molybdenum, the tendency towards the predominant formation of dimeric species at high acid concentrations are in agreement with the calculations from the formation constants [52, 62]. Furthermore, the results indicate that the polymerization of molybdenum is enhanced as the acid concentration decreases, which is in good agreement with the findings of Ng *et al.* and Coddington *et al.* [52, 53], who described these phenomena before, without being able to characterize the solution species and their sum formulas.

The measurement during the dissolutions of the pellet shows that the relative abundance of the trimeric species increases with increasing Mo concentration in the solution, and larger species form with the dissolution of the Mo pellet.

Besides stable Mo (VI) species, a fraction of molybdenum in the oxidation state +V is observed in the spectra. Through the measurement of $^{98}MoO_3$ samples, explanation of Mo(V) as intermediate product of the oxidation process can be excluded. The formation of Mo(V) as an artefact due to the CID process is rather unlikely, as all the measurement are performed in very soft condition, that a water shell of 4-21 water molecules remains around the species.

Table 4-4: Relative abundance of species in sample **P1**, **P2**, **P3, P4** and **P5**. ^{98}Mo-pellet placed in 1 mol/L nitric acid. **P1**:[^{98}Mo] = 2.4 mmol/L, **P2**:[^{98}Mo] = 7.6 mmol/L, **P3**:[^{98}Mo] = 11.4 mmol/L, **P4**:[^{98}Mo] = 19.7 mmol/L, **P5**:[^{98}Mo] = 19.3 mmol/L,

species	Sum formula	m/q	plot colour	P1	P2	P3	P4	P5
Mo(V) monomers	$[Mo^{V}O_2]^+$	129.90	blue		3.3	2.8	1.7	
	$[Mo^{V}O(OH)(NO_3)]^+$	192.91	yellow	1.5	2.4	1.4	1.3	0.2
Dimers	$[Mo_2O_5(OH)]^+$	292.81	magenta	41.5	27.0	19.2	17.5	14.8
	$[Mo_2O_5(NO_3)]^+$	337.81	white	14.1	4.0		2.8	4.9
Trimers	$[Mo_3O_8(OH)]^+$	438.71	green	34.3	27.1	21.0	22.6	26.8
	$[Mo_3O_8(NO_3)]^+$	483.71	red					2.2
Tetramers	$[Mo_4O_{11}(OH)]^+$	584.62	yellow	8.7	16.5	18.5	14.4	10.8
	$[Mo_4O_{11}(NO_3)]^+$	629.61	magenta				5.3	8.8
Pentamers	$[Mo_5O_{14}(OH)]^+$	730.52	blue		19.7	19.7	17.7	16.7
Heptamers	$[Mo_7O_{20}(OH)]^+$	1022.32	green			9.4	9.0	8.0
Octamers	$[Mo_8O_{23}(OH)]^+$	1168.23	yellow			8.2	7.8	5.9

5 Mixed system

Beside molybdenum as an inert matrix of Mo-cermet fuel, other substances are present in the reprocessing solution. In order to increase the dissolution rate of molybdenum, ferric nitrate could be added into the reprocessing solution. Characterisation of the solution species is a necessary prerequisite to gain a microscopic understanding of the underlying processes Transuranic (TRU) elements such as plutonium (Pu), and minor actinides (MAs), which are the primary contributors to long term radiotoxicity in spent fuel.

How about the influence of iron on the dissolution behaviour of molybdenum? How about the solution chemistry of mixed Mo and TRU, MAs system? As mentioned above, in this work zirconium and thorium would be used as analog for tetravalent actinides, particularly Pu. Europium would be used as analog for trivalent actinides, particularly Am. The mixed solution species Mo and Fe, Mo and Zr, Mo and Th, Mo and Eu will be discussed in the chapter.

5.1 Mo-Fe

The addition of Iron (III) nitrate is known to significantly increase the solubility of uranyl molybdate and enhance the dissolution rate in nitric acid [83]. Anion exchange resin studies indicate that a negatively charged iron-molybdenum complex ion is present in such solutions [161].

$$2Fe^{3+} + 12MoO_3 + 6H_2O \rightarrow (Fe_2Mo_{12}O_{42})^{6-} + 12H^+ \qquad [83]$$

The addition of ferric nitrate to the acid increases the dissolution rate of the Mo pellet as confirmed by project partner FZ Jülich. The Mo pellet can be completely dissolved in 1 mol/L HNO_3 containing at least 1 mol/L Fe(lll) within one day. In 1 mol/L HNO_3 without the addition of Fe(lll) only about 40% of the pellet are dissolved after 3 days [162].

In the reprocessing process, a high dissolution rate of Mo will improve effectiveness of the first dissolutions process. In this section, Mo-Fe samples are measured by use of ESI-MS to investigate the influence of iron on the dissolution behaviour of molybdenum.

5.1.1 Sample preparation

Isotopically pure ^{98}Mo metal powder was dissolved ([^{98}Mo] = 10 mmol/L) with 1 mol/L nitric acid containing $Fe(NO_3)_3$ ([Fe] = 10 mmol/L) within one day. The resulting solutions were investigated by means of *nano* ESI-MS in order to characterize and quantify the solution species. After 431 days, the aged mixed solution was measured by *nano* ESI-MS again.

5.1.2 Results and discussion

Besides the expected molybdenum species that were also observed in the pure ^{98}Mo powder sample **M2**, which is with the same Mo concentration at the same acidity (1 mol/L nitric acid), mixed Mo-Fe species were detected. The spectrum is shown in Figure 5-1 TOP. To better differentiate the species, the same color is used for the same group of the species. Pure molybdenum species with hydroxide ions are marked in magenta, with nitrate ion are marked in white. Mo dimers are the dominant species with a total relative abundance of 39.6% ($[Mo_2O_5(OH)]^+$ 31.8% and $[Mo_2O_5(NO_3)]^+$ 7.8%). The relative abundance of all detected species are shown in Table 5-1. There is no significant change in the relative abundance trends compare to sample **M2**. Trimers are the largest pure Mo species, with significant peak intensity. $[Mo_3O_8(OH)]^+$ has relative abundance of 34.3%, this value is similar to the relative abundance of $[Mo_2O_5(OH)]^+$. As can be observed in metal powder sample **M1**-**M3**, one Mo(V) species $[MoO(OH)(NO_3)]^+$, is also detected in the mixed Mo-Fe sample (marked in cyan), the relative abundance is also very small (4.6%).

Mixed Mo-Fe species are marked with green in the spectrum, $[MoO_2Fe(NO_3)(OH)_3]^+$ (rel. abundance about 7.0% with respect to Mo) and $[Mo_2O_5Fe(NO_3)(OH)_3]^+$ (rel. abundance about 14.0% with respect to Mo) [in short (Mo, Fe 1, 1), and (Mo, Fe 2, 1)]. (Mo, Fe 1, 1) has a relative abundance of 7.0% with respect to Mo, although no Mo (VI) monomeric species is detected in the solution. Thus, we can deduce that the Mo-Fe mixed species are actual mixed solution species, which may be precursors of the soluble Mo-Fe complex.

Furthermore, two pure Fe species are found in the solution. The Fe(III) species $[Fe(III)NO_3]^+$ (blue, m/q 251.91~468.09, relative abundance 62.2% with respect to Fe) is detected in the solution. Additionally, the peak at m/q value between 207.92 and 370.06 (marked in yellow, relative abundance 16.3% with respect to Fe) indicates that the species $[Fe(III)NO_3]^+$ undergoes a reduction to species $[Fe(II)(NO_3)_2]^+$. The Fe(II) forms in spite of the oxidizing conditions in both, strong nitric acid and the nano-ESI needle tip. In nano-ESI positive mode, oxidation may take place due to the high voltage applied at the ESI-capillary. The tip acts as an anode that would lead to an oxidation

process. An alteration of the oxidation state of Fe-complexes was also found under nano-ESI conditions [86, 87]. Weber *et al.* observed ~5% Fe(III) of Fe(II)nicotianamine(NA) complex both in negative ionization mode and positive ionization mode. Reduction is likely occurring only in negative ionization mode, hence, the authors found, the reduced form Fe(II) does not originate from the ionization process. Likewise in our measurement, the appearance of a Fe(II) species in Fe(III) solution could not occur in the ESI positive mode, rather take place already in solution.

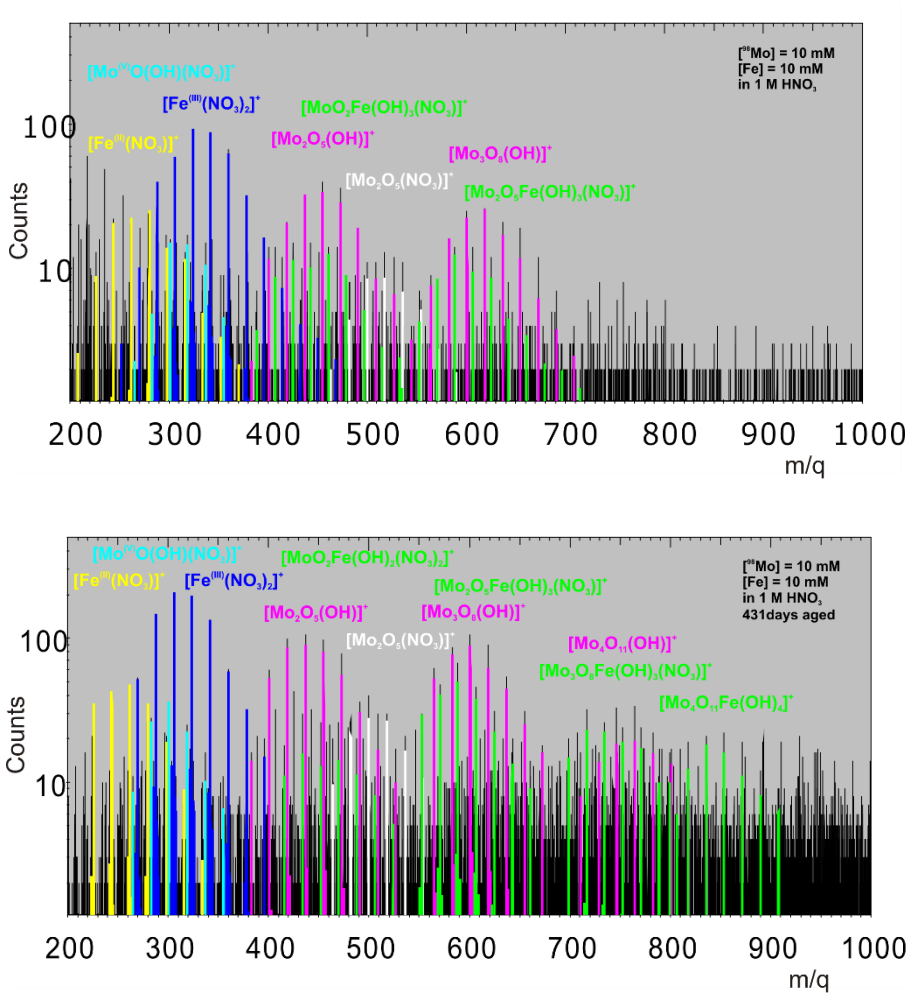

Figure 5-1: Mass spectra of sample [^{98}Mo] = 10 mmol/L, [Fe] = 10 mmol/L, [HNO_3] = 1 mol/L. TOP: fresh solution. Pure Mo(VI) species，$[Mo_2O_5(OH)]^+$ and $[Mo_3O_8(OH)]^+$ are marked in magenta, $[Mo_2O_5(NO_3)]^+$ is marked in white. One Mo(V) species is detected with relative abundance 4.5%. Pure Fe(III) and Fe(II) species are marked in blue and yellow respectively. Mixes Mo-Fe species $[MoO_2Fe(NO_3)(OH)_3]^+$ and $[Mo_2O_5Fe(NO_3)(OH)_3]^+$ are formed. BOTTOM: sample after 431 days. Mo(V) and Fe(II) peaks remain in the spectrum. Larger mixed species $Mo^{VI}_3O_8Fe^{III}(NO_3)(OH)_3^+$, $Mo^{VI}_4O_{11}Fe^{III}(OH)_4^+$ are formed. The relative abundance of the mixed species is increased after 431 days.

Table 5-1: relative species abundance of Mo-Fe sample in 1 mol/L HNO_3, [^{98}Mo] = 10 mmol/L, [Fe] = 10 mmol/L, [HNO_3] = 1 mol/L.

	species	Sum formula	m/q	fresh relative abundance in %		431 aged relative abundance in %	
				Mo	Fe	Mo	Fe
Pure Mo	Mo(V)	$[Mo^{V}O(OH)(NO_3)]^+$	192.91	4.5		2.2	
	Dimers	$[Mo_2O_5(OH)]^+$	292.81	31.8		19.7	
		$[Mo_2O_5(NO_3)]^+$	337.81	7.8		5.4	
	Trimers	$[Mo_3O_8(OH)]^+$	438.71	34.8		27.9	
	Tetramers	$[Mo_4O_{11}(OH)]^+$	584.62			11.6	
Pure Fe	Fe (II)NO_3	$[FeNO_3]^+$	117.85		16.3		11.1
	Fe(III)NO_3	$[Fe(NO_3)_2]^+$	179.85		62.2		51.9
Mixed species		$Mo^{VI}O_2Fe^{III}(NO_3)(OH)_3^+$/ $Mo^{VI}O_2Fe^{III}(NO_3)_2(OH)_2^+$	298.77/ 343.77	7.0	10.8	2.0	5.5
		$Mo^{VI}{}_2O_5Fe^{III}(NO_3)(OH)_3^+$	444.68	14.0	10.8	11.2	15.4
		$Mo^{VI}{}_3O_8Fe^{III}(NO_3)(OH)_3^+$	590.58			10.2	9.4
		$Mo^{VI}{}_4O_{11}Fe^{III}(OH)_4^+$	691.48			9.7	6.7

To investigate the stability of Mo-Fe mixed species and Fe(II) species, a 431 days aged sample solution was measured again by use of *nano* ESI-MS. The ESI spectrum is shown in Figure 5-1, bottom. In comparison to fresh sample, there are no significant changes, pure Mo, pure Fe and mixed Mo-Fe species are detected also in the aged solution, Mo(V) and Fe(II) species are observed. The relative abundance of Mo(V) decreases to 2.2%, and Fe(II) species decrease to 11.1% after 431 days. It seems that species, with unstable oxidation states decrease with time. However, while in the pellet sample Mo(V) species nearly vanished after 461 days, in the Mo-Fe sample Mo(V) species still accounts for 2.2% after 431 days, this may be due to the existence of iron in the solution.

In the 431 days aged solution, larger mixed Mo-Fe species formed: $Mo^{VI}{}_3O_8Fe^{III}(NO_3)(OH)_3^+$, $Mo^{VI}{}_4O_{11}Fe^{III}(OH)_4^+$ [in short (Mo, Fe 3, 1) and (Mo, Fe 4, 1)]. The relative abundance of all mixed species increases from 21.0% to 33.1% with respect to Mo, and from 21.6% to 37.0% with respect to Fe. This means, the addition of iron (III) nitrate did not only lead to significant increase of the solubility of molybdenum and the dissolution rate in nitric acid but also the formation of Mo-Fe species prevents forming precipitates. However, our investigations do still not provide clear evidence whether this is the driving force in the enhancement of the dissolution kinetics of Mo metal, or whether it rather is the involvement of Fe(III) as redox partner.

For the actual reprocessing, the advantageous increase in dissolution rate by addition

of $Fe(NO_3)_3$ and the lower abundance of large Mo-polymers is paid for by the formation of mixed species which might hinder efficient partitioning. It is, however, obvious that the tendency for precipitation decreases in the aged Mo solution.

5.2 Mo-Zr

^{90}Zr(IV) is used in this work as analogue for Pu(IV) to investigate how Mo species change when Zr is added to the Mo containing solutions and whether mixed solution species are formed and the relation of solution species to ZMH precipitation. The following chapter describes the measurement of Mo and Zr mixed system, the mixed system is measured by ESI-MS with two different acid concentrations ($[HNO_3]$ = 0.5 mol/L and 1 mol/L). For each acid concentration series, the metal concentration ratio is varied by changing the Zr concentration to give ratios of [Mo]:[Zr] = 1:1, 2:1 and 10:1 (see Table 5-2, samples **A1**, **A2**, **A3**, **B1**, **B2** and **B3**)

5.2.1 Sample preparation

Since there are five naturally occurring Zr isotopes, for larger signal intensities of ion count isotopically enriched ^{90}Zr is used in this system. Stock solutions of $[^{98}Mo]$ = 10 mmol/L are prepared as described in chapter 4.1.1. Isotopically pure ^{90}Zr (> 99% ^{90}Zr) metal powder is obtained from STB Isotope Germany GmbH and further processed in the department of Nuclear Engineering Kyoto University (Japan). The water soluble compound $^{90}ZrCl_4$ is synthesized by a dry process. 200 mg of ^{90}Zr metal powder is reacted with pure Cl_2 gas (20 ml/min) in a quartz reaction vessel heated to 320°C. Only the chloride product vaporizes, and the light-organish-white powder is deposited at the cold trap. The product is assigned to be anhydrous $^{90}ZrCl_4$ by X-ray diffraction analysis and thermogravimetry-differential thermal analysis. Though the chemical yield of product is only 64%, the non-volatile residue is found to be zirconium oxide originally produced on the surface of metal powder in ambient conditions.

Stock solutions of ^{90}Zr (50 mmol/L) are prepared by dissolution of isotopically pure $^{90}ZrCl_4$ in $[HNO_3]$ = 1 mol/L. The concentrations of ^{98}Mo and ^{90}Zr stock solutions are measured by ICP-MS. The mixed ^{98}Mo and ^{90}Zr samples are prepared in two series in 0.5 mol/L nitric acid and in 1 mol/L nitric acid. For each series, there are three samples with different concentration ratios of Mo and Zr (1:1, 2:1 and 10:1). The samples are prepared by mixing appropriate amounts of stock solution of Mo and Zr and measured normally on the same day by use of *nano* ESI-MS. Sample **A1** and sample **A3** (see Table 5-2) are measured eight days and six days after the mixture respectively. The concentrations of six samples are calculated from the concentration of stock Mo and Zr solutions considering the total volume. After 200 days of aging, the concentrations of six samples are measured by ICP-MS. The concentrations of the fresh samples are

summarized in Table 5-2.

Table 5-2: Summary of Mo-Zr samples examined by *nano* ESI-MS. Concentration ratios of molybdenum and zirconium and the concentrations in the fresh samples respectively.

Sample ID	acid	concentration ratio ^{98}Mo: ^{90}Zr	concentration of ^{98}Mo (mmol/L)	concentration of ^{90}Zr (mmol/L)
A1	$[HNO_3]$ = 0.5 mol/L	1:1	8.0	8.0
A2		2:1	9.0	4.5
A3		10:1	9.0	0.9
B1	$[HNO_3]$ = 1 mol/L	1:1	8.0	8.0
B2		2:1	9.0	4.5
B3		10:1	9.0	0.9

5.2.2 ESI-measurement Results and discussion

5.2.2.1 Solution species in 0.5 mol/L nitric acid

The ESI mass spectra of the samples **A1**, **A2** and **A3** are shown in Figure 5-2. Monomeric up to pentameric pure Mo species are detected in sample **A1** ([Mo] = 8.0 mmol/L, [Zr] = 8.0 mmol/L, Mo:Zr ratio 1:1) and **A2** ([Mo] = 9.0 mmol/L, [Zr] = 4.5 mmol/L, Mo:Zr ratio 2:1). In the sample **A3** ([Mo] = 9.0 mmol/L, [Zr] = 0.9 mmol/L, Mo:Zr ratio 10:1) Mo forms a considerable fraction of polymers up to the octamer with relative abundance 2.9%, the largest polymer which can be quantified in sample **A3**. There are some small signals of octamers, nonamers and decamers, however, statistics is very poor hindering a meaningful calculation of the relative abundances. The relative abundances of species in the three samples are summarized in Table 5-3. Mo trimers ($[Mo_3O_8(OH)]^+$ and $[Mo_3O_8(NO_3)]^+$) are the dominant pure Mo species (a total of 27.6% in **A1**, 29.5% in **A2** and 27.0% in **A3**, respectively) in all three samples. This is not similar with the result of pure Mo solutions without any addition of Zr (sample **M3**, see chapter 4.1.2) the dominant pure Mo species is pentameric with an abundance of 27.3%). By comparing the relative abundances with the ones in the pure Mo systems **A1**, **A2**, **A3** and **M3, i**t can be seen, that the presence of Zr in solution suppresses to a degree the formation of larger Mo species.

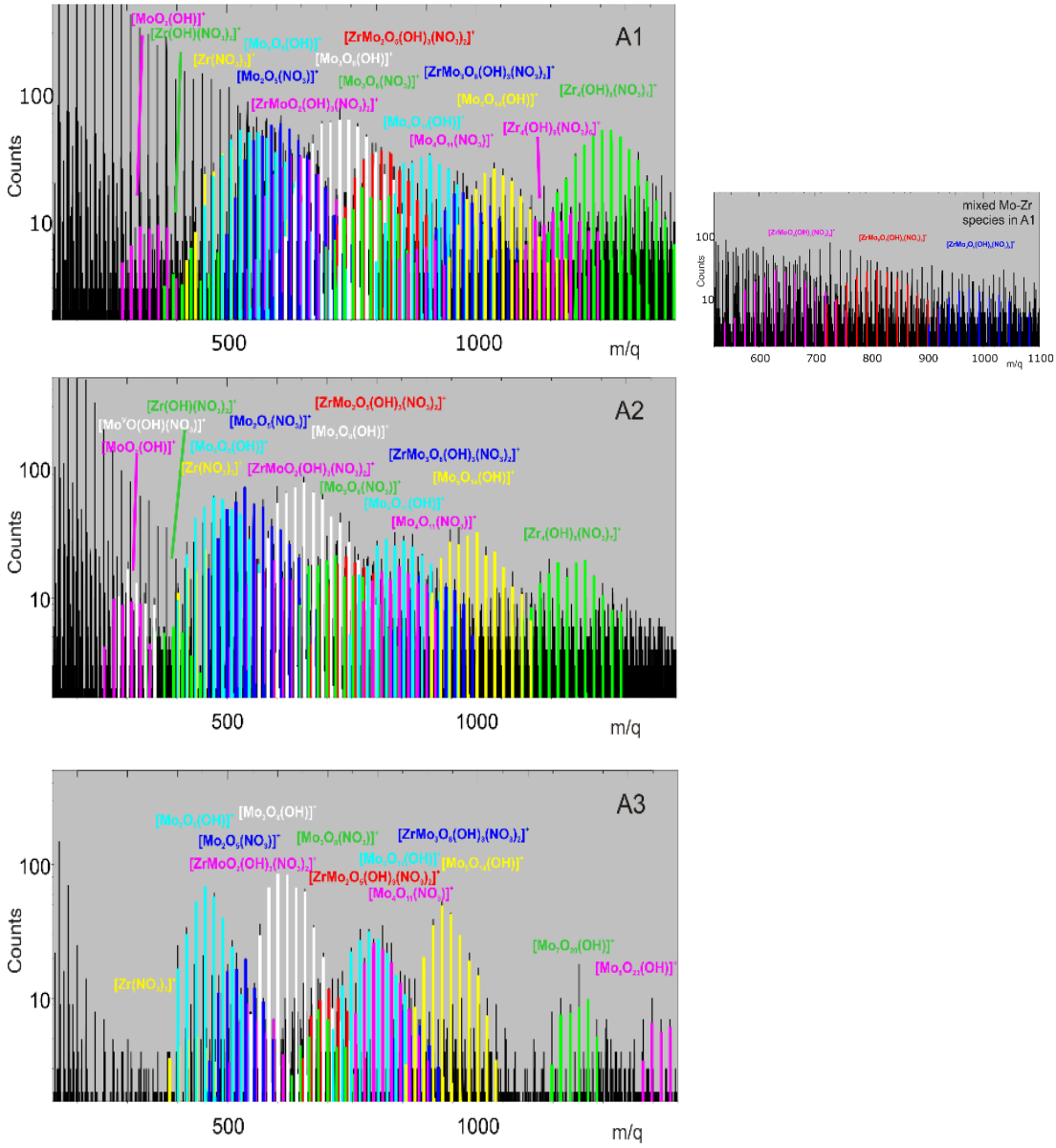

Figure 5-2: Mass spectra of sample **A1**, **A2** and **A3**. Sample **A1**, **A2** und **A3** are prepared in 0.5 mol/L HNO_3 with different concentration ratios of Mo and Zr (1:1, 2:1 and 10:1). In these samples, similar pure Mo, pure Zr and mixed Zr-Mo species are observed. **Top right:** Three mixed Mo-Zr species are observed also in samples **A1**: $[ZrMoO_2(OH)_3(NO_3)_2]^+$ (1, 1), $[ZrMo_2O_5(OH)_3(NO_3)_2]^+$ (1, 2) and $[ZrMo_3O_8(OH)_3(NO_3)_2]^+$ (1, 3). For the sake of clarity, the other species have not been fitted in this zoom. The relative abundance of the three mixed species with respect to Mo decreases with decreasing concentration of Zr in the sample.

Table 5-3: Relative abundance of species in three samples in 0.5 mol/L HNO_3 (sample **A1**: [Mo] = 8.0 mmol/L, [Zr] = 8.0 mmol/L, sample **A2**: [Mo] = 9.0 mmol/L, [Zr] = 4.5 mmol/L, sample **A3**: [Mo] = 9.0 mmol/L, [Zr] = 0.9 mmol/L). The Mo:Zr ratios are 1:1, 2:1 and 10:1. The relative abundance of pure Mo species are given with respect to Mo, pure Zr species are with respect to Zr and mixed species are with respect to Mo and Zr respectively.

	Solution species	relative abundance in %					
		A1 Mo:Zr ratio 1:1		A2 Mo:Zr ratio 2:1		A3 Mo:Zr ratio 10:1	
		Mo	Zr	Mo	Zr	Mo	Zr
Pure Mo species	$[Mo^{V}O(OH)(NO_3)]^+$	-	-	0.6	-	-	-
	$[MoO_2(OH)]^+$	0.5	-	0.5	-	-	-
	$[Mo_2O_5(OH)]^+$	10.9	-	9.4	-	9.7	-
	$[Mo_2O_5(NO_3)]^+$	11.8	-	11.6	-	3.1	-
	$[Mo_3O_8(OH)]^+$	22.4	-	23.1	-	24.9	-
	$[Mo_3O_8(NO_3)]^+$	5.2	-	6.4	-	2.1	-
	$[Mo_4O_{11}(OH)]^+$	15.9	-	13.7	-	13.1	-
	$[Mo_4O_{11}(NO_3)]^+$	2.1	-	6.9	-	9.5	-
	$[Mo_5O_{14}(OH)]^+$	14.8	-	17.6	-	23.5	-
	$[Mo_5O_{14}(NO_3)]^+$	-	-	-	-	-	-
	$[Mo_7O_{20}(OH)]^+$	-	-	-	-	6.5	-
	$[Mo_8O_{23}(OH)]^+$	-	-	-	-	2.9	-
Pure Zr species	$[Zr(NO_3)_3]^+$	-	6.8	-	9.7	-	14.7
	$[Zr(OH)(NO_3)_2]^+$		0.7		2.0		
	$[Zr_4(OH)_8(NO_3)_7]^+$	-	62.9	-	60.3	-	-
	$[Zr_4(OH)_9(NO_3)_6]^+$	-	12.3	-	-	-	-
Mixed species	$[ZrMoO_2(OH)_3(NO_3)_2]^+$	3.3	6.4	1.7	9.2	0.7	26.1
	$[ZrMo_2O_5(OH)_3(NO_3)_2]^+$	7.4	7.3	4.2	11.3	2.0	36.2
	$[ZrMo_3O_8(OH)_3(NO_3)_2]^+$	5.6	3.7	4.2	7.5	1.9	23.0

In addition to the pure Mo species in the samples, four pure Zr species are detected: Zr forms primarily monomers $[Zr(NO_3)_3]^+$ (yellow), and tetramers $[Zr_4(OH)_9(NO_3)_6]^+$ (magenta) and $[Zr_4(OH)_8(NO_3)_7]^+$ (green) and very small amounts of $[Zr(OH)(NO_3)_2]^+$ (green). For the Zr complexes a coordination of nitrate in the first coordination sphere is considered less likely at the rather low nitrate concentration of $[HNO_3]$ = 0.5 mol/L. Pure Zr species consist of two groups, monomeric Zr^{4+}, and the tetramers $[Zr_4(OH)_8]^{8+}$ and $[Zr_4(OH)_9]^{7+}$. For all these ions the charge is partly compensated for by an adequate number of nitrate anions until only a singly charged nanodroplet containing the Zr species remains, for instance seven NO_3^- ions in the case of $[Zr_4(OH)_8(NO_3)_7]^+$. Both Zr

hydroxide tetrameric complexes with the same number of Zr atoms but 8 and 9 hydroxide ions, respectively, are present simultaneously. The total number of polymers with the same number of Zr(IV) ions *x* is obtained by the sum

$$N(x) = N(Zr_x) = \sum_b N\{[Zr_x(OH)_b]^q\}.$$

The species and their abundances are in good accord with the results on the hydrolysis behaviour of Zr(IV) reported before [29] as well as with the review of Brown and Ekberg [89], which was presented in detail in the chapter 2.2. At $pH_C = 0.3$, the Zr tetrameric species with about 70% relative abundance are the dominant species. As shown in Figure 2-7, the $[Zr_4(OH)_8]^{8+}$ is the predominant Zr(IV) species at pH = 0.3 and log [Zr] = -2 to -3. The relative abundance of Zr monomers increases with increasing [Mo]:[Zr] ratio in the sample. The relative abundance of Zr tetramers does not notably change.

Nevertheless, in sample **A3** ([Mo]:[Zr] = 10:1) zirconium tends to form more mixed Mo-Zr species, rather than Zr-tetramers. Three mixed Mo-Zr species are observed in all three samples **A1**, **A2** and **A3**: $[ZrMoO_2(OH)_3(NO_3)_2]^+$ (Mo, Zr 1, 1) (magenta), $[ZrMo_2O_5(OH)_3(NO_3)_2]^+$ (Mo, Zr 2, 1) (red) and $[ZrMo_3O_8(OH)_3(NO_3)_2]^+$ (Mo, Zr 3, 1) (blue). Here the advantage of the *nano* ESI-MS method becomes obvious: mixed species even of rather low relative abundance can be characterized unambiguously, as each cationic solution species gives rise to a specific mass spectrometric signal. The (Mo, Zr 2, 1) species has the highest relative abundance of the mixed species (with respect to both Zr and Mo). The relative abundance of the three mixed species with respect to Mo decreases with decreasing concentration of Zr in the sample. The sum formula of solution species (Mo, Zr 2, 1) $[ZrMo_2O_5(OH)_3(NO_3)_2]^+$ resembles the one of the solid ZMH phases ($[ZrMo_2O_7(OH)_2]\cdot 2H_2O$), that tend to form in Mo-Zr mixtures. Furthermore, one or more chemical equilibria between the three mixed solution species (Mo, Zr 1, 1), (Mo, Zr 2, 1) and (Mo, Zr 3, 1) are highly likely to exist in the system. Therefore, we conclude that mixed solution species are the precursors of the ZMH precipitate.

During aging, various precipitates form in $[HNO_3]$ = 0.5 mol/L solutions after 200 days (Figure 5-3). In sample **A1** [Mo]:[Zr] = 1:1 a white precipitate is forming after 200 days and in sample **A2** with [Mo]:[Zr] = 2:1 white sediments are observed on the bottom of the vial. The sample **A3** with [Mo]:[Zr] = 10:1 becomes turbid during the course of the experiment but no precipitate forms at the bottom of the vial. The concentrations of Mo and Zr in the supernatant of aged solutions were measured by use of ICP-MS and shown in Table 5-4.

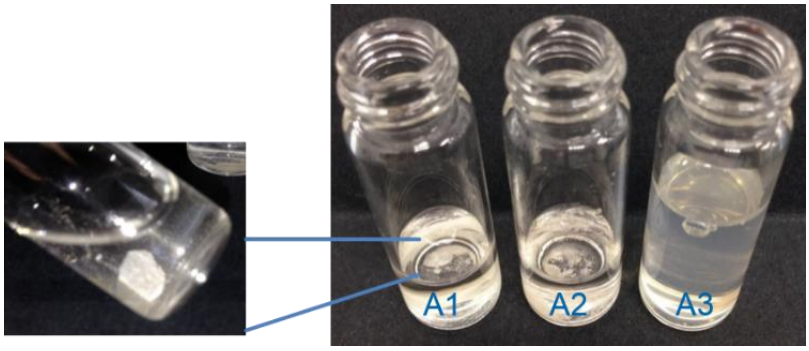

Figure 5-3: precipitates form in samples **A1**, **A2** and **A3** after 200 days.

Table 5-4: Mo and Zr concentration in samples A1. A2 and A3 fresh and 200 days aged solutions, respectively.

		fresh (mmol/L)	aged (mmol/L)	concentration
A1	Mo	8.0	1.2	6.8
	Zr	8.0	4.5	3.5
A2	Mo	9.0	2.0	7
	Zr	4.5	0.8	3.7
A3	Mo	9.0	8.9	0.1
	Zr	0.9	0.5	0.4

ZMH has a stoichiometric ratio of N(Mo)/N(Zr) = 2 as described in chapter 2.6. After formation of the precipitate the decrease of [Mo] and [Zr] in the solutions follow this ratio to good approximation: in sample **A1** the Mo concentration decreases by Δ[Mo] = 6.8 mmol/L the one of Zr by Δ[Zr] = 3.5 mmol/L which gives a ratio of Δ[Mo]/Δ[Zr] = 1.94. Similarly, the ratio of the decreases in sample A2 is Δ[Mo]/Δ[Zr] = 1.89. This finding corroborates the assumption of mixed Mo-Zr species being the precursors of the ZMH precipitate. Since no precipitate forms in sample A3, the ratio of concentration difference cannot be interpreted as it was done for the other two samples.

We measured the supernatant of 200 days aged sample **A1** by use of *nano* ESI-MS. The ESI-spectrum is shown in Figure 5-4. In the aged filtrate, Mo species could not be detected except a small amount of Mo-Zr mixed species $[ZrMoO_2(OH)_3(NO_3)_2]^+$ (Mo, Zr 1, 1) (magenta). The rest of Zr in solution forms monomeric and polymeric species, such as, Zr monomeric, dimeric, tetrameric and pentameric species. The decrease of Mo-Zr mixed species is not only true for (Mo, Zr 2, 1), which has the same ration of Mo and Zr in ZMH, but also occurs for the other two mixed solution species (Mo, Zr 1, 1) and (Mo, Zr 3, 1). This is further proof of the hypothesis, that one or more chemical equilibria between the three mixed solution species (Mo, Zr 1, 1), (Mo, Zr 2, 1) and (Mo, Zr 3, 1) exist.

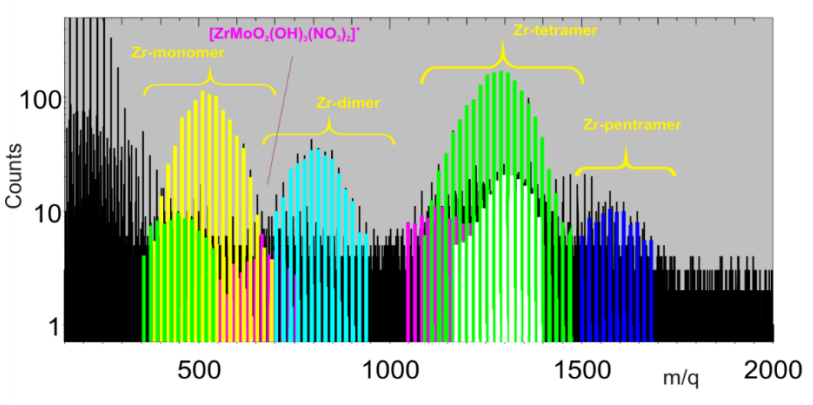

Figure 5-4: ESI spectrum of 200 days aged sample A1 ([Mo] = 1.2 mmol/L, [Zr] = 4.5 mmol/L, in 0.5 mol/L HNO_3). Mo species could not be seen in the spectrum except a small amount of Mo-Zr 1:1 mixed species $[ZrMoO_2(OH)_3(NO_3)_2]^+$ (1, 1) (magenta). Zr forms more polymeric species. Zr monomeric, dimeric, tetrameric and pentameric species.

5.2.2.2 Solution species in 1 mol/L nitric acid

In order to determine the influence of the proton concentration on the speciation three more samples with higher acid concentration ($[HNO_3]$ = 1 mol/L) are investigated by *nano* ESI-MS measurements. As for the previous samples, the concentration of ^{98}Mo is 8.0 mmol/L to 9.0 mmol/L and the concentrations of ^{90}Zr is varied from 8.0 mmol/L to 0.9 mmol/L. The ratios [Mo]:[Zr] are 1:1 (**B1**), 2:1 (**B2**) and 10:1 (**B3**). As an example, a part of the ESI-MS spectrum from m/q 250-1400 of the sample **B3** ([Mo] = 9.0 mmol/L, [Zr] = 0.9 mmol/L, $[HNO_3]$ = 1 mol/L) is shown in Figure 5-5. The relative species abundances of these three samples are summarized in Table 5-5.

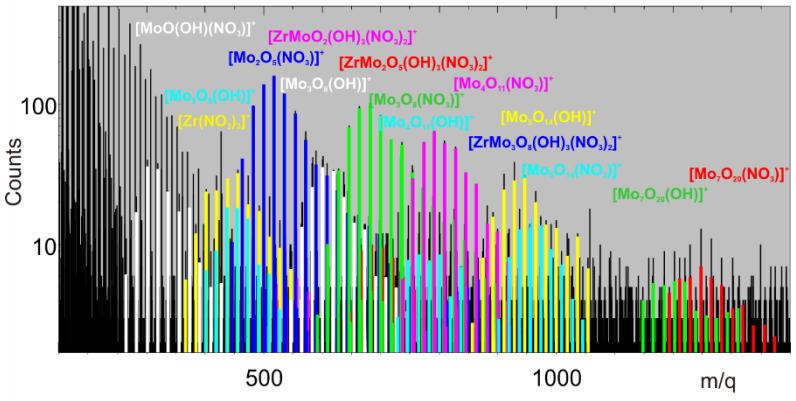

Figure 5-5: ESI spectrum of the sample B3 ([Mo] = 9.0 mmol/L, [Zr] = 0.9 mmol/L, $[HNO_3]$ = 1 mol/L). Some small signals of heptamers (with hydroxide and with nitrate anions, respectively), are shown in the spectrum, but due to poor statistics cannot be evaluated in terms of relative abundances.

Mo(V) species are detected in all three samples: ($[Mo^VO(OH)(NO_3)]^+$) in sample **B2** and **B3** and $[Mo^VO_2]^+$ in sample **B1** and **B2**. The relative abundances of Mo(V) species are between 0.8% and 2.0%. Compared with the samples in $[HNO_3]$ = 0.5 mol/L, more

Mo(V) species form in systems of higher acid concentration. The fraction of dimers increases compared to the relative abundances in samples **A1**, **A2** and **A3** (Table 5-3). The dimers $[Mo_2O_5(OH)]^+$ and $[Mo_2O_5(NO_3)]^+$ with a total relative abundance of ca. 30% are the dominant species in samples **B1** and **B2**, whereas in sample **B3** the trimers (31.8%) are more abundant than the dimers (22.9%). This contrasts with the samples at lower acidity where the trimers dominate in all three samples. The increase of dimers is due to the cumulative effect of the addition of Zr and the higher acid strength of the samples: The presence of Zr leads to a lower abundance of larger Mo polymeric species in the solution. On the other hand, the influence of the proton concentration comes into play: in stronger acid, the formation of large Mo polymeric species is suppressed. Only in sample **B3** the addition of Zr does not suffice to make dimers the dominant species, but due to the effect of proton concentration, the total of dimers in sample **B3** (22.9%) exceeds the total of dimers in sample in **A3** (12.8%). There are some heptamers detected in sample **B3**, however, as mentioned before due to poor statistics the species are not considered for the relative abundance calculation. Pure Mo polymeric species containing hydroxide or nitrate, respectively, are observed in each of the samples. As discussed above, nitrate species are considered as doubly charged Mo species, the presence of Zr in solution may prevent formation of doubly charged species in nitric acid. In the sample **B3**, as a special case, the relative abundance of species with nitrate is higher than of those containing an additional hydroxide. In the measurement with pure Mo samples, the amount of nitrate species increases after 258 days (see chapter 4.1.2).

Zr forms primarily monomers and tetramers. In addition to the monomer $[Zr(NO_3)_3]^+$ in ($[HNO_3]$ = 0.5 mol/L there are other monomers in ($[HNO_3]$ = 1 mol/L samples, namely $[ZrONO_3]^+$ and $[ZrOH(NO_3)_2]^+$. The relative abundance of these three Zr monomeric species is 16.3% in sample **B1**. It is higher than in sample **A1** (7.5%), with [Zr] = 8.0 mmol/L. This tendency is in accord with the literature (NEA-TDB [163]): the amount of Zr monomeric species increased with increasing acid concentration. These trends can also be seen in Figure 2-7, in the low pH range, with decreasing pH value monomeric Zr predominate. Here again *nano* ESI-MS shows its strengths, not only the predominate species can be detected, but also the minor species can be observed and identified.

The three mixed Zr-Mo species observed in samples **B1**, **B2** and **B3** equal the ones identified in samples **A1**, **A2** and **A3**: $[ZrMoO_2(OH)_3(NO_3)_2]^+$, $[ZrMo_2O_5(OH)_3(NO_3)_2]^+$, and $[ZrMo_3O_8(OH)_3(NO_3)_2]^+$. The relative abundance of these three mixed species with respect to Mo decreases with decreasing concentration of Zr in the sample. As precursors of the ZMH precipitate Mo-Zr mixed species are directly observed in all three samples by ESI-MS measurement.

Table 5-5: Relative species abundances of three samples in 1 mol/L HNO_3. (Sample **B1**: [Mo] = 8.0 mmol/L, [Zr] = 8.0 mmol/L, sample **B2**: [Mo] = 9.0 mmol/L, [Zr] = 4.5 mmol/L, sample **B3**: [Mo] = 9.0 mmol/L, [Zr] = 0.9 mmol/L). The [Mo]:[Zr] ratios are 1:1, 2:1 and 10:1. The relative abundances of pure Mo species are calculated with respect to [Mo], pure Zr species with respect to [Zr] and mixed species are with respect to [Mo] and [Zr] respectively.

	Solution species	**relative abundance in %**					
		B1 Mo:Zr ratio 1:1		**B2** Mo:Zr ratio 2:1		**B3** Mo:Zr ratio 10:1	
		Mo	Zr	Mo	Mo	Zr	Mo
Pure Mo species	$[Mo^{V}O_2]^+$	1.4		0.8			
	$[Mo^{V}O(OH)(NO_3)]^+$	-	-	2.0	-	1.8	-
	$[MoO_2(OH)]^+$	1.0	-	-	-	-	-
	$[Mo_2O_5(OH)]^+$	27.3	-	17.7	-	1.9	-
	$[Mo_2O_5(NO_3)]^+$	4.6	-	14.0	-	21.0	-
	$[Mo_3O_8(OH)]^+$	22.3	-	23.1	-	6.7	-
	$[Mo_3O_8(NO_3)]^+$		-	4.1	-	25.1	-
	$[Mo_4O_{11}(OH)]^+$	8.0	-	8.7	-	2.5	-
	$[Mo_4O_{11}(NO_3)]^+$	-	-	3.1	-	19.3	-
	$[Mo_5O_{14}(OH)]^+$	-	-	6.5	-	13.1	-
	$[Mo_5O_{14}(NO_3)]^+$			-	-	5.3	
Pure Zr species	$[Zr(NO_3)_3]^+$	-	11.8	-	17.9	-	58.9
	$[ZrO(NO_3)]^+$	-	2.3	-	2.6	-	-
	$[Zr(OH)(NO_3)_2]^+$	-	2.2	-	5.2	-	
	$[Zr_4(OH)_8(NO_3)_7]^+$	-	33.1	-	30.7	-	-
	$[Zr_4(OH)_9](NO_3)_6]^+$	-	20.5	-	9.6	-	-
Mixed species	$[ZrMoO_2(OH)_3(NO_3)_2]^+$	11.0	15.8	5.8	16.4	0.3	7.5
	$[ZrMo_2O_5(OH)_3(NO_3)_2]^+$	11.6	8.3	9.0	12.8	1.5	19.8
	$[ZrMo_3O_8(OH)_3(NO_3)_2]^+$	12.7	6.0	5.2	4.9	1.6	13.8

Unlike the samples in $[HNO_3]$ = 0.5 mol/L (**A1**, **A2** and **A3**), no precipitates form in samples **B1**, **B2** and **B3** in $[HNO_3]$ = 1 mol/L after 200 days, therefore no significant concentration differences are observed in the three aged ($[HNO_3]$ = 1 mol/L) samples. The formation of ZMH in nitric acid depends on temperature and concentration of nitric acid [118, 122, 164]. The higher the temperature and the lower the concentration of nitric acid the higher becomes the precipitation rate of ZMH phases. At room temperature precipitation is not observed in $[HNO_3]$ = 3 mol/L after 248 hours by Lin [128] and the solubility equilibrium is slower to achieve than at higher temperature [165]. Accordingly, precipitation is observed after 200 days in $[HNO_3]$ = 0.5 mol/L samples and no precipitation in $[HNO_3]$ = 1 mol/L samples.

5.2.3 Validation of existence of detected species by ESI-MS measurement

While discussing ESI-MS measurements, the question arises frequently, whether the detected species really exist in solution, or the species are artefacts due to up-concentration effects during the ESI process. To validate ESI-MS measurement suitability for Mo-Zr samples, Poisson's distribution calculation with a sticking factor is used. In the present case, there are two possibilities: the first possibility is that the larger polymeric species are only composed of two smaller species that reach the detector in the same droplet by chance. The second is that lager species exist in the sample solution (real solution species) and are not formed due to the ESI process. In order to decide which is true we calculate the number of ion counts from the ESI-MS measurements for each single species (note: not the relative abundance of species but the normalized number of detected ions). Knowing the number of molecules per unit volume and droplet size one can calculate the expectation value for the mean number of molecules per droplet (which should be <<1 at reasonable conditions). Since the distribution of molecules in the droplets is a random statistical process, the number of molecules in one droplet follows Poisson's law. Subsequently, we calculate the probability for finding two species in the same droplet by chance. An example for sample **A1** is given in Table 5-6. The calculations for the other samples are given in the supplementary material.

If the calculated probability to find an artefact polymer is close to zero, the polymer must be a true aquatic species. For instance, if no monomers are present in solution, dimers cannot be artefacts and similarly without monomers, trimers cannot be formed by adding one to a dimer. If the probability value equals or exceeds the amount of ion counts, artefacts cannot be ruled out. We infer for our sample **A1**, that Mo dimer, Mo trimer, Zr monomer, Zr tetramer and mixed Mo-Zr species (1, 1) are actual solution species. The amount of ion counts from ESI-MS measurement of Mo monomers is 0.0108 ± 0.0006, Mo dimers is 0.2238 ± 0.0031. The upper limit of the probability of the trimer being an artefact (meaning that one monomer and one dimer in the same droplet reach the detector) is 0.0108 * 0.2238 = 0.0024 (± 0.0001). In this sample, the amount of ion counts of Mo trimers (0.1817 ± 0.0027) is higher than the calculated probability. Thus, it is highly likely that the species is actually present in solution and not only generated by the ESI process. Likewise, Mo pentamer and mixed (1, 2) and mixed (1, 3) species are actual solution species, however, part of the detected species could be artefacts. The Poisson's distribution calculation can verify the existence of detected species by ESI-MS measurement.

Table 5-6: Amount of ion counts from ESI-MS measurements for each species in sample **A1** with the probability calculated from Poisson's distribution. If the calculated probability to find an artefact species is zero, the species must be present in solution. If the probability value equals or exceeds the amount of ion counts, artefacts cannot be ruled out.

solution species by ESI-MS measurement			Amount of ion counts from ESI-MS measurements	probability Poisson for artefact species
Pure Mo species	monomer	$[MoO_2(OH)]^+$	0.0108 ± 0.0006	0
	dimer	$[Mo_2O_5(OH)]^+$, $[Mo_2O_5(NO_3)]^+$	0.2238 ± 0.0031	0.0001 ± 1.3·E-5
	trimer	$[Mo_3O_8(OH)]^+$, $[Mo_3O_8(NO_3)]^+$	0.1817 ± 0.0027	0.0024 ±0.0001
	tetramer	$[Mo_4O_{11}(OH)]^+$, $[Mo_4O_{11}(NO_3)]^+$	0.0883 ± 0.0018	0.0521 ± 0.0014
	pentamer	$[Mo_5O_{14}(OH)]^+$	0.0583 ± 0.0014	0.0416 ± 0.0008
Pure Zr species	monomer	$[Zr(NO_3)_3]^+$, $[Zr(OH)(NO_3)_2]^+$	0.0744 ± 0.0016	0
	tetramer	$[Zr_4(OH)_8(NO_3)_7]^+$, $[Zr_4(OH)_9(NO_3)_6]^+$	0.1884 ± 0.0028	3.1·E-5 ± 0.27·E-5
Mixed species	(1, 1)	$[ZrMoO_2(OH)_3(NO_3)_2]^+$	0.0641 ± 0.0015	0.0008 ± 4.9·E-5
	(1, 2)	$[ZrMo_2O_5(OH)_3(NO_3)_2]^+$	0.0732 ± 0.0016	0.0167 ± 0.0004
	(1, 3)	$[ZrMo_3O_8(OH)_3(NO_3)_2]^+$	0.0370 ± 0.0011	0.0135 ± 0.0004

5.2.4 Mo-Zr mixed system Conclusion

ESI-MS is successfully applied to investigate mixtures of Mo and Zr in nitric acid solutions. The sensitivity of the method combined with the ability to cover a large mass range at once is helpful to characterize all solution species in this very complicated system. Pure Mo species, pure Zr species and mixed Mo-Zr species are identified and quantified at the same time. Pure Mo solution species are detected as monomer, dimer and polymer. The Mo polymers decrease in size with increasing acid strength, and the presence of Zr in solution leads to a decreasing fraction of large Mo polymeric species. Three mixed Mo-Zr species, which are precursor of ZMH precipitates in nitric acid, are detected in each of the samples. Their relative abundance increases with increasing acidity of the solution and increasing concentration of Zr. Although in the higher acidic system ($[HNO_3]$ = 1 mol/L), the concentration of ZMH precursor is higher than in the $[HNO_3]$ = 0.5 mol/L system, after 200 days in the aged solution precipitations are formed in 0.5 mol/L nitric acid samples; no precipitates are formed in 1 mol/L nitric acid samples. The amount of ZMH precursor in solution depends on acid concentration, but the formation of ZMH precipitates does not depend on the amount of precursor, but rather on the acid concentration. So, to minimize the formation of ZMH in reprocessing, higher acid strength is more appropriate.

5.3 Mo-Th

In order to clarify whether the Mo-Matrix forms mixed species with tetravalent actinides from the fuel, the investigations on the Mo-Th system are a further step towards the investigation on the Mo-Pu system. Th is used here since it has only one stable oxidation state +IV. The Th system has the advantage that the complex redox chemistry of Pu does not come into play and we can focus on the oxidation state +IV. The measurements are performed with three different concentration ratios of ^{98}Mo and Th (1:1, 2:1 and 10:1) at different acidic strengths ([HNO_3] = 0.5, 1 and 3 mol/L). The concentration of ^{98}Mo was kept at about 10 mmol/L.

5.3.1 Sample preparation

Three Thorium stock solutions ([Th(IV)] = 0.1 mol/L) were prepared by dissolving weighed amounts of thorium nitrate ($Th(NO_3)_4 \cdot 5H_2O$) (Merck, Darmstadt, Germany, analytical grade) in 3 mol/L, 1 mol/L and 0.5 mol/L nitric acid, respectively. The mixed ^{98}Mo and Th samples are prepared in three series in 3 mol/L, in 1 mol/L and in 0.5 mol/L nitric acid. Samples **M1** (10 mmol/L ^{98}Mo in 3 M HNO_3), **M2** (10 mmol/L ^{98}Mo in 1 M HNO_3), **M3** (10 mmol/L ^{98}Mo in 0.5 M HNO_3) were used as ^{98}Mo stock solution. For each series, there are three samples with different concentration ratios of Mo and Th (1:1, 2:1 and 10:1), which are prepared by mixing appropriate amounts of stock solution of ^{98}Mo and stock solution of Th and measured normally on the same day by use of *nano* ESI-MS. No precipitates appeared in any of the nine samples. The concentrations of samples were measured by ICP-MS as summarized in Table 5-7.

Table 5-7: Summary of Mo-Th samples examined by *nano* ESI-MS. Concentration ratios of ^{98}Mo and Th and the concentrations in the samples respectively.

Sample ID	acid	planned concentration ratio ^{98}Mo: Th	concentration of ^{98}Mo (mmol/L)	concentration of Th (mmol/L)
C1	[HNO_3] = 0.5 mol/L	1:1	11.0	8.1
C2		2:1	10.4	4.2
C3		10:1	10.7	1.1
D1	[HNO_3] = 1 mol/L	1:1	10.0	8.8
D2		2:1	10.0	4.6
D3		10:1	9.8	1.1
E1	[HNO_3] = 3 mol/L	1:1	10.8	9.0
E2		2:1	10.4	4.7
E3		10:1	10.6	1.2

As can be seen in Table 5-7, the concentration of Mo in samples are higher than expected, therefore, the ratios of ^{98}Mo and Th are not exactly reached as planned. However, the trends of the concentration are following the plan, that the concentrations of ^{98}Mo remain around 10 mmol/L in all of the nine samples, the concentration of Th progressively decreases in the three series.

5.3.2 ESI-measurement Results and discussion

The ESI-MS spectra of altogether 9 samples of the Mo-Th system are shown in Figure 5-6. The relative abundances of species are summarized in Table 5-8.

The three spectra in the upper row are 0.5 mol/L HNO_3 series. (sample **C1** [^{98}Mo] = 11.0 mmol/L, [Th] = 8.1 mmol/L, sample **C2** ([^{98}Mo] = 10.4 mmol/L, [Th] = 4.2 mmol/L and sample **C3** [^{98}Mo] = 10.7 mmol/L, [Th] = 1.1 mmol/L). In every of the spectra three types of species are detected, pure Mo species, pure Th species and mixed Mo-Th species.

The largest pure Mo polymer, which can be quantified, is the pentamer $[Mo_5O_{14}(OH)]^+$. The relative abundance of pentamers increases with decreasing Th amount in solution. Mo trimers $[Mo_3O_8(OH)]^+$ are the dominant pure Mo species (28.3% in **C1**, 30.5% in **C2** and 35.4% in **C3**, respectively) in all three samples. This is not similar with the result of pure Mo solutions without any Th (sample **M3**, see chapter 4.1.2, the dominant pure Mo species is pentameric with relative abundance of 27.3%), but rather resembles the result of sample **A1**, **A2** and **A3** in the Mo–Zr system, with the same acid strength as **C1**, **C2** and **C3**. The presence of Th in solution has an effect as of Zr in the Mo-Zr samples. Th suppresses the formation of large Mo species. The spectra of other two acidity series, 1 mol/L HNO_3 series and 3 mol/L HNO_3 series, are shown in middle row and bottom row of Figure 5-6, respectively. The dimers $[Mo_2O_5(OH)]^+$ and $[Mo_2O_5(NO_3)]^+$ become the dominant species at higher acidity (in **D1**, **D2**, **D3**, **E1**, **E2** and **E3**). The relative abundance of dimer increases with increasing acid strength of the samples (**C1** in comparison to **D1** and **E1**, **C2** in comparison to **D2** and **E2**, **C3** in comparison to **D3** and **E3**). The presence of Th leads to not only a lower abundance of large Mo polymeric species but also dimeric species. That means, the presence of Th suppresses the formation of pure Mo species.

In addition to the pure Mo species, pure Th species are detected in all of the nine samples. Th monomeric species are forming with different numbers of OH^- ligands $[Th(OH)_y(NO_3)_{3-y}]^+$ (y=0-3). In sample **C1** ([Th] = 8.1 mmol/L in 0.5 mol/L HNO_3), $[Th(NO_3)_3]^+$ (y=0, yellow, + 6 ~ 16 H_2O, m/q = 526.14 ~ 706.30) is by far the dominating solution species accounting for almost 50% of the thorium amount in solution. $[Th(NO_3)_3]^+$ predominate also in the other eight samples with > 50% of the [Th] concentration (see Table 5-8). For the samples **C1**, **D1** and **E1**, with Th concentrations

between 8.1 mmol/L ~ 9.0 mmol/L, the following trends for pure Th hydrolysis and polymerization are observed:

- The relative abundance of monomeric Th species increases with increasing acid strength. Less fractions of the complexes $[Th(OH)_y(NO_3)_{3-y}]^+$ are forming at high acidity (sample **C1** y = 0, 1, 2 and 3, sample **D1** y = 0, 1 and 2, sample **E1** y = 0 and 1).
- The largest and only Th polymers measured in the samples are dimers with various numbers of hydroxide ligands $[Th_2(OH)(NO_3)_6]^+$ and $[Th_2(OH)_2(NO_3)_5]^+$. The lower the acidity, the higher the abundance of Th-dimers.
- The relative abundance of pure Th species of total Th concentration increases with increasing acid strength.

For the samples **C2**, **D2** and **E2**, with Th concentrations between 4.2 mmol/L ~ 4.7 mmol/L:

- The relative abundance of monomeric Th species at $[HNO_3]$ = 3 mol/L (56.8%) is less than in **C2** (72.4%, $[HNO_3]$ = 0.5 mol/L) and **D2** (74.4%, $[HNO_3]$ = 1 mol/L). Less fraction of monomers complexes $[Th(OH)_y(NO_3)_{3-y}]^+$ are forming at high acidity (sample **C2** y = 0, 1, 2 and 3, sample **D2** y = 0, 1 and 2, sample **E2** y = 0 and 1).
- More dimers form at $[HNO_3]$ = 3 mol/L.
- The relative abundances of pure Th species of total Th concentration are similar. (**C2** 80.2%, **D2** 80.8% and **E2** 79.5%).

For the samples **C3**, **D3** and **E3**, with Th concentrations between 1.1 mmol/L ~ 1.2 mmol/L:

- The relative abundances of pure Th species of total Th concentration in sample **D3** and **E3** are similar, and higher than in sample **C3**. It follows the trends, that relative abundance of pure Th increases with increasing acid strength. (**C3** 62.5%, **D3** 77.1% and **E3** 77.8%).
- At this series, a higher fraction of $[Th(OH)_y(NO_3)_{3-y}]^+$ forms at high acidity. (sample **C3** y = 0 and 1, sample **D3** y = 0, 1 and 2, sample **E3** y = 0, 1, 2 and 3)
- No dimer is forming in sample **C3** and **D3**, at $[HNO_3]$ = 3 mol/L sample **E3** 8.6% dimers are forming in solution.

In the first (**C1**, **D1** and **E1**) and second (**C2**, **D2** and **E2**) series, Th(IV) monomeric species $[Th(OH)_y(NO_3)_{3-y}]^+$ form decreasing fractions with increasing acidity, the trend is in accordance with a ESI-MS study performed at [Th(IV)] = 6×10^{-6}–10^{-1} mol/L in HCl at $[H^+] = 10^{-4}$ – 0.1 mol/L [46]. Obviously, this is due to increasing concentration of HNO_3 in sample solution, less free OH^- ions are produced and more NO_3^- are present in the samples, which as competing ions of OH^-, lower fractions of the Th complex are forming. The third series (**C3**, **D3** and **E3**), with concentration ratios of Mo and Th of about 10 : 1, does not follow the trend as in pure Th(IV) solutions. It seems like, that the presence of Mo in solution has a strong influence on the formation of the

hydrolyzed species. The measurement by Walther *et al.* shows, that with decreasing acidity more polynuclear species of Th form [46]. These trends are observed in the first series ([Th] ≈ 9 mmol/L), but not in the ([Th] ≈ 4 mmol/L) and third series ([Th] ≈ 1 mmol/L). It seems, that the present of Mo in solution has also an influence on the formation of large Th polymers. That is to say, due to the presence of Mo in the Th solution, a higher fraction of Th monomeric species and larger amount of Th polymeric species are forming. For increasing acidity, Th tends to form pure Th species.

Moulin *et al.* [31] studied the hydrolysis of Th at [Th(IV)] = 10^{-3} mol/L in perchloric acid at pH = 0 – 3. At pH 0, the Th monomeric species $[Th(ClO_4)_3(H_2O)_3]^+$ and very weakly peak of $[Th(OH)(ClO_4)_2(H_2O)_3]^+$ are identified. At pH 1, $[Th(ClO_4)_3(H_2O)_3]^+$ still gives the most intense peaks in the mass spectra. The intensity of $[Th(ClO_4)_3(H_2O)_3]^+$ (ca. 5% of $[Th]^{4+}$) peak increases. Furthermore, in our work at similar Th concentration, the very weak peak of $[Th(OH)(NO_3)_2]^+$ can be observed at lower pH range and the relative abundance can be calculated (about 2% of total $[Th]^{4+}$ concentration at $[HNO_3]$ = 3 mol/L, pH -0.5; about 4% of total $[Th]^{4+}$ at $[HNO_3]$ = 1 mol/L, pH 0; about 5% of total $[Th]^{4+}$, at $[HNO_3]$ = 0.5 mol/L, pH 0.3). The result agrees very well with the study by Moulin [31] and shows the advantage of *nano* ESI-MS, that the minor species can be more simply observed and identified in the logarithmic scale.

Mixed species $[Mo_xTh_yO_z(OH)_a(NO_3)_b]^+$ (x = 1-3, y = 1-2 and z = 2, 5 and 8) are observed in all of the nine samples at three different acid strengths. At $[HNO_3]$ = 0.5 mol/L, the lowest acid strength in this work, $[ThMoO_2(OH)_a(NO_3)_b]^+$ (a = 3, b = 2, magenta and a = 2, b = 3, blue) are the dominant mixed species in samples **C1** (12.2% with respect to Mo, 6.9% with respect to Th), **C2** (7.4% with respect to Mo, 7.8% with respect to Th) and **C3** (3.7% with respect to Mo, 20.3% with respect to Th)**.** It is important to keep in mind that the relative abundance of species is calculated by multiplying the intensity of peak areas of the species (summing over all different numbers of water molecules) by weighting with the number of Mo or Th atoms in the species. In sample **C1**, for instance, $[Th_2MoO_2(OH)_4(NO_3)_5]^+$ has the relative abundance 6.1% with respect to Th, which is multiplying the weighting of Th (here 2). Therefore, the peak areas of $[Th_2MoO_2(OH)_4(NO_3)_5]^+$ (Figure 5-6, spectrum **C1**, magenta, + 8 ~ 14 H_2O, m/q = 1116~1224) are smaller than $[ThMoO_2(OH)_3(NO_3)_2]^+$ (Figure 5-6, spectrum **C1**, magenta + 8 ~ 14 H_2O, m/q = 638~785), which can be clearly see in the spectrum. No Mo (VI) monomeric species exist in the solution, which could form artefacts together with Th monomers in the same ESI droplet, therefor, the species $[ThMoO_2(OH)_a(NO_3)_b]^+$ is most likely a real solution species.

At $[HNO_3]$ = 1 mol/L, $[ThMoO_2(OH)_a(NO_3)_b]^+$ (a = 3, b = 2 and a = 2, b = 3) remain the dominant mixed species in samples **D1**, **D2** and **D3** as the samples at $[HNO_3]$ = 0.5 mol/L. The relative abundance of these dominant species decreases with increasing acid strength (see Table 5-8). At $[HNO_3]$ = 3 mol/L, $[ThMoO_2(OH)_a(NO_3)_b]^+$ are no more dominant in the samples, but rather $[ThMo_2O_5(OH)_a(NO_3)_b]^+$ (a = 3, b = 2

and a = 2, b = 3) (**E1**, 16.3% with respect to Mo, 3.1% with respect to Th; **E2**, 19.8% with respect to Mo, 7.8% with respect to Th; **E3**, 7.9% with respect to Mo, 13.5% with respect to Th). With increasing acid strength, Th and Mo form more species with ratio Th:Mo = 1:2. However, mixed Mo-Th species like $[ThMo_2O_5(OH)_3(NO_3)_2]^+$ at least partly formation during the measurement process cannot be fully excluded.

Unknown peaks, which are nearly in the m/q range 514 ~ 604 and plotted as red lines, are detected in all Mo-Th samples, but **C3**. The intensity of these peaks varies in different samples. For example, in sample **C1** and **D2** they have relatively high intensity as compared with in samples **E3**. The m/q value of the peak is very similar to $[^{208}Pb(NO_3)]2N^+$, however, by use of ICP-OES, the present of Pb in the sample is excluded. For the relative abundance of the species, this unknown peak is not included in the calculation.

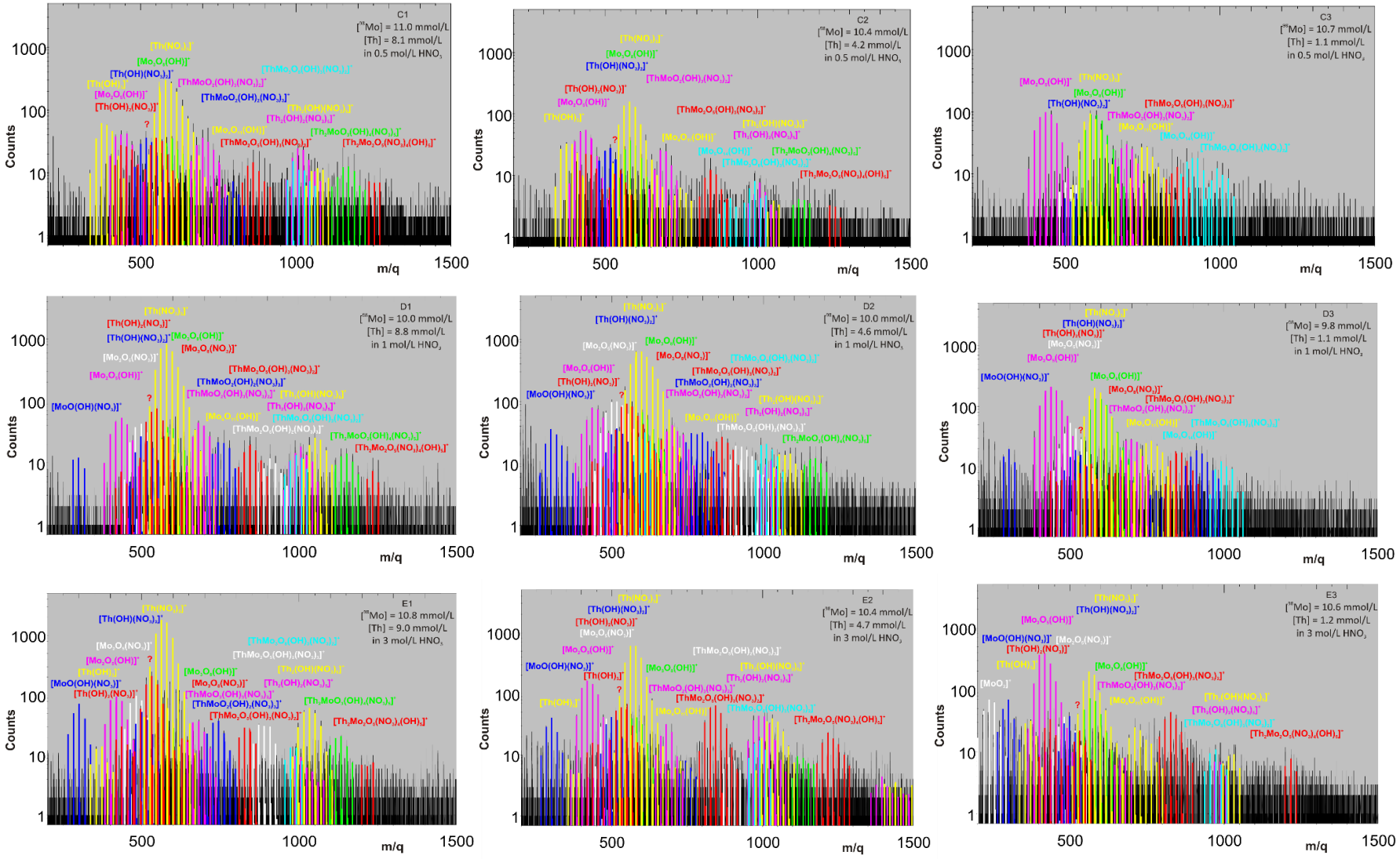

Figure 5-6: ESI-spectra of samples. UPPER ROW: **C1**, **C2** and **C3** (Mo-Th samples in 0.5 mol/L HNO_3); SECOND ROW: **D1**, **D2** and **D3** (Mo-Th samples in 1 mol/L HNO_3); THIRD ROW: **E1**, **E2** and **E3** (Mo-Th samples in 3 mol/L HNO_3). $[Th(NO_3)_3]^+$ (yellow) is by far the dominating solution species accounting for almost 50% of the all Th in sample solution. Mo and Th form two mixed Mo-Th species (1, 1) and (2, 1). The relative abundance of (1, 1) decreases with increasing acidity of the solution. (2, 1) increases with increasing solution acidity.

Table 5-8: Relative abundance of species in nine samples: **C1**, **C2** and **C3** (Mo-Th samples in 0.5 mol/L HNO_3); **D1**, **D2** and **D3** (Mo-Th samples in 1 mol/L HNO_3); **E1**, **E2** and **E3** (Mo-Th samples in 3 mol/L HNO_3). Pure Mo, pure Th and mixed Mo-Th species are formed. The relative abundance of pure Mo species are given with respect to Mo, pure Th species are with respect to Th and mixed species are with respect to Mo and Th respectively.

	Solution species	relative abundance in %																	
		0.5 mol/L HNO_3						1 mol/L HNO_3						3 mol/L HNO_3					
		C1 Mo:Th ratio 1:1		C2 Mo:Th ratio 2:1		C3 Mo:Th ratio 10:1		D1 Mo:Th ratio 1:1		D2 Mo:Th ratio 2:1		D3 Mo:Th ratio 10:1		E1 Mo:Th ratio 1:1		E2 Mo:Th ratio 2:1		E3 Mo:Th ratio 10:1	
		Mo	Th	Mo	Th	Mo	Th	Mo	Th	Mo	Th	Mo	Th	Mo	Th	Mo	Th	Mo	Th
Pure Mo species	$[Mo^{V}O_2]^+$																	3.3	
	$[Mo^{V}O(OH)(NO_3)]^+$							1.1		2.4		0.6		5.2		2.5		3.0	
	$[Mo_2O_5(OH)]^+$	21.5		29.3		22.5		17.3		13.5		28.9		19.9		32.6		49.5	
	$[Mo_2O_5(NO_3)]^+$							14.5		22.3		7.1		20.4		7.6		5.2	
	$[Mo_3O_8(OH)]^+$	28.3		30.5		35.3		20.6		19.6		33.5		15.0		13.3		17.0	
	$[Mo_3O_8(NO_3)]^+$							2.9		8.4		1.9		5.0					
	$[Mo_4O_{11}(OH)]^+$	6.2		7.7		16.2		2.5		4.0		10.8				3.9		9.7	
	$[Mo_5O_{14}(OH)]^+$			6.0		14.5						8.3							
Pure Th species	$[Th(NO_3)_3]^+$		49.4		51.2		60.7		69.5		68.8		68.3		78.4		53.6		51.4
	$[Th(OH)(NO_3)_2]^+$		4.9		7.3		1.8		3.8		2.7		3.2		1.9		3.2		6.8
	$[Th(OH)_2(NO_3)]^+$		3.4		5.2				1.9		2.9		5.6						5.7
	$[Th(OH)_3]^+$		7.4		8.7														5.3
	$[Th_2(OH)(NO_3)_6]^+$		4.6		2.1				6.0		4.2				8.1		10.8		5.4
	$[Th_2(OH)_2(NO_3)_5]^+$		9.9		5.6				4.2		2.3				1.5		11.9		3.2
Mixed species	$[ThMoO_2(OH)_3(NO_3)_2]^+$	10.5	6.0	7.4	7.8	3.7	20.3	8.0	3.7	4.3	4.0	2.2	10.2	4.5	1.7	3.1	2.5	0.6	1.9
	$[ThMoO_2(OH)_2(NO_3)_3]^+$	1.7	0.9					4.6	2.1	4.6	4.3			5.2	2.0				
	$[ThMo_2O_5(OH)_3(NO_3)_2]^+$	8.7	2.5	8.2	4.3	3.2	8.7	8.3	1.9	6.0	2.8	3.2	7.4	6.7	1.3	17.8	7.0	7.9	13.5
	$[ThMo_2O_5(OH)_2(NO_3)_3]^+$							5.5	1.3	5.8	2.7			9.6	1.8	2.0	0.8		
	$[ThMo_3O_8(OH)_3(NO_3)_2]^+$	14.0	2.7	7.6	2.7	4.6	8.5	8.9	1.4	7.6	2.4	3.5	5.3	5.2	0.7	6.5	1.7	2.8	3.2
	$[Th_2MoO_2(OH)_4(NO_3)_5]^+$	5.3	6.1	1.5	3.2			3.4	3.1	1.5	2.9			3.3	2.6		2.3		
	$[Th_2Mo_2O_5(OH)_5(NO_3)_4]^+$	3.8	2.2	1.8	1.9			2.4	1.1							10.7	6.2	1.0	3.6

5.3.3 Validation of existence of detected species by ESI-MS measurement

To validate ESI-MS measurement suitability for Mo-Th samples, Poisson's distribution calculation with a sticking factor, which was described in the chapter 5.2.3, is used. To note, that not the relative abundance of species but the normalized number of detected ions are used for this calculation.

Sample **C1** is used here as an example to analyze the Mo-Th system. In sample **C1** there are no Mo-monomers present in solution, Mo-dimers cannot be artefacts and similarly without monomers, trimers cannot be formed by adding one to a dimer. If the probability value equals or exceeds the amount of ion counts, artefacts cannot be ruled out. We infer for our sample **C1**, that Mo dimer, Mo trimer, Th monomer and mixed Mo-Th species $[ThMoO_2(OH)_a(NO_3)_b]^+$ (1, 1) and $[Th_2MoO_2(OH)_4(NO_3)_5]^+$ (2, 1) are highly likely that the species are actually present in solution and not only generated by the ESI process.

Moulin[31] described in his work, that at a pH range of 0 – 3 and [Th(IV)] = 10^{-3} mol/L Th polymerization is very unlikely to occur. This agrees with our Poisson's distribution calculation result, that the probability value of dimer (0.4049 ± 0.0085) is significantly higher than the amount of ion counts (0.0707 ± 0.0018). That means Th dimers are most likely artefacts by the ESI process. In addition, the calculation result shows that mixed Mo-Th species (1, 2) (1, 3) (2, 2) as artefacts cannot be ruled out.

Table 5-9: Amount of ion counts from ESI-MS measurements for each species in sample **C1** with the probability calculated from Poisson's distribution. If the calculated probability to find an artefact species is zero, the species must be present in solution. If the probability value equals or exceeds the amount of ion counts, artefacts cannot be ruled out.

solution species by ESI-MS measurement			Amount of ion counts from ESI-MS measurements	probability Poisson for artefact species
Pure Mo species	monomer	$[MoO_2(OH)]^+$	0	0
	dimer	$[Mo_2O_5(OH)]^+$, $[Mo_2O_5(NO_3)]^+$	0.0792 ± 0.0018	0.0001 ± 1.3·E-5
	trimer	$[Mo_3O_8(OH)]^+$, $[Mo_3O_8(NO_3)]^+$	0.0527 ± 0.0015	0.0024 ±0.0001
	tetramer	$[Mo_4O_{11}(OH)]^+$, $[Mo_4O_{11}(NO_3)]^+$	0.0086± 0.0006	0.0521 ± 0.0014
Pure Th species	monomer	$[Th(NO_3)_3]^+$, $[Th(OH)(NO_3)_2]$+, $[Th(OH)_2(NO_3)]^+$, $[Th(OH)_3]^+$	0.6363 ± 0.0067	0
	dimer	$[Th_2(OH)(NO_3)_6]^+$, $[Th_2(OH)_2(NO_3)_5]^+$	0.0707 ± 0.0018	0.4049 ± 0.0085
Mixed species	(1, 1)	$[ThMoO_2(OH)_3(NO_3)_2]^+$, $[ThMoO_2(OH)_2(NO_3)_3]^+$	0.0679 ± 0.0018	0
	(1, 2)	$[ThMo_2O_5(OH)_3(NO_3)_2]^+$	0.0244 ± 0.0010	0.0464 ± 1.3·E-3
	(1, 3)	$[ThMo_3O_8(OH)_3(NO_3)_2]^+$	0.0261 ± 0.0011	0.0335 ±1.0·E-3
	(2, 1)	$[Th_2MoO_2(OH)_4(NO_3)_5]^+$	0.0298 ± 0.0011	0
	(2, 2)	$[Th_2Mo_2O_5(OH)_5(NO_3)_4]^+$	0.0105 ± 0.007	0.0347 ± 0.002

5.3.4 Mo-Th mixed system Conclusion

Mixtures of Mo and Th in the concentration range of 1 mmol/L to 10 mmol/L in three different concentration of nitric acid ([HNO_3] = 0.5, 1 and 3 mol/L) is investigated by use of *nano* ESI-MS. The existence of detected species is validated by Poisson's distribution calculation. Pure Mo solution species are detected as monomer, dimer and polymer. The Mo polymers decrease in size with increasing acid strength, and the presence of Th suppresses the formation of pure Mo species and large Mo polymeric species. Validated by Poisson's distribution calculation, Th dimers are not present in solution, Th forms only monomers in this concentration and pH range as Moulin[31] described in his work. $[Th(NO_3)_3]^+$ is the predominant pure Th species. Mo and Th form two mixed Mo-Th species (1, 1) and (2, 1). The relative abundance of (1, 1) decreases with increasing acidity of the solution. Conversely, (2, 1) increases with increasing acidity. In all of the three different concentration ratios of Mo and Th, the relative abundance of mixed species (1, 1) and (2, 1) decreases with increasing acid strength. (for **C1**, **D1** and **E1**: relative abundance of mixed species 17.5%, 16% and 13.0%, for **C2**, **D2** and **E2**: relative abundance of mixed species 8.9%, 10.4% and 3.1%, for **C3**, **D3** and **E3**: relative abundance of mixed species 3.7%, 2.2% and 0.6%). That means, the high concentration of nitric acid can suppress the formation of mixed Mo-Th species.

5.4 Mo-Eu

The mixed system of ^{98}Mo and Eu(III) has been measured by use of *nano* ESI-MS [166], in order to investigate whether the Mo-Matrix forms mixed species with trivalent actinides from the fuel. Eu is used as analogue of trivalent actinides.

5.4.1 Sample preparation

Three europium stock solutions ([Eu(III)] = 0.5 mol/L, 0.25 mol/L and 0.05 mol/L) were prepared by dissolving weighed amounts of the Europium(III) nitrate pentahydrate ($Eu(NO_3)_3 \cdot 5H_2O$) (Sigma-Adrich, analytical grade) in 3 mol/L, 1 mol/L and 0.5 mol/L nitric acid, respectively. The mixed ^{98}Mo and Eu samples were prepared in three series in 3 mol/L, in 1 mol/L and in 0.5 mol/L nitric acid. Samples **M1** (10 mmol/L ^{98}Mo in 3 M HNO_3), **M2** (10 mmol/L ^{98}Mo in 1 M HNO_3), **M3** (10 mmol/L ^{98}Mo in 0.5 M HNO_3) were used as ^{98}Mo stock solution. For each series, there are three samples with different concentration ratios of Mo and Eu (1:1, 2:1 and 10:1), which were prepared by mixing appropriate amounts of stock solution of ^{98}Mo and stock solution of Eu (for 1:1 samples [Eu(III)] = 0.5 mol/L was used, for 2:1 samples [Eu(III)] = 0.25 mol/L was used and for 10:1 samples [Eu(III)] = 0.05 mol/L was used). The samples were measured normally on the same day by use of *nano* ESI-MS. No precipitates appeared in any of the nine samples. The concentration of ^{98}Mo and Eu were measured by ICP-MS and

summarized in Table 5-10.

Table 5-10: Summary of Mo-Eu samples examined by *nano* ESI-MS. Concentration ratios of ^{98}Mo and Eu and the concentrations in the samples respectively [166].

Sample ID	acid	planned concentration ratio ^{98}Mo: Eu	concentration of ^{98}Mo (mmol/L)	concentration of Eu (mmol/L)
F1	[HNO_3] = 0.5 mol/L	1:1	10.2	7.8
F2		2:1	10.2	3.9
F3		10:1	10.2	0.8
G1	[HNO_3] = 1 mol/L	1:1	9.4	8.0
G2		2:1	9.5	4.1
G3		10:1	9.5	0.8
H1	[HNO_3] = 3 mol/L	1:1	9.9	8.2
H2		2:1	9.8	4.2
H3		10:1	9.6	0.8

As can be seen in Table 5-10, the concentration of Eu in the samples are lower than expected, therefore, the ratios of ^{98}Mo and Eu are not exactly as planned. However, the trends of the concentration are in compliance with the plan, that the concentration of ^{98}Mo remain around 10 mmol/L in all of the nine samples, the concentration of Eu progressively decreasing in the three series.

5.4.2 Results and discussion

The ESI mass spectra of altogether 9 samples of the Mo-Eu system are shown in Figure 5-7. The relative abundances of species are summarized in Table 5-12.

The three spectra in the upper row are 0.5 mol/L HNO_3 series. (sample **F1** [Mo] = 10.2 mmol/L, [Eu] = 7.8 mmol/L, sample **F2** ([Mo] = 10.2 mmol/L, [Eu] = 3.9 mmol/L and sample **F3** [Mo] = 10.2 mmol/L, [Eu] = 0.8 mmol/L). In each of the spectra three types of species are detected, pure Mo species, pure Eu species and mixed Mo-Eu species.

The largest pure Mo polymer, which can be quantified, is the nonamer $[Mo_9O_{26}(OH)]^+$. The relative abundance of large pure Mo species increases with decreasing Eu amount in solution. Mo trimers $[Mo_3O_8(OH)]^+$ are the dominant pure Mo species (21.3% in **F1**, 23.3% in **F2** and 24.9% in **F3**, respectively) in all three samples. This is not similar with the result of pure Mo solutions without any addition of Eu, but rather similar with the result of sample **A1**, **A2** and **A3** in Mo-Zr system and **C1**, **C2** and **C3** in Mo-Th system, which are with same acid strength as **F1**, **F2** and **F3**. The presence of Eu in solution has similar effects of Zr and Th in the mixed system, suppresses the formation of larger Mo

species. The spectra of the other two acidity series, 1 mol/L HNO_3 series and 3 mol/L HNO_3 series, are shown in middle row and bottom row of Figure 5-7, respectively. More dimers $[Mo_2O_5(OH)]^+$ and $[Mo_2O_5(NO_3)]^+$ are formed in higher acidity (1 mol/L HNO_3) samples (**G1**, **G2**, and **G3**). Mo dimeric species get the dominant species in 3 mol/L HNO_3 samples (**H1**, **H2** and **H3**). More pure Mo species are formed in higher acid strength samples. The presence of Eu leads to a lower abundance of large Mo polymeric species and less pure Mo species.

In addition to the pure Mo species, pure Eu species are detected in all of the nine samples. $[Eu(NO_3)_2]^+$ (green peak in spectrum, Figure 5-7) is the dominating pure Eu species with different relative abundance (see Table 5-12) in the nine Mo-Eu mixed samples. In 3 mol/L HNO_3 (**H1**, **H2** and **H3**) samples a larger fraction of monomeric species are forming with different number of OH^- ligands $[Eu(OH)_y(NO_3)_{2-y}]^+$ (y=0-2). Table 5-11 summarizes the relative abundance of Eu monomeric, dimeric and trimeric species. The relative abundance of monomeric species, three fractions of monomeric species added together, increase with decreasing Eu concentration in the samples. Less polymeric species are detected with increasing nitride acid concentration.

Table 5-11: Relative abundance of pure Eu species in Mo-Eu system. Eu(III) and Eu(II) are detected. Eu(III) monomer are detected with different fraction $[Eu(OH)_y(NO_3)_{2-y}]^+$ (y=0-2), the relative abundance of monomer added together.

Pure Eu Solution species	**relative abundance in %**								
	0.5 mol/L HNO_3			**1 mol/L HNO_3**			**3 mol/L HNO_3**		
	F1	**F2**	**F3**	**G1**	**G2**	**G3**	**H1**	**H2**	**H3**
$[Eu(II)(NO_3)]^+$	1.2	2.5		5.9	6.3		12.8	16.6	20.6
Eu (III) monomer	31.7	32.8	100	35.9	55.8	76.0	61.7	61.2	74.9
Eu (III) dimer $[Eu_2(NO_3)_5]^+$	29.3	22.5		26.3	18.1		15.8	9.7	
Eu (III) trimer $[Eu_3(NO_3)_8]^+$	6.8			9.5			5.1	8.5	

Assuming that the europium nuclei in polymers are bridged by nitrates, the increase of the relative abundance of $[Eu_2(NO_3)_5]^+$ could be understood as a result of increasing acid concentration. However, as showed in Table 5-11 the relative abundance of $[Eu_2(NO_3)_5]^+$ decreases with increasing concentration of nitric acid. It suggests that Eu polymeric species might be artefacts, which are generated during the ESI process. The existence of Eu monomeric and polymeric species is validated by Poisson's distribution calculation and will be discussed in chapter 5.4.3.

A reduction to $[Eu(II)NO_3]^+$ is apparent in the Mo-Eu system, in spite of the oxidizing conditions in both, strong nitric acid and the nano-ESI needle tip. As described in chapter 5.1.2 the appearance of the reduced species in solution should not occur in the ESI positive mode. Reduced species of Lanthanides have been observed by Stewart [147] in ESI positive mode. As described in chapter 3.3, reduced species as illustrated by Stewart, does not generally originate from the ESI process, rather it tends to

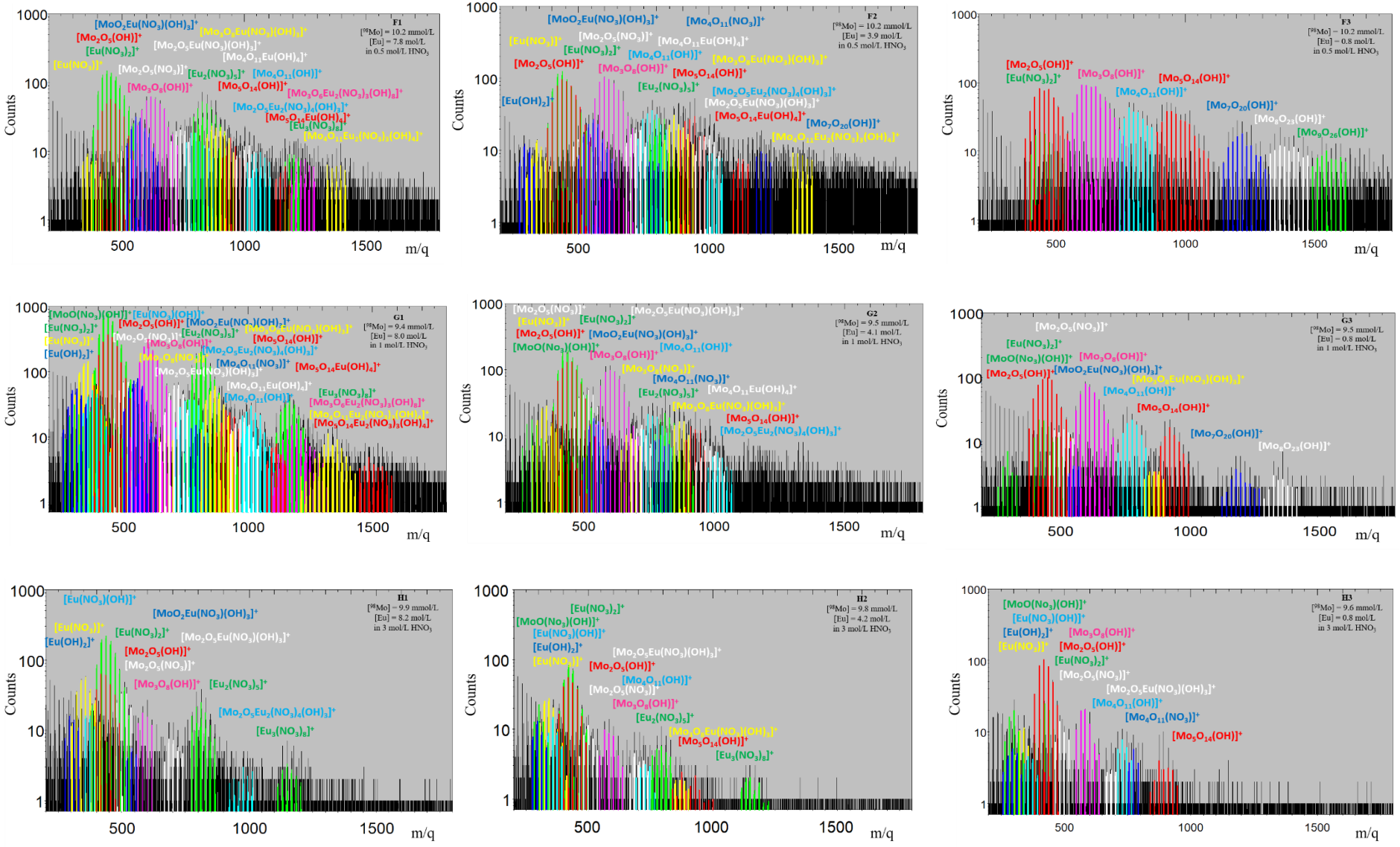

Figure 5-7: ESI-spectra of samples. Upper row: **F1**, **F2** and **F3** (Mo-Eu samples in 0.5 mol/L HNO_3); second row: **G1**, **G2** and **G3** (Mo-Eu samples in 1 mol/L HNO_3); third row: **H1**, **H2** and **H3** (Mo-Eu samples in 3 mol/L HNO_3) [166].

Table 5-12: Relative abundance of species in nine samples: **F1**, **F2** and **F3** (Mo-Eu samples in 0.5 mol/L HNO_3); **G1**, **G2** and **G3** (Mo-Eu samples in 1 mol/L HNO_3); **H1**, **H2** and **H3** (Mo-Eu samples in 3 mol/L HNO_3). Pure Mo, pure Eu and mixed Mo-Eu species are formed. The relative abundance of pure Mo species are given with respect to Mo, pure Eu species are with respect to Eu and mixed species are with respect to Mo and Eu respectively [166].

	Solution species	relative abundance in %																	
		0.5 mol/L HNO_3						1 mol/L HNO_3						3 mol/L HNO_3					
		F1 Mo:Eu ratio 1:1		F2 Mo:Eu ratio 2:1		F3 Mo:Eu ratio 10:1		G1 Mo:Eu ratio 1:1		G2 Mo:Eu ratio 2:1		G3 Mo:Eu ratio 10:1		H1 Mo:Eu ratio 1:1		H2 Mo:Eu ratio 2:1		H3 Mo:Eu ratio 10:1	
		Mo	Eu	Mo	Eu	Mo	Eu	Mo	Eu	Mo	Eu	Mo	Eu	Mo	Eu	Mo	Eu	Mo	Eu
Pure Mo species	$[Mo^{V}O_2]^+$																		
	$[Mo^{V}O(OH)(NO_3)]^+$																		
	$[Mo_2O_5(OH)]^+$	10.3		12.1		10.4		18.7		23.5		26.1		43.7		51.8		53.0	
	$[Mo_2O_5(NO_3)]^+$	1.2		1.5				3.5		8.5		3.9		20.7		8.9		5.8	
	$[Mo_3O_8(OH)]^+$	21.3		23.3		24.9		23.0		25.6		33.0		16.8		15.2		17.9	
	$[Mo_3O_8(NO_3)]^+$							0.9		2.6									
	$[Mo_4O_{11}(OH)]^+$	7.7		10.1		13.0		5.4		8.9		11.9				5.7		8.2	
	$[Mo_4O_{11}(NO_3)]^+$			1.6				1.5		2.7								4.7	
	$[Mo_5O_{14}(OH)]^+$	5.6		9.8		19.2		4.3		6.2		11.9				7.6		8.7	
	$[Mo_7O_{20}(OH)]^+$			3.1		12.4						5.3							
	$[Mo_8O_{23}(OH)]^+$					11.6						4.8							
	$[Mo_9O_{26}(OH)]^+$					8.5													
Pure Eu species	$[Eu(NO_3)]^+$		1.2		2.5				5.9		6.3				12.8		16.6		20.6
	$[Eu(OH)_2]^+$														2.5		5.7		13.0
	$[Eu(NO_3)(OH)]^+$														2.4		4.4		9.5
	$[Eu(NO_3)_2]^+$		31.7		32.8		100		35.9		55.8		76.0		56.8		51.1		52.4
	$[Eu_2(NO_3)_5]^+$		29.3		22.5				26.3		18.1				15.8		9.7		
	$[Eu_3(NO_3)_8]^+$		6.8						9.5						5.1		8.5		

Mixed species	$[MoO_2Eu(OH)_3(NO_3)]^+$	4.5	5.3	2.9	7.4		3.8	3.8	2.6	4.7	0.6	9.3	2.5	0.9				
	$[Mo_2O_5Eu(OH)_3(NO_3)]^+$	15.1	3.7	4.1	5.2		6.3	3.1	4.1	3.8			11.9	2.1	7.1	2.9	1.8	4.5
	$[Mo_2O_5Eu_2(OH)_3(NO_3)_4]^+$	5.8	5.2	2.0	5.1		4.2	4.2	7.1	4.3								
	$[Mo_3O_8Eu(OH)_3(NO_3)]^+$	5.9	5.8	11.1	9.5		9.9	3.3	2.4	4.3	2.7	14.8	4.4	1.5	3.6	1.0		
	$[Mo_3O_6Eu_2(OH)_8(NO_3)_3]^+$	8.4	4.5				5.0	3.3										
	$[Mo_4O_{11}Eu(OH)_4]^+$	4.6	2.4	8.7	5.6		5.1	1.3	5.8	2.7								
	$[Mo_4O_{11}Eu_2(OH)_3(NO_3)_2]^+$	3.1	3.4	5.8	7.3		2.3	0.9										
	$[Mo_5O_{14}Eu(OH)_4]^+$	6.4	0.7	3.9	2.0		1.6	0.3										
	$[Mo_5O_{14}Eu_2(OH)_4(NO_3)_3]^+$						4.5	2.2										

facilitate the transfer from pre-existing solutions. Hence, the reduction of Eu in Mo-Eu samples could be taking place already in solution.

A large number of mixed species $[Mo_xO_yEu_z(OH)_a(NO_3)_b]^+$ (x = 1-5, y = 2-14 and z = 1, 2) are detected in Mo-Eu system. In sample **F1**, **F2** (0.5 mol/L HNO_3) and **G1**, **G2** (1 mol/L HNO_3) Mo and Eu form several mixed species with different Mo:Eu ratios (x:z = 1:1, 2:1, 2:2, 3:1, 3:2, 4:1, 4:2, 5:1 and 5:2). In sample **G3** and 3 mol/L HNO_3 samples **H1**, **H2** and **H3** less mixed Mo-Eu are detected, and those have the low stoichiometric ratios 1 to 1 and 2 to 1. In sample **F3**, no mixed species are detected. As demonstrated in Figure 5-8, Mo-Eu mixed species with x:z ratios 2:1, 3:1 have the highest relative abundance. The overall trend for the mixed species is dependent on the ratio of Eu in the sample, and acid strength. At higher acidic strength, the mixed species distribution is rather simple. However, mixed Mo-Eu species at least partly formed during the measurement process cannot be fully excluded, Poisson's distribution calculation with a sticking factor is used by the Mo-Eu system to validate ESI-MS measurement suitability for Mo-Eu samples.

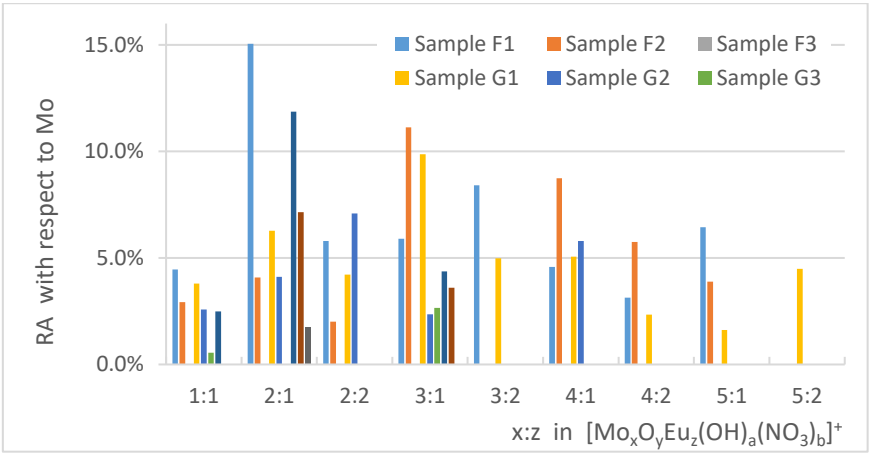

Figure 5-8: relative abundance of mixed Mo-Eu species with respect to Mo in samples **F1**, **F2**, **F3**, **G1**, **G2**, **G3**, **H1**, **H2** and **H3**. Mo and Eu form several mixed species with different Mo:Eu ratios (x:z = 1:1, 2:1, 2:2, 3:1, 3:2, 4:1, 4:2, 5:1 and 5:2). The species with x:z ratios 2:1, 3:1 have the highest relative abundance. No mixed species are detected in sample **F3**. With increasing acidic strength and decreasing Eu concentration in the samples, less mixed species are formed.

5.4.3 Validation of existence of detected species by ESI-MS measurement

In the case of europium, some species appeared likely to be concentration artefacts. In order to validate the existence of mixed Mo-Eu species, samples **F1** is used as an example to probe the Mo-Eu system by Poisson's distribution for quality control [166]. Table 5-13 shows the comparison of the amount of ion counts from the ESI measurements for each respective species with the probability calculated from Poisson's distribution to find two species in the same droplet by chance. It is found that the pure Eu polymer-species are very likely artefact species. If it is assumed that

nitrate is not coordinated in the first coordination sphere as discussed in chapter 5.2.2.1, the dominant pure Eu species $[Eu(NO_3)_2]^+$ in sample **F1** is free europium Eu^{3+}. This result is in good agreement with the species distribution, which is shown in Figure 2-8, only free europium Eu^{3+} present in solution below pH 5.5. ESI-MS shows the advantage, that not only the dominant species Eu^{3+}, but also minor species can be observed and identified.

The values of Mo species calculated by means of Poisson distribution are usually lower than the values of the measured data: the species are true solution species. Only with the tetramers and pentamers can a proportion of concentration artefacts not be completely ruled out. Most importantly, the mixed Mo-Eu species $MoO_2Eu(NO_3)(OH)_3^+$ is definitely a real solution species. The monomeric molybdenum (VI) species, which is required for an artefact species does not appear in the spectra. In the case of $Mo_2O_5Eu(NO_3)(OH)_3^+$ the situation is less clear. It cannot be ruled out that this species occurs at least partially as an artefact. The remaining mixed complexes, which according to Poisson should have lower probabilities to form in the ESI process, are likely to be true solution species.

Table 5-13: Comparison of the amount of ion counts from ESI measurement for each respective species with the probability for species to be artefacts, calculated from the Poisson distribution for sample **F1** (Mo: Eu=1:1) in 0.5 mol/L HNO_3. If the calculated probability is much lower than the number of ion counts for the respective species, it is highly likely, that the species is present in solution and not an artefact species.[166]

	solution species by ESI measurement		**Amount of ion counts from ESI measurements**	**probability Poisson for artefact species**
Pure Mo species	dimer	$[Mo_2O_5(OH)]^+$, $[Mo_2O_5](NO_3)^+$	0.1088	0.0000
	trimer	$[Mo_3O_8(OH)]^+$	0.0782	0.0000
	tetramer	$[Mo_4O_{11}(OH)]^+$	0.0168	0.0118
	pentamer	$[Mo_5O_{14}(OH)]^+$	0.0085	0.0085
Pure Eu species	monomer	$[Eu(NO_3)]^+$	0.3754	0.0000
	dimer	$[Eu_2(NO_3)_5]^+$	0.1298	0.1410
	Trimer	$[Eu_3(NO_3)_8]^+$	0.0314	0.0529
Mixed species	(1. 1)	$MoO_2Eu(NO_3)(OH)_3^+$	0.0572	0.0000
	(2. 1)	$Mo_2O_5Eu(NO_3)(OH)_3^+$	0.0402	0.0409
	(2. 2)	$Mo_2O_5Eu_2(NO_3)_4(OH)_3^+$	0.0279	0.0141
	(3. 1)	$Mo_3O_8Eu(NO_3)(OH)_3^+$	0.0627	0.0294
	(3. 2)	$Mo_3O_6Eu_2(NO_3)_3(OH)_8^+$	0.0242	0.0102

5.4.4 Mo-Eu mixed system Conclusion

In this system, europium was used as homologue for the trivalent actinides. Solutions with ^{98}Mo-metal in different concentrations and nitric acid concentrations were measured by use of ESI-MS. The relative abundance of large pure Mo species decreases with increasing Eu amount in solution. The appearance of europium polymer species in the mass spectra seem to arise as concentration artefacts in the ESI measurement process. $[Eu(NO_3)_2]^+$ is the predominant Eu species, in good agreement with the species distribution, which is shown in Figure 2-8, only free europium Eu^{3+} is present in solution below pH 5.5.

In addition, mixed Mo-Eu species are formed in the Mo-Eu mixtures. In the case of $MoO_2Eu(NO_3)(OH)_3^+$, it can be safely determined that these are not concentration artefacts and really exist in the solution. With other mixed complexes, it cannot be ruled out that at least some of the mixed complexes identified in the mass spectra result from concentration effects in the measurement process. The overall trend for the mixed species is dependent on the ratio of Eu in the sample, and acid strength. At higher acidic strength, the mixed species distribution is rather simple.

5.5 Comprehensive discussion of 4 mixed systems

The addition of Iron (III) nitrate leads to significant increase of the solubility of molybdenum and dissolution rate in nitric acid. The mixed species of Mo-Fe species (Mo, Fe 1, 1) and (Mo, Fe 2, 1) are directly observed by use of ESI-MS. In the 431 days aged solution, larger mixed Mo-Fe species formed and the relative abundance of all mixed species increases. The formation of mixed species could be not only leading to significantly increase the solubility of molybdenum and dissolution rate in nitric acid but also preventing the formation of precipitates. However, our investigations do still not show unequivocally whether this is the driving force in the enhancement of the dissolution kinetics of Mo metal, or it is the involvement of Fe(III) as redox partner.

In the other three mixed systems, mixed species are directly observed also. The influence of nitric acid concentration remains the way as in the pure Mo solution, higher acidic strengths lead to less large Mo polymeric species. The higher concentration of Zr(IV), Th(IV) and Eu(III) the less large Mo polymeric species are formed. In the Mo-Zr system, three mixed species are detected (Zr, Mo 1, 1), (Zr, Mo 1, 2) and (Zr, Mo 1, 3). Through the validation of Poisson's distribution calculation three mixed species are proven to be actual solution species. Larger amounts of mixed Mo-Zr species are formed in higher nitric acid concentration solutions. In the Mo-Th system, seven mixed species are detected, which have enough intensity peaks for the relative abundance calculation. By use of Poisson's distribution calculation two mixed Mo-Th species (Th, Mo 1, 1) and (Th, Mo 2, 1) are validated as actual solution species. The

relative abundance of mixed species decreases with increasing acid strength. That means, the high concentration of nitric acid can suppress the formation of mixed Mo-Th species. In the case of the Mo-Eu system, mixed Mo-Eu species with Mo: Eu ratios 1:1, 2:1 and 3:1 are likely to be true mixed solution species. The relative abundance of the mixed species Mo-Eu, decreases with increasing acid strength. The trend of the Mo-Zr system, higher nitric acid more mixed Mo-Zr species, is different from the other two systems Mo-Th and Mo-Eu. This could be due to the particularity of the ZMH precipitate precursors.

In all the mixed systems as well as pure Mo system, except Zr and Th, the other metals have been observed to a small extent in their reduced forms, such as Mo(V) of Mo(VI), Fe(II) of Fe(III), Eu(II) of Eu(III). Reduction is unlikely to occur in positive ionization mode of ESI-MS, even more since the voltage setting between the sampling plate and the skimmer were chosen in a very mild condition that the detected molecules remain in droplets of some 10–30 water molecules, this makes a CID process for the reduction of the metal cation rather unlikely. It seems to be related with reduced forms actually present in fresh solution. However, no reduction of Zr and Th is observed in the measurement, Zr and Th have one thing in common: the IV state is the only stable one. It is due to the one stable oxidation state, under the same setting of the orifice-skimmer region of the mass spectrometer, no reduced form is detected of Zr and Th. It is further verified our assumption, that reduced form metal could be not occur in the ESI process, rather take place already in solution.

6 Summary and Outlook

Dissolution behavior of Mo-CerMet fuel in reprocessing was investigated by use of *nano* ESI-MS. Pure Mo solution as well as 4 mixed systems (Mo-Fe, Mo-Zr, Mo-Th and Mo-Eu) solutions are qualitative and quantitative analyzed in 0.5 - 3 mol/L nitric acid. The sensitivity of the method combined with the ability to cover a large mass range at once is helpful to characterize all solution species in this very complicated system. Therefore, the sum formulas and relative abundances of many solution species can be investigated at the same time, even if the system of aqua Mo is rather complicated.

In the pure Mo solutions, Mo dimer is the dominant species in the sample of 1 mol/L and 3 mol/L nitric acid, pentameric $[Mo_5O_{14}(OH)]^+$ becomes the dominant species in the sample with 0.5 mol/L nitric acid. At lower acid concentration, the tendency towards formation of polymeric species increases. The solution species are measured during the dissolutions of the Mo pellet. With increasing concentration of Mo and increasing dissolution time, larger polymeric species form. The species distribution becomes more complicated during dissolution of the pellet, due to the increasing Mo concentration. There is no cationic hexameric Mo-species detected in any of the spectra. The possibility of the absence would be anionic hexameric species or neutral hexamers in solution present at the conditions of present investigation. Further investigation of Mo hexameric species are needed to fully understand this behavior.

As an inert matrix of Mo-cermet fuel, molybdenum is expected to be separated from nitric acid containing solution by reprocessing. For this process, each of the many species can exhibit a different behavior during liquid-liquid extraction steps. The solution with the simplest species distribution will be handled in liquid-liquid extraction most easily. Two effects in our investigation led to the more pronounced formation of larger cationic polymeric molybdenum species. First, a decrease in acid concentration to 0.5 mol/L leads to a higher abundance of larger polymers. The same is true for an increase of molybdenum concentration, as can be seen in the molybdenum pellet dissolution series. Therefore, higher acidic strengths and low Mo concentration are favorable to the reprocessing step.

In the study of Mo-Fe system, there is no significant change in the relative abundance trends compared to pure Mo samples, of the same concentration of nitric acid. Mo dimers are the dominant species. Two mixed Mo-Fe species (Mo, Fe 1, 1) and (Mo, Fe 2, 1) are formed. The formation of mixed Mo-Fe species could explain the enhanced dissolution kinetics of Mo in the presence of Fe(III). In the 431 days aged solution,

larger mixed Mo-Fe species formed: (Mo, Fe 3, 1) and (Mo, Fe 4, 1). The addition of Fe(III) nitrate not only lead to significantly increase of the solubility of molybdenum and dissolution rate in nitric acid but also the formation of Mo-Fe species prevents formation of precipitates.

In all of the three mixed system, Mo-Zr, Mo-Th and Mo-Eu, pure Mo species, pure Zr, Th or Eu species and mixed species are identified and quantified at the same time.

In the Mo-Zr system, the Mo polymers decrease in size with increasing acid strength, and the presence of Zr in solution leads to a decreasing fraction of large Mo polymeric species. Pentamers are no longer the dominant pure Mo species but Mo trimers. The predominance of tetramers $[Zr_4(OH)_8]^{8+}$ of Zr(IV) at pH = 0.3, log [Zr] in the range = -2 to -3 is in agreement with a recent review of Brown and Ekberg [89]. Three mixed Mo-Zr species (Mo, Zr 1, 1), (Mo, Zr 2, 1) and (Mo, Zr 3, 1), which are precursor of ZMH precipitates in nitric acid, are detected in each of the samples. Their relative abundance increases with increasing acidity of the solution and increasing concentration of Zr. Although in the higher acidic system ($[HNO_3]$ = 1 mol/L), the concentration of ZMH precursor is higher than in the $[HNO_3]$ = 0.5 mol/L system, after 200 days in the aged solution precipitates formed in 0.5 mol/L nitric acid samples, but no precipitates formed in 1 mol/L nitric acid samples. That is, the amount of ZMH precursor in solution depends on acid concentration, but the formation of ZMH precipitation does not depend on the amount of the precursor, but rather on the acid concentration. Therefore, to minimize the formation of ZMH in reprocessing, higher acid strength is more appropriate.

In the Mo-Th system, Mo polymers decrease in size with increasing acid strength, and the presence of Th suppresses the formation of pure Mo species and large Mo polymeric species. Th forms only monomers in the concentration range 1 mM to 10 mM and pH range of -0.5 to 0.3. This is in good agreement with literature. $[Th(NO_3)_3]^+$ is the predominate pure Th species. Mo and Th form two mixed Mo-Th species (1, 1) and (2, 1). The relative abundance of (1, 1) decreases with increasing acidity of the solution. Conversely, (2, 1) increases with increasing acidity. In all of the three different concentration ratios of Mo and Th, the relative abundance of mixed species (1, 1) and (2, 1) decreases with increasing acid strength. That means, the high concentration of nitric acid can suppress the formation of mixed Mo-Th species.

In the Mo-Eu system, the relative abundance of large pure Mo species decreases with increasing Eu amount in solution. The presence of Eu suppresses the formation of pure Mo species and large Mo polymeric species. $[Eu(NO_3)_2]^+$ is the predominant Eu species in the concentration range 1 mM to 10 mM and pH range of -0.5 to 0.3. Mixed Mo-Eu $MoO_2Eu(NO_3)(OH)_3^+$ is detected by ESI-MS and can be confirmed to really exist in the solution. At higher acidic strength, the mixed species distribution is rather simple.

Throughout the three mixed system, higher acidic strengths and the presence of Zr, Th or Eu suppresses the formation of pure Mo species and the formation of large Mo polymeric species. High concentration of nitric acid can suppress the formation of mixed Mo-Th species and mixed Mo-Eu species. In contrast, in higher concentration of nitric acid more mixed Mo-Zr species are formed. This could be due to the particularity of the ZMH precipitate precursors. For easier handling in liquid-liquid extraction, higher concentration of nitric acid is favorable to the reprocessing step.

The reduced forms of the metal, such as Mo(V) of Mo(VI), Fe(II) of Fe(III), Eu(II) of Eu(III), observed in the ESI-MS spectra are considered not to be caused by the ESI process but rather take place already in solution.

Since each species could behave differently in liquid-liquid extraction steps, solutions containing less different species are easier to be handled in reprocessing. Working at higher acid strengths could be advantageous for future reprocessing processes, as there are significantly fewer dissolution species in the system.

Due to the complexity of the Mo system the ESI measurement time is rather long, and routine measurements could be achieved in this work. More routine measurements could perform now with the availability of the much more sensitive orbitrap spectrometer in order to obtain more precise results. A further measurement of ^{98}Mo pellet dissolution in presence of Fe(lll) with ESI-MS will enabled a deeper understanding of the enhancement of Mo pellet dissolution kinetics by iron. Two possible reasons for the absence of Mo hexameric species are given in this work, for more understanding Quantum chemical calculation are being applied. In terms of high acid concentration and trace concentration of metal in the samples, a suitable method, such as hybrid ion trap MS, for species structure analyzes should be applied in the future.

References

[1] IAEA, NUCLEAR POWER REACTORS IN THE WORLD, INTERNATIONAL ATOMIC ENERGY AGENCY, VIENNA, 2018.

[2] IAEA, Global Energy and CO2 Status Report 2018, 2018.

[3] IAEA, NUCLEAR POWER REACTORS IN THE WORLD, VIENNA, 2017.

[4] G.I.I. Forum, A Technology Roadmap for Generation IV Nuclear Energy Systems, 2002.

[5] IAEA, Classification of Radioactive Waste, IAEA, Vienna, 2009.

[6] IAEA, Implications of Partitioning and Transmutation in Radioactive Waste Management, VIENNA, 2004.

[7] IAEA, Viability of inert matrix fuel in reducing plutonium amounts in reactors, (2006).

[8] C. Walther, From hydrolysis to the formation of colloids. Polymerization of tetravalent actinide ions, Forschungszentrum Karlsruhe, INE, Karlsruhe, 2008.

[9] Technology Roadmap Update for Generation IV Nuclear Energy Systems, Generation IV International Forum, 2014.

[10] NEA, Potential Benefits and Impacts of Advanced Fuel Cycles with Partitioning and Transmutation, in: OECD (Ed.), Nuclear Energy Agency of the OECD (NEA), France, 2011.

[11] M. Salvatores, G. Palmiotti, Radioactive waste partitioning and transmutation within advanced fuel cycles: Achievements and challenges, Progress in Particle and Nuclear Physics, 66 (2011) 144-166.

[12] W.D. Loveland, D.J. Morrissey, G.T. Seaborg, Modern nuclear chemistry, Second edition. ed., Wiley, Hoboken, NJ, USA, (2017), pp. xviii, 744 pages.

[13] NEA, Spent Nuclear Fuel Reprocessing Flowsheet, 2012.

[14] IAEA, Studies on fuels with low fission gas release. Proceedings of a technical committee meeting, International Atomic Energy Agency (IAEA), 1997.

[15] A. Fernandez, R.J.M. Konings, J. Somers, Design and fabrication of specific ceramic-metallic fuels and targets, Journal of Nuclear Materials, 319 (2003) 44-50.

[16] D. Haas, A. Fernandez, D. Staicu, J. Somers, W. Maschek, P. Liu, X. Chen, CERMET fuel behavior and properties in ADS reactors, Energ Convers Manage, 49 (2008) 1928-1933.

[17] J. Wallenius, Neutronic aspects of inert matrix fuels for application in ADS, Journal of Nuclear Materials, 320 (2003) 142-146.

[18] K. Bakker, F.C. Klaassen, R.P.C. Schram, A. Hogenbirk, R.K. Meulekamp, The use of molybdenum-based ceramic-metal (CerMet) fuel for the actinide management in LWRs, Nucl Technol, 146 (2004) 325-331.

[19] D. Haas, A. Fernandez, C. Nastren, D. Staicu, J. Somers, W. Maschek, X. Chen, Properties of cermet fuels for minor actinides transmutation in ADS, Energ Convers Manage, 47 (2006) 2724-2731.

[20] J. Wallenius, S. Pillon, L. Zaboudko, Fuels for accelerator-driven systems, Nucl Instrum Meth A, 562 (2006) 625-629.

[21] N. Ouvrier, H. Boussier, Recycling of MgO, Mo, & ZrO2 based actinide-bearing matrices: assessment of reprocessing feasibility & waste production, Procedia Chem, 7 (2012) 322-327.

[22] C. Ekberg, Y. Albinsson, M.J. Comarmond, P.L. Brown, Studies on the Complexation Behavior of Thorium(IV). 1. Hydrolysis Equilibria, J Solution Chem, 29 (2000) 63-86.

[23] M. Altmaier, X. Gaona, T. Fanghänel, Recent Advances in Aqueous Actinide Chemistry and Thermodynamics, Chem Rev, 113 (2013) 901-943.

[24] I.A. Dement'ev, A.O. Kozin, Y.V. Kondrat'ev, D.V. Korol'kov, A.A. Proyavkin, Mononuclear, polynuclear, and cluster complexes of molybdenum and their reactions as models of biochemical systems and processes, Russ J Gen Chem+, 77 (2007) 822-843.

[25] M. Yamashita, J.B. Fenn, Electrospray ion source. Another variation on the free-jet theme, The Journal of Physical Chemistry, 88 (1984) 4451-4459.

[26] J.B. Fenn, M. Mann, C.K. Meng, S.F. Wong, C.M. Whitehouse, Electrospray Ionization for Mass-Spectrometry of Large Biomolecules, Science, 246 (1989) 64-71.

[27] M.J. Keith-Roach, A review of recent trends in electrospray ionisation-mass spectrometry for the analysis of metal-organic ligand complexes, Anal Chim Acta, 678 (2010) 140-148.

[28] L.W. McDonald, J.A. Campbell, S.B. Clark, Failure of ESI Spectra to Represent Metal-Complex Solution Composition: A Study of Lanthanide-Carboxylate Complexes, Anal Chem, 86 (2014) 1023-1029.

[29] C. Walther, J. Rothe, M. Fuss, S. Buchner, S. Koltsov, T. Bergmann, Investigation of polynuclear Zr(IV) hydroxide complexes by nanoelectrospray mass-spectrometry combined with XAFS, Anal Bioanal Chem, 388 (2007) 409-431.

[30] C. Walther, M. Fuss, S. Buchner, H. Geckeis, Stability of Th(IV) polymers measured by electrospray mass spectrometry and laser-induced breakdown detection, J Radioanal Nucl Ch, 282 (2009) 1003-1008.

[31] C. Moulin, B. Amekraz, S. Hubert, V. Moulin, Study of thorium hydrolysis species by electrospray-ionization mass spectrometry, Anal Chim Acta, 441 (2001) 269-279.

[32] C. Walther, J. Rothe, B. Brendebach, M. Fuss, M. Altmaier, C.M. Marquardt, S. Buechner, H.R. Cho, J.I. Yun, A. Seibert, New insights in the formation processes of Pu(IV) colloids, Radiochim Acta, 97 (2009) 199-207.

[33] N.G. Tsierkezos, J. Roithová, D. Schröder, M. Ončák, P. Slavíček, Can Electrospray Mass Spectrometry Quantitatively Probe Speciation? Hydrolysis of Uranyl Nitrate Studied by Gas-Phase Methods, Inorg Chem, 48 (2009) 6287-6296.

[34] M. Steppert, C. Walther, Mass spectrometric characterization and quantification of Pu(VI) hydrolysis products, Radiochim Acta, 101 (2013) 307-311.

[35] D.K. Walanda, R.C. Burns, G.A. Lawrance, E.I. von Nagy-Felsobuki, Electrospray mass spectral study of isopolyoxomolybdates, J Chem Soc Dalton, (1999) 311-321.

[36] M.J. Deery, O.W. Howarth, K.R. Jennings, Application of electrospray ionisation mass spectrometry to the study of dilute aqueous oligomeric anions and their reactions, J Chem Soc Dalton, (1997) 4783-4788.

[37] H.N. Miras, E.F. Wilson, L. Cronin, Unravelling the complexities of inorganic and supramolecular self-assembly in solution with electrospray and cryospray mass spectrometry, Chem Commun, (2009) 1297-1311.

[38] M. Takahashi, Y. Abe, M. Tanaka, Elucidation of molybdosilicate complexes in the

molybdate yellow method by ESI-MS, Talanta, 131 (2015) 301-308.

[39] L. Vila-Nadal, E.F. Wilson, H.N. Miras, A. Rodriguez-Fortea, L. Cronin, J.M. Poblet, Combined Theoretical and Mass Spectrometry Study of the Formation-Fragmentation of Small Polyoxomolybdates, Inorg Chem, 50 (2011) 7811-7819.

[40] S. Hietanen, Studies on the Hydrolysis of Metal Ions. IX. The Hydrolysis of the Thorium Ion, Th4+. Acta Chem Scand, (1954) 1626-1642.

[41] S. Hietanen, L.G. Sillen, Studies on the Hydrolysis of Metal Ions-22 - Equilibrium Studies in Self-Medium - Application to the Hydrolysis of Th4+, Acta Chem Scand, 13 (1959) 533-550.

[42] C.F. Baes, R.E. Mesmer, The hydrolysis of cations, Wiley-Interscience, New York, (1976).

[43] J.J. Cruywagen, J.B.B. Heyns, E.F.C.H. Rohwer, Dimeric Cations of Molybdenum(VI), J Inorg Nucl Chem, 40 (1978) 53-59.

[44] J.J. Cruywagen, J.B.B. Heyns, Molybdenum(VI) equilibria at high perchloric acid concentration, Polyhedron, 19 (1999) 907-911.

[45] J.J. Cruywagen, A.G. Draaijer, J.B.B. Heyns, E.A. Rohwer, Molybdenum(VI) equilibria in different ionic media. Formation constants and thermodynamic quantities, Inorg Chim Acta, 331 (2002) 322-329.

[46] C. Walther, M. Fuss, S. Buchner, Formation and hydrolysis of polynuclear Th(IV) complexes - a nano-electrospray mass-spectrometry study, Radiochim Acta, 96 (2008) 411-425.

[47] C. Walther, J. Rothe, B. Schimmelpfennig, M. Fuss, Thorium nanochemistry: the solution structure of the Th(IV)-hydroxo pentamer, Dalton T, 41 (2012) 10941-10947.

[48] V. Neck, J.I. Kim, Solubility and hydrolysis of tetravalent actinides, Radiochim Acta, 89 (2001) 1-16.

[49] T. Fujii, H. Yamana, M. Watanabe, H. Moriyama, Extraction of molybdenum from nitric acid by octyl(phenyl)-N,N-diisobutylcarbamoylmethyl-phosphine oxide, Solvent Extr Ion Exc, 19 (2001) 127-141.

[50] A. Kumar, P.K. Mohapatra, P.N. Pathak, V.K. Manchanda, Extraction of Mo(VI) from nitric acid medium by di(octyl-phenyl) phosphoric acid, Solvent Extr Ion Exc, 19 (2001) 491-505.

[51] P. Tkac, A. Paulenova, Speciation of Molybdenum (VI) In Aqueous and Organic Phases of Selected Extraction Systems, Separation Science and Technology, 43 (2008) 2641-2657.

[52] K.Y.S. Ng, E. Gulari, Spectroscopic and Scattering Investigation of Isopoly-Molybdate and Tungstate Solutions, Polyhedron, 3 (1984) 1001-1011.

[53] J.M. Coddington, M.J. Taylor, Mo-95 Nuclear Magnetic-Resonance and Vibrational Spectroscopic Studies of Molybdenum(VI) Species in Aqueous-Solutions and Solvent Extracts from Hydrochloric and Hydrobromic Acid - Evidence for the Complexes [Mo2O5(H2O)6]2+, [MoO2X2(H2O)2] (X = Cl or Br), and [MoO2Cl4]2-, J Chem Soc Dalton, (1990) 41-47.

[54] C. Knobler, B.R. Penfold, W.T. Robinson, C.J. Wilkins, S.H. Yong, Molybdenum(Vi) Complexes from Diols and Aminoalcohols - Occurrence of Moo2, Mo2o3, and Mo2o5 Core Structures, J Chem Soc Dalton, (1980) 248-252.

[55] N.L. Banik, S. Büchner, R. Burakham, M. Fuss, F. Geyer, H. Geckeis, M. Lagos, C.M. Marquardt, C. Walther, B. Kuczewski, J. Aupiais, N. Baglan, S. Topin, A.G. Maslennikov, Annual Report 2009, Institut für Nukleare Entsorgung, 2009, pp. 81-84.

[56] F. Chauveau, P. Souchay, G. Tridot, Etude Des Composes Permolybdiques, B Soc Chim Fr, (1955) 1519-1524.

[57] F. Chauveau, Sur Les Composes De Movl Et Des Acides Chlorhydrique Et Sulfurique Concentres, Cr Hebd Acad Sci, 242 (1956) 2154-2157.

[58] Krumenac.L, Very Acidic Sodium Molybdate Solutions by Ultraviolet Spectrophotometry .4. New Interpretation of Measurements - Very Dilute Solutions, B Soc Chim Fr, (1971) 2820-&.

[59] Krumenac.L, Study of Highly Acidic Sodium Molybdate Solutions by Ultraviolet Absorption Spectrophotometry .3. Influence of Acidity on Absorption Spectrum of Dimeric Form Predominant in Concentrated Molybdate Solutions, B Soc Chim Fr, (1971) 362-&.

[60] M.T. Paffett, F.C. Anson, Electrochemical Generation of Monomeric Aquamolybdenum(V) by Reduction of Molybdenum(Vi) at High Dilution in Trifluoromethanesulfonic Acid, Inorg Chem, 20 (1981) 3967-3972.

[61] J. F. Ojo, R.S. Taylor, A.G. Sykes, Kinetics of the Rapid Monomer-Dimer Equilibration of Molybdenum(VI) in Aqueous Perchloric Acid Solutions Journal of the Chemical Society, Dalton Transactions, (1975) 500-505.

[62] J.J. Cruywagen, Protonation, Oligomerization, and Condensation Reactions of Vanadate(V), Molybdate(VI), and Tungstate(VI), 49 (1999) 127-182.

[63] S. Himeno, M. Hasegawa, Raman-Spectroscopic Evidence of Dimeric Molybdenum(VI) Species in Acidic Solutions, Inorg Chim a-Art Let, 83 (1984) L5-L6.

[64] J.J. Cruywagen, J.B.B. Heyns, Equilibria and Uv Spectra of Mononuclear and Polynuclear Molybdenum(VI) Species, Inorg Chem, 26 (1987) 2569-2572.

[65] M.-S. Lee, S.-H. Sohn, M.-H. Lee, Ionic Equilibria and Ion Exchange of Molybdenum(VI) from Strong Acid Solution, Bulletin of the Korean Chemical Society, 32 (2011) 3687-3691.

[66] E. Esbelin, P. Gareil, M. Masson, J.L. Emin, Investigation of Mo(VI) monomer-dimer equilibrium in highly acidic solutions by UV absorbance spectroscopy using refined numerical processing, Anal Chim Acta, 433 (2001) 299-310.

[67] Z.H. Zhou, H.L. Wan, K.R. Tsai, Molybdenum(VI) complex with citric acid: Synthesis and structural characterization of 1:1 ratio citrate molybdate K2Na4[(MoO2)(2)O(cit)(2)]center dot 5H(2)O, Polyhedron, 16 (1997) 75-79.

[68] F.A. Cotton, J.S. Wood, S.M. Morehouse, Identification + Characterization by X-Ray Diffraction of New Binuclear Molybdenum(6) Oxalate Complex, Inorg Chem, 3 (1964) 1603-&.

[69] K. Yokoi, N. Matsubayashi, T. Miyanaga, I. Watanabe, K. Murata, S. Ikeda, Studies on the Structure of Cationic Dimer of Molybdenum(VI) in Acidic Solution by Xanes and Exafs, Chem Lett, (1987) 1453-1456.

[70] K. Yokoi, N. Matsubayashi, T. Miyanaga, I. Watanabe, S. Ikeda, Studies on the Structure of Molybdenum(Vi) in Acidic Solution by Xanes and Exafs, Polyhedron, 12 (1993) 911-914.

[71] T. Sato, H. Watanabe, H. Suzuki, Liquid-Liquid-Extraction of Molybdenum(Vi) from Aqueous Acid-Solutions by Tbp and Topo, Hydrometallurgy, 23 (1990) 297-308.

[72] S.P. Vorobev, I.P. Davydov, I.V. Shilin, Russ. J. Inorg. Chem., 12 (1967) 1129-1132.

[73] P.J. Coope, W.P. Thistlethwaite, The Absorption Spectra of Acidified Molybdate Solutions, J Inorg Nucl Chem, 2 (1956) 125-127.

[74] D. Gras, K. H. Tytko, Gmelin Handbook of Inorganic and Organometallic Chemistry, Springer, Berlin, (1989).

[75] F. Jalilehvand, V. Mah, B.O. Leung, D. Ross, M. Parvez, R.F. Aroca, Structural characterization of Molybdenum(V) species in aqueous HCl solutions, Inorg Chem, 46 (2007) 4430-4445.

[76] M. Ardon, A. Pernick, Molybdenum(V) in Aqueous-Solution, Inorg Chem, 12 (1973) 2484-2485.

[77] S. Himeno, M. Hasegawa, Raman Studies on Molybdenum(V) Species in HCl Solutions, Inorg Chim a-Art Let, 83 (1984) L17-L18.

[78] S. Himeno, A. Saito, M. Hasegawa, Polarographic and Spectrophotometric Studies on the Equilibration of Mo(V) Species in HCl Solutions, Inorg Chim a-Art Let, 88 (1984) 93-98.

[79] W.W. Schulz, E.M. Duke, Reprocessing of low-enrichment uranium-molybdenum alloy fuels, (1959).

[80] L.M. Ferris, Aqueous processes for dissolution of uranium-molybdenum alloy reactor fuel elements (1961).

[81] W.W. Schulz, E.M. Duke, R.E. Burns, Nitric Acid Dissolution of Uranium-Molybdenum Alloy Reactor Fuels, Ind Eng Chem Proc Dd, 1 (1962) 156-160.

[82] P.A. Anderson, Laboratory Simulation of High-Level Liquid Waste Evaporation and Storage, Nucl Technol, 47 (1980) 173-180.

[83] L.M. Ferris, Aqueous processes for dissolution of uranium-molybdenum alloy reactor Fuel Elements, Ind Eng Chem, 53 (1961) 279-281.

[84] M. Gledhill, Electrospray ionisation-mass spectrometry of hydroxamate siderophores, Analyst, 126 (2001) 1359-1362.

[85] I. Spasojevic, H. Boukhalfa, R.D. Stevens, A.L. Crumbliss, Aqueous solution speciation of Fe(III) complexes with dihydroxamate siderophores alcaligin and rhodotorulic acid and synthetic analogues using electrospray ionization mass spectrometry, Inorg Chem, 40 (2001) 49-58.

[86] R. Rellan-Alvarez, J. Abadia, A. Alvarez-Fernandez, Formation of metal-nicotianamine complexes as affected by pH, ligand exchange with citrate and metal exchange. A study by electrospray ionization time-of-flight mass spectrometry, Rapid Commun Mass Sp, 22 (2008) 1553-1562.

[87] G. Weber, N. von Wiren, H. Hayen, Analysis of iron (II)/iron(III) phytosiderophore complexes by nano-electrospray ionization Fourier transform ion cyclotron resonance mass spectrometry, Rapid Commun Mass Sp, 20 (2006) 973-980.

[88] T.K. Sham, J.B. Hastings, M.L. Perlman, Structure and Dynamic Behavior of Transition-Metal Ions in Aqueous-Solution - an Exafs Study of Electron-Exchange Reactions, J Am Chem Soc, 102 (1980) 5904-5906.

[89] P. Brown, C. Ekberg, Hydrolysis of Metal Ions, Wiley-VCH Verlag GmbH & Co. KGaA, Weinheim, (2016).

[90] A. Stefansson, Iron(III) hydrolysis and solubility at 25 degrees C, Environ Sci Technol, 41 (2007) 6117-6123.

[91] H.R. Cho, C. Walther, J. Rothe, V. Neck, M.A. Denecke, K. Dardenne, T. Fanghanel, Combined LIBD and XAFS investigation of the formation and structure of Zr(IV) colloids, Anal Bioanal Chem, 383 (2005) 28-40.

[92] J.I. Yun, H.R. Cho, V. Neck, M. Altmaier, A. Seibert, C.M. Marquardt, C. Walther, T. Fanghanel, Investigation of the hydrolysis of plutonium(IV) by a combination of spectroscopy and redox potential measurements, Radiochim Acta, 95 (2007) 89-95.

[93] C. Ekberg, G. Kallvenius, Y. Albinsson, P.L. Brown, Studies on the hydrolytic behavior of zirconium(IV), J Solution Chem, 33 (2004) 47-79.

[94] T. Sasaki, T. Kobayashi, I. Takagi, H. Moriyama, Solubility measurement of zirconium(IV) hydrous oxide, Radiochim Acta, 94 (2006) 489-494.

[95] A. Clearfield, P.A. Vaughan, The Crystal Structure of Zirconyl Chloride Octahydrate and Zirconyl Bromide Octahydrate, Acta Crystallogr, 9 (1956) 555-558.

[96] A.J. Zielen, R.E. Connick, The Hydrolytic Polymerization of Zirconium in Perchloric Acid Solutions, J Am Chem Soc, 78 (1956) 5785-5792.

[97] G.M. Muha, P.A. Vaughan, Structure of the Complex Ion in Aqueous Solutions of Zirconyl and Hafnyl Oxyhalides, J Chem Phys, 33 (1960) 194-199.

[98] M. Aberg, X-Ray Investigation of Some Aqueous Zirconium(IV) Halide, a Hafnium(Iv) Chloride, and Some Zirconium(IV) Perchlorate Solutions, Acta Chem Scand A, 31 (1977) 171-181.

[99] J. Rose, T.J.M. De Bruin, G. Chauveteau, R. Tabary, J.L. Hazemann, O. Proux, A. Omari, H. Toulhoat, J.Y. Bottero, Aqueous zirconium complexes for gelling polymers. A combined X-ray absorption spectroscopy and quantum mechanical study, J Phys Chem B, 107 (2003) 2910-2920.

[100] C. Hagfeldt, V. Kessler, I. Persson, Structure of the hydrated, hydrolysed and solvated zirconium(IV) and hafnium(IV) ions in water and aprotic oxygen donor solvents. A crystallographic, EXAFS spectroscopic and large angle X-ray scattering study, Dalton T, (2004) 2142-2151.

[101] P.L. Brown, Chemical hemical thermodynamics of zirconium OECD Nuclear Energy Agency, Issy-les-Moulineaux, France, 2005.

[102] PSI, The PSI/Nagra Chemical Thermodynamic, Switzerland, 2014.

[103] M. Wickleder, B. Fourest, P. Dorhout, Thorium, The Chemistry of the Actinide and Transactinide Elements, Springer, Dordrecht, 2006.

[104] R.D. Shannon, Revised Effective Ionic-Radii and Systematic Studies of Interatomic Distances in Halides and Chalcogenides, Acta Crystallogr A, 32 (1976) 751-767.

[105] V. Neck, J.I. Kim, An electrostatic approach for the prediction of actinide complexation constants with inorganic ligands-application to carbonate complexes, Radiochim Acta, 88 (2000) 815-822.

[106] G.L. Johnson, L.M. Toth, Plutonium(IV) and thorium(IV) hydrous polymer chemistry, Technicalreport TM-6365, (1978).

[107] C. Ekberg, P. Brown, J. Comarmond, Y. Albinsson, On the hydrolysis of tetravalent metal ions, Scientific Basis for Nuclear Waste Management Xxiv, 663 (2000) 1091-1099.

[108] G. Johannson, The Structure of a dinuclear hydroxo complex of thorium, Acta Chemica Scandinavica 22 (1968) 389-398.

[109] R.E. Wilson, S. Skanthakumar, G. Sigmon, P.C. Burns, L. Soderholm, Structures of dimeric hydrolysis products of thorium, Inorg Chem, 46 (2007) 2368-2372.

[110] M. Osaka, M. Koi, S. Takano, Y. Yamane, T. Misawa, A novel concept for americium-

containing target for use in fast reactors, J Nucl Sci Technol, 43 (2006) 367-374.

[111] V. Neck, T. Fanghänel, J.I. Kim, Aquatische Chemie und thermodynamische Modellierung von trivalenten Actiniden, 1998.

[112] N. Wiberg, A. Holleman, E. Wiberg, Lehrbuch der Anorganischen Chemie, Walter de Gruyter, Berlin, New York, (2007).

[113] B. Ribar, A. Kapor, G. Argay, A. Kalman, Tetraaquatrinitratoeuropium(III) monohydrate, Acta Crystallographica Section C, 42 (1986) 1450-1452.

[114] Y. Suzuki, T. Nankawa, T. Yoshida, T. Ozaki, T. Ohnuki, A.J. Francis, S. Tsushima, Y. Enokida, I. Yamamoto, Biodegradation of Eu(III)-citrate complexes by Pseudomonas fluorescens, J Radioanal Nucl Ch, 266 (2005) 199-204.

[115] E. Bentouhami, G.M. Bouet, J. Meullemeestre, F. Vierling, M.A. Khan, Physicochemical study of the hydrolysis of Rare-Earth elements (III) and thorium (IV), Cr Chim, 7 (2004) 537-545.

[116] M. Jimenez-Reyes, M. Solache-Rios, A. Rojas-Hernandez, Behaviour of europium (III) and its hydroxo and carbonate complexes in a solvent extraction system with HDBM in 2 M NaCl at 303 K, Radiochim Acta, 87 (1999) 125-133.

[117] D.L. Clark, D.E. Hobart, M.P. Neu, Actinide Carbonte Complexes and Their Importance in Actinide Environmental Chemistry, Chem Rev, 95 (1995) 25-48.

[118] M.H. Lloyd, Instabilities and Solids Formation in Lwr Reprocessing Solutions, T Am Nucl Soc, 24 (1976) 233-234.

[119] R.A. Penneman, R.G. Haire, M.H. Lloyd, Polymolybdates as plutonium (IV) hosts, American Chemical Society; Washington, DC(1980), pp. 571-581.

[120] A. Clearfield, R.H. Blessing, Preparation and Crystal-Structure of a Basic Zirconium Molybdate and Its Relationship to Ion-Exchange Gels, J Inorg Nucl Chem, 34 (1972) 2643-2663.

[121] H. Kleykamp, J.O. Paschoal, R. Pejsa, F. Thummler, Composition and Structure of Fission-Product Precipitates in Irradiated Oxide Fuels - Correlation with Phase Studies in the Mo-Ru-Rh-Pd and BaO-UO2-ZrO2-MoO2 Systems, Journal of Nuclear Materials, 130 (1985) 426-433.

[122] B.S.M. Rao, E. Gantner, H.G. Muller, J. Reinhardt, D. Steinert, H.J. Ache, Solids Formation from Synthetic Fuel-Reprocessing Solutions - Characterization of Zirconium Molybdate by ICP, XRF, and Raman Microprobe Spectroscopy, Appl Spectrosc, 40 (1986) 330-336.

[123] K. Gonda, K. Oka, T. Nemoto, Characteristics and Behavior of Emulsion at Nuclear-Fuel Reprocessing, Nucl Technol, 57 (1982) 192-202.

[124] T. Usami, T. Tsukada, T. Inoue, N. Moriya, T. Hamada, D. Serrano Purroy, R. Malmbeck, J.P. Glatz, Formation of zirconium molybdate sludge from an irradiated fuel and its dissolution into mixture of nitric acid and hydrogen peroxide, Journal of Nuclear Materials, 402 (2010) 130-135.

[125] L. Zhang, Takeuchi, M., Koizumi, T., Hirasawa I. , Evaluation of precipitation behavior of zirconium molybdate hydrate, Frontiers of Chemical Science and Engineering, 7 (2013) 65-71.

[126] B.S.M. Rao, E. Gantner, J. Reinhardt, D. Steinert, H.J. Ache, Characterization of the Solids Formed from Simulated Nuclear-Fuel Reprocessing Solutions, Journal of Nuclear Materials, 170 (1990) 39-49.

[127] T. Izumida, F. Kawamura, Precipitates Formation Behavior in Simulated High Level Liquid Waste of Fuel Reprocessing, J Nucl Sci Technol, 27 (1990) 267-274.

[128] C.S. Lin, Wang, X. Y., Zhang, C. H., Study of precipitation behavior of Mo and Zr in nitric acid solution. Journal of Nuclear Radiochemistry, Journal of Nuclear and Radiochemistry, 14 (1992).

[129] D. Zhu, C.S. Lin, Study of solubiluty product on precipitate of molybdenum and zirconium in nitric acid, Journal of Nuclear and Radichemistry, 24 (2002) 77-83.

[130] A. Magnaldo, M. Masson, R. Champion, Nucleation and crystal growth of zirconium molybdate hydrate in nitric acid, Chemical Engineering Science, 62 (2007) 766-774.

[131] F.J. Doucet, D.T. Goddard, C.M. Taylor, I.S. Denniss, S.M. Hutchison, N.D. Bryan, The formation of hydrated zirconium molybdate in simulated spent nuclear fuel reprocessing solutions, Physical Chemistry Chemical Physics, 4 (2002) 3491-3499.

[132] X.G. Liu, J. Chen, Y.C. Zhang, J.C. Wang, Precipitation of zirconium and molybdenum in simulated high-level liquid waste concentration and denitration process, Procedia Chem, 7 (2012) 575-580.

[133] N. Paul, R.B. Hammond, T.N. Hunter, M. Edmondson, L. Maxwell, S. Biggs, Synthesis of nuclear waste simulants by reaction precipitation: Formation of caesium phosphomolybdate, zirconium molybdate and morphology modification with citratomolybdate complex, Polyhedron, 89 (2015) 129-141.

[134] C. Fourdrin, S. Esnouf, V. Dauvois, J.P. Renault, L. Venault, M. Tabarant, D. Durand, A. Cheniere, C. Lamouroux-Lucas, F. Cochin, Irradiation effects in hydrated zirconium molybdate, Journal of Nuclear Materials, 426 (2012) 38-44.

[135] T. Bergmann, T.P. Martin, H. Schaber, High-Resolution Time-of-Flight Mass Spectrometers: Part I. Effects of Field Distortions in the Vicinity of Wire Meshes, Rev Sci Instrum, 60 (1989) 347-349.

[136] T. Bergmann, H. Goehlich, T.P. Martin, H. Schaber, G. Malegiannakis, High-Resolution Time-of-Flight Mass Spectrometers. Part II. Cross Beam Ion Optics, Rev Sci Instrum, 61 (1990) 2585-2591.

[137] T. Bergmann, T.P. Martin, H. Schaber, High-Resolution Time-of-Flight Mass Spectrometers. Part III. Reflector Design, Rev Sci Instrum, 61 (1990) 2592-2600.

[138] M.S. Wilm, M. Mann, Electrospray and Taylor-Cone Theory, Doles Beam of Macromolecules at Last, Int J Mass Spectrom, 136 (1994) 167-180.

[139] I.I. Stewart, Electrospray mass spectrometry: a tool for elemental speciation, Spectrochimica Acta Part B-Atomic Spectroscopy, 54 (1999) 1649-1695.

[140] M. Dole, L.L. Mack, R.L. Hines, Molecular Beams of Macroions, J Chem Phys, 49 (1968) 2240-&.

[141] H.M. Dole, Bridging Gas Gap, Am Gas Assoc Mon, 52 (1970) 34-&.

[142] J.V. Iribarne, B.A. Thomson, Evaporation of Small Ions from Charged Droplets, J Chem Phys, 64 (1976) 2287-2294.

[143] B.A. Thomson, J.V. Iribarne, Field-Induced Ion Evaporation from Liquid Surfaces at Atmospheric-Pressure, J Chem Phys, 71 (1979) 4451-4463.

[144] P. Kebarle, A brief overview of the present status of the mechanisms involved in electrospray mass spectrometry, J Mass Spectrom, 35 (2000) 804-817.

[145] M. Gamero-Castano, J.F. de la Mora, Mechanisms of electrospray ionization of singly and multiply charged salt clusters, Anal Chim Acta, 406 (2000) 67-91.

[146] G.R. Agnes, G. Horlick, Effect of Operating Parameters on Analyte Signals in Elemental Electrospray Mass Spectrometry, Appl Spectrosc, 49 (1995) 324-334.

[147] I.I. Stewart, G. Horlick, Developments in the electrospray mass spectrometry of inorganic species, Trac-Trend Anal Chem, 15 (1996) 80-90.

[148] E.d. Hoffmann, V. Stroobant, Mass Spectrometry, John Wiley & Sons Ltd, Chichester, England, (2007).

[149] R.J. Cotter, The new time-of-flight mass spectrometry, Anal Chem, 71 (1999) 445a-451a.

[150] M.S. Espinosa, R. Servant, P.A. Babay, Study of metal-ligand species by ESI-MS: The case of La, Nd and Th complexes with EDTA, Microchem J, 129 (2016) 151-157.

[151] D. Schroder, Ion clustering in electrospray mass spectrometry of brine and other electrolyte solutions, Physical Chemistry Chemical Physics, 14 (2012) 6382-6390.

[152] J.M. Daniel, S.D. Friess, S. Rajagopalan, S. Wendt, R. Zenobi, Quantitative determination of noncovalent binding interactions using soft ionization mass spectrometry, Int J Mass Spectrom, 216 (2002) 1-27.

[153] A.T. Blades, P. Jayaweera, M.G. Ikonomou, P. Kebarle, Ion-Molecule Clusters Involving Doubly Charged Metal-Ions (M2+), International Journal of Mass Spectrometry and Ion Processes, 102 (1990) 251-267.

[154] A.T. Blades, P. Jayaweera, M.G. Ikonomou, P. Kebarle, FIRST STUDIES OF THE GAS PHASE ION CHEMISTRY OF M3+ METAL ION LIGANDS *, International Journal of Mass Spectrometry and Ion Processes, 101 (1990) 325-336.

[155] I.I. Stewart, G. Horlick, Electrospray Mass-Spectra of Lanthanides, Anal Chem, 66 (1994) 3983-3993.

[156] Y. Sasaki, A.G. Sykes, Formation and dissociation of the ethylenediaminetetra-acetic acid complex of the molybdenum(V) dimer Mo2O42+ in aqueous perchloric acid solution, Journal of the Chemical Society, Dalton Transactions, (1974) 1468-1473.

[157] C. Moulin, N. Charron, G. Plancque, H. Virelizier, Speciation of uranium by electrospray ionization mass spectrometry: Comparison with time-resolved laser-induced fluorescence, Appl Spectrosc, 54 (2000) 843-848.

[158] C. Galindo, M. Del Nero, Trace Level Uranyl Complexation with Phenylphosphonic Acid in Aqueous Solution: Direct Speciation by High Resolution Mass Spectrometry, Inorg Chem, 52 (2013) 4372-4383.

[159] M. Steppert, C. Walther, M. Fuss, S. Buchner, On the polymerization of hexavalent uranium. An electrospray mass spectrometry study, Rapid Commun Mass Sp, 26 (2012) 583-591.

[160] E.L. Mühr-Ebert, Dissolution Behaviour of Innovative Inert Matrix Fuels for Recycling of Minor Actinides, Fakultät für Georessourcen und Materialtechnik Rheinisch-Westfälischen Technischen Hochschule Aachen, 2017.

[161] W.W. Schulz, E.M. Duke, Reprocessing of low-enrichment uranium-molybdenum alloy fuels, Richland, 1959.

[162] E.L. Ebert, ASGARD-Report, FZJ, 2015.

[163] P.L. Brown, G.R. Erickson, J.V. Evans, The Chemical Characterization of Zirconium

Molybdate Gels, Colloid Surface, 62 (1992) 11-21.

[164] M. Kubota, T. Fukase, Formation of Precipitate in High-Level Liquid Waste from Nuclear-Fuel Reprocessing, J Nucl Sci Technol, 17 (1980) 783-790.

[165] L. Zhu. D., C. S., study of solubility product on precipitation of molybdenum and zirconium in nitric acid, Journal of Nuclear and Radiochemistry, 24 (2002) 77-83.

[166] X. Chen, Speziation von gemischten Molybdän-Europium-Komplexen mittels nano ESI-TOF, IRS, Leibniz Universität Hannover, 2014.

Publications and Presentations of this Work

Publications

- M. Cheng, Elena Ebert, M. Patzschke, M. Steppert, G. Modolo, C. Walther, On the speciation of Mo(VI) in strongly acidic media: a combined mass spectrometric and theoretical study, in process
- Meijie Cheng, Takayuki Sasaki, Michael Steppert, Clemens Walther, Mo-Zr interaction in nitric acid solutions: mass spectrometric proof for the formation of mixed Mo-Zr solution species, in process

Conference Presentation and Poster

1. M. Cheng, M. Steppert, C. Walther (2012): $^{98}Mo_nO_m$ species distributions in acidic solution measured by Electrospray Ionization Mass-Spectrometry. ATAS workshop 2012, Dresden, 05.-07. November.
2. M. Cheng, M. Steppert, C. Walther (2013): Mo_nO_m species distributions in acidic solution measured by Electrospray Ionization Mass-Spectrometry. DPG Frühjahrstagung 2013, Hannover, 18. - 22. März
3. M. Cheng, M. Steppert, C. Walther (2013): On the dissolution behavior of new Mo fuel matrices for Generation IV reactors. GDCh-Wissenschaftsforum Chemie 2013, Darmstadt, 1.-4. September
4. A. Hartmann, M. Cheng, M. Steppert, C. Walther (2014): Wie invasiv ist der Electrospray-Ionisationseffekt? DPG Frühjahrstagung 2014, Berlin, 17.-21. März
5. M. Cheng, M. Steppert, C. Walther (2014): Investigation of new Mo fuel matrices for Generation IV Reactors by Electrospray Ionization Mass-Spectrometry. ATAS workshop 2014, Dresden, 03.-07. November.
6. M. Cheng, M. Steppert, C. Walther (2015), Characterization of mixed Mo-Zr solution species by nano-Electrospray Ionization Mass Spectrometry. DPG Frühjahrstagung 2015, Heidelberg, 23. - 27. März.
7. M. Cheng, M. Steppert, C. Walther (2015), How does Iron influence the dissolution behavior of Mo based generation IV reactor fuel? New insights using nano ESI-TOF-MS. E-MRS 2015 Spring Meeting, Lille, France, 11.-15. Mai.
8. M. Steppert, M. Cheng, Elena Ebert, C. Walther (2015), Investigations on the solution behavior of new Mo fuel matrices for generation IV reactors by means of electrospray ionization mass spectrometry. E-MRS 2015 Spring Meeting, Lille, France, 11.-15. Mai.

9. M. Steppert, M. Cheng, C. Walther (2015), Bildung von gemischten Molybdän-Zirkonium Lösungsspezies als Vorläufer schwerlöslicher hydratisierter Zirkoniummolybdat-Phasen in Wiederaufarbeitungsschritten. GDCh WiFo 2015, Dresden, 30. Aug. - 01. September
10. M. Cheng, M. Steppert, C. Walther (2015), How does Iron influence the dissolution behavior of Mo based generation IV reactor fuel? New insights using nano ESI-TOF-MS. GDCh WiFo 2015, Dresden, 30. Aug. - 01. September

Danksagung

Herr Prof. Dr. Clemens Walther sage ich meinen herzlichsten Dank für die Ermöglichung dieser Arbeit, die Hilfsbereitschaft und die vielen guten Ratschläge und konstruktiven Kommentare. Insbesondere Du hast mir geholfen und mich ermutigt hast, wenn es mal eine schwerere Phase gegeben hat. Das habe ich nie als selbstverständlich angesehen. Herzlichen Dank!

Vielen Dank an Prof. Dr. Georg Steinhauser, Prof. Dr. Christian Ekberg für die freundliche Übernahme des Korreferats.

Mein besonderer Dank gilt Dr. Michael Steppert für die jahrelange, umfassende Unterstützung in allen Arbeitsbereichen, insbesondere für die intensive, fachliche Betreuung der Labortätigkeiten und die hilfreichen Hinweise und motivierenden Worte beim Verfassen der Arbeit.

Sebastian Büchner danke ich für die stete Unterstützung in aller Reparatur, Aufbau, Programmiere an dem Gerät.

Zudem bin ich folgenden Personen dankbar für die unterstützende Hilfe bei Messungen und Berechnungen: Dr. Elena Mühr-Ebert (Zusammenarbeit bei der Mo-Pellet), Dr. Alex Hölzer (ICP-MS, ICP-OES).

Ich danke allen Mitgliedern des Instituts für Radioökologie und Strahlenschutz für ihre Freundlichkeit, Hilfsbereitschaft und Unterstützung. Besonders danke ich Frau G. Erb-Bunnenberg und Herr Dr. C. Bunnenberg Euere umfangreiche Unterstützung und Ermutigung in allen letzten vielen Jahren.

Financial support for this research was provided by the European Atomic Energy Community‘s 7th Framework Program (FP7 2007-2011), project ASGARD – grant agreement No. 295825. I would like to thank all members of the project for the great collaboration.

Schließlich möchte ich mich noch bei meiner Familie von ganzem Herzen bedanken. Mein Mann Dr. Jianfeng Cui für die liebevolle Unterstützung während der Promotionszeit und die Motivation meine Dissertation zu vollenden. Meine beiden Töchter Lisa und Luna für das Verständnis und die Zeit, dass mich nach Hannover fahren lassen und am Computer schreiben lassen. Meine Eltern und Schwiegereltern für die Ermöglichung meines Studiums.

Eidesstattliche Erklärung

Hiermit erkläre ich, dass die vorliegende Arbeit ohne jegliche Hilfe dritter und ausschließlich von mir selbst verfasst wurde. Ich versichere, dass ich keine anderen, außer den genannten Literaturquellen und Hilfsmitteln, verwendet habe.

Hannover, den 18.11.2019

Meijie Cheng